Methods[1]

J.M. Jaeger, S.P.S. Gulick, L.J. LeVay, H. Asahi, H. Bahlburg, C.L. Belanger, G.B.B. Berbel, L.B. Childress, E.A. Cowan, L. Drab, M. Forwick, A. Fukumura, S. Ge, S.M. Gupta, A. Kioka, S. Konno, C.E. März, K.M. Matsuzaki, E.L. McClymont, A.C. Mix, C.M. Moy, J. Müller, A. Nakamura, T. Ojima, K.D. Ridgway, F. Rodrigues Ribeiro, O.E. Romero, A.L. Slagle, J.S. Stoner, G. St-Onge, I. Suto, M.H. Walczak, and L.L. Worthington[2]

Chapter contents

Introduction 1
Lithostratigraphy 5
Paleontology and biostratigraphy 9
Stratigraphic correlation 11
Geochemistry 14
Physical properties 16
Paleomagnetism 22
Downhole logging 23
References 28
Figures 31
Tables 55

[1] Jaeger, J.M., Gulick, S.P.S., LeVay, L.J., Asahi, H., Bahlburg, H., Belanger, C.L., Berbel, G.B.B., Childress, L.B., Cowan, E.A., Drab, L., Forwick, M., Fukumura, A., Ge, S., Gupta, S.M., Kioka, A., Konno, S., März, C.E., Matsuzaki, K.M., McClymont, E.L., Mix, A.C., Moy, C.M., Müller, J., Nakamura, A., Ojima, T., Ridgway, K.D., Rodrigues Ribeiro, F., Romero, O.E., Slagle, A.L.,Stoner, J.S., St-Onge, G., Suto, I., Walczak, M.H., and Worthington, L.L., 2014. Methods. *In* Jaeger, J.M., Gulick, S.P.S., LeVay, L.J., and the Expedition 341 Scientists, *Proc. IODP,* 341: College Station, TX (Integrated Ocean Drilling Program). doi:10.2204/iodp.proc.341.102.2014
[2] **Expedition 341 Scientists' addresses.**

Introduction

This chapter documents the procedures and methods employed in the various shipboard laboratories of the R/V *JOIDES Resolution* during Integrated Ocean Drilling Program (IODP) Expedition 341. This information applies only to shipboard work described in the Expedition Reports section of the Expedition 341 *Proceedings of the Integrated Ocean Drilling Program* volume. Methods used by investigators for shore-based analyses of Expedition 341 data will be described in separate, individual publications. This introductory section provides an overview of operations, curatorial conventions, depth scale terminology, and general core handling and analyses.

Authorship of site chapters

All shipboard scientists contributed to this volume. However, certain sections were written by discipline-based groups of scientists as listed below (listed alphabetically):

Background and objectives: S. Gulick, J. Jaeger
Operations: S. Gulick, J. Jaeger, L. LeVay, S. Midgley
Lithostratigraphy: H. Bahlburg, L. Childress, E. Cowan, M. Forwick, C. Moy, J. Müller, K. Ridgway, F. Rodrigues Ribeiro
Biostratigraphy: H. Asahi, C. Belanger, A. Fukumura, S. Gupta, S. Konno, L. LeVay, K. Matsuzaki, O. Romero, I. Suto
Stratigraphic correlation: A. Mix, G. St-Onge
Geochemistry: G. Berbel, C. März, E. McClymont, A. Nakamura
Physical properties: A. Kioka, T. Ojima, M. Walczak, L. Worthington
Paleomagnetism: S. Ge, J. Stoner
Downhole logging: L. Drab, A. Slagle
Core-log-seismic integration: L. Drab, S. Gulick, C. Moy, K. Ridgway, A. Slagle, L. Worthington

Site locations

GPS coordinates from precruise site surveys were used to position the vessel at all Expedition 341 sites. A Syquest Bathy 2010 compressed high-intensity radar pulse (CHIRP) subbottom profiler was used to monitor the seafloor depth on the approach to each site to reconfirm the depth profiles from precruise surveys. Once the vessel was positioned at a site, the thrusters were lowered and a positioning beacon was dropped to the seafloor. The dynamic positioning control of the vessel used navigational input from the

doi:10.2204/iodp.proc.341.102.2014

GPS system and triangulation to the seafloor beacon, weighted by the estimated positional accuracy. The final position for each hole of a given site was the mean position calculated from the GPS data collected over a significant portion of the time the hole was occupied. A survey of the seafloor was conducted at Site U1420 using the underwater camera system to ensure that it was free of obstructions.

Coring and drilling operations

The advanced piston corer (APC), extended core barrel (XCB), and rotary core barrel (RCB) systems were used during Expedition 341. At Sites U1417–U1419 and U1421, multiple holes were drilled to build a composite depth scale and a stratigraphic splice for continuous subsampling after the expedition (see **"Sample depth calculations"** and **"Stratigraphic correlation"**).

The APC system cuts soft-sediment cores with minimal coring disturbance relative to other IODP coring systems. After the APC core barrel is lowered through the drill pipe and lands near the bit, the drill pipe is pressured up until one or two shear pins that hold the inner barrel attached to the outer barrel fail. The inner barrel then advances into the formation and cuts the core. The driller can detect a successful cut, or "full stroke," from the pressure gauge on the rig floor.

The depth limit of the APC system, often referred to as APC refusal, is indicated in two ways: (1) the piston consistently fails to achieve a complete stroke (as determined from the pump pressure reading) because the formation is too hard and limited core recovery is achieved, or (2) excessive force (>60,000 lb; ~267 kN) is required to pull the core barrel out of the formation. When a full stroke could not be achieved, one or more additional attempts were typically made, and each time the bit was advanced by the length of recovered core. Note that this resulted in a nominal recovery of ~100% based on the assumption that the barrel penetrated the formation by the length of core recovered. During Expedition 341, there were a number of partial strokes that still returned nearly full core liners. In these cases, the partial strokes were not viewed as refusal and additional full-length APC cores were attempted.

The standard APC system contains a 9.5 m long core barrel. Expedition 341 was the first IODP expedition to make use of the half APC system, which uses a 4.7 m long core barrel. In most instances, the half APC system was deployed after the standard APC system reached refusal but was also employed in second or later holes at a site when coring particular depth intervals where previous full APC cores failed to achieve a full stroke. During use of the half APC system, the same criteria were applied in terms of refusal as for the full-length APC system. Use of the half APC system allowed for significantly greater APC sampling depths to be attained than would have otherwise been possible.

Nonmagnetic core barrels were used during all full-length APC system deployments, and steel core barrels were used for the half APC system. Orientation using the FlexIT tool (see **"Paleomagnetism"**) was completed on standard APC cores taken in various holes at each site, depending on operational conditions. Formation temperature measurements were made when operationally feasible to obtain temperature gradients and heat flow estimates using the advanced piston corer temperature tool (APCT-3) (see **"Physical properties"**).

The XCB system was used to advance the hole when half APC refusal occurred before the target depth was reached. The XCB is a rotary system with a small cutting shoe that extends below the large rotary APC/XCB bit. The smaller bit can cut a semiindurated core with less torque and fluid circulation than the main bit, optimizing recovery. The XCB cutting shoe (bit) extends ~30.5 cm ahead of the main bit in soft sediment but retracts into the main bit when hard formations are encountered. XCB core barrels are 9.5 m long.

The bottom-hole assembly (BHA) is the lowermost part of the drill string. A typical APC/XCB BHA consists of a drill bit (outer diameter = 11 7/16 inch), a bit sub, a seal bore drill collar, a landing saver sub, a modified top sub, a modified head sub, a nonmagnetic drill collar (for APC/XCB), a number of 8 inch (~20.32 cm) drill collars, a tapered drill collar, six joints (two stands) of 5½ inch (~13.97 cm) drill pipe, and one crossover sub. A lockable flapper valve was used so we could collect downhole logs without dropping the bit when APC/XCB coring.

The RCB system was deployed when APC or XCB coring rates diminished below an acceptable level if the formation was expected to be too indurated for APC/XCB coring (e.g., Site U1420), or if the bit was destroyed by an increasingly hard formation. The RCB is a conventional rotary drilling system that requires a dedicated RCB BHA and a dedicated RCB drilling bit (outer diameter = 9⅞ inches). A typical BHA for RCB coring includes an RCB drill bit, a mechanical bit release, a modified head sub, an outer core barrel, a modified top sub, and a series of drill collars followed by a tapered drill collar and 5½ inch drill pipe.

Drilling disturbance

Cores may be significantly disturbed as a result of the drilling process and may contain extraneous ma-

terial as a result of the coring and core handling process. In formations with loose sand or gravel layers, material from intervals higher in the borehole may be washed down by drilling circulation, accumulate at the bottom of the hole, and be sampled with the next core. The uppermost 10–50 cm of each core must therefore be examined critically during description for potential "cave-in." Common coring-induced deformation includes the concave-downward appearance of originally horizontal bedding. Piston action may result in fluidization (flow-in) at the bottom of APC cores. Retrieval from depth to the surface may result in elastic rebound. Gas that is in solution at depth may become free and drive core segments within the liner apart. When gas content is high, pressure must be relieved for safety reasons before the cores are cut into segments. This is accomplished by drilling holes into the liner, which forces some sediment as well as gas out of the liner. Holes are also drilled into the liner for rhizon sampling of pore waters. Drilling disturbances are described in "Lithostratigraphy" in each site chapter and are graphically indicated on the graphic core summary reports (see **"Core descriptions"**).

Core handling and curatorial procedures

Cores recovered during Expedition 341 were extracted from the core barrel in plastic liners. These liners were carried from the rig floor to the core processing area on the catwalk outside the Core Laboratory and cut into ~1.5 m long sections. The exact section length was noted and later entered into the database as "created length" using the Sample Master application. This number was used to calculate recovery. Headspace samples were taken from selected section ends (typically one per core if recovery allowed) using a syringe for immediate hydrocarbon analysis as part of the shipboard safety and pollution prevention program. Similarly, microbiology samples were taken immediately after the core was sectioned. Whole-round samples for interstitial water (IW) and physical properties were cut on the catwalk. Core catcher samples were taken for biostratigraphic analysis. When catwalk sampling was complete, liner caps (blue = top; colorless = bottom; yellow = bottom, whole-round cut) were glued with acetone onto liner sections and the sections were placed in core racks in the laboratory for analysis. Rarely, APC cores were plugged and the liner could not be easily extracted; see the drillers core tech summary sheet for a list of cores for which this was required. In this situation, the liner was hydraulically extruded on the rig floor into half-round liner sections and curated the same as normally extracted liners.

The numbering of sites, holes, cores, and samples followed standard IODP procedure. A full curatorial sample identifier consists of the following information: expedition, site, hole, core number, core type, section number, and offset in centimeters measured from the top of a given section. For example, a sample identification of "341-U1417A-1H-2, 10–12 cm" represents a sample taken from the interval between 10 and 12 cm below the top of Section 2 of Core 1 ("H" designates that this core was taken with the APC system) of Hole A of Site U1417 during Expedition 341. The "U" preceding the hole number indicates that the hole was drilled by the United States Implementing Organization (USIO) platform, the *JOIDES Resolution*. Other core types are designated by "R" for cores taken with the RCB system and "X" for cores taken by the XCB system. Half APC cores also were given the "H" designation, and the usage of the half APC system was noted in the core tech summary sheet by the drillers.

Shipboard core analysis

Whole-round core sections were immediately run through the Special Task Multisensor Logger (STMSL) when necessary for stratigraphic correlation after being cut on the catwalk. The STMSL measures density and magnetic susceptibility at a low resolution and is used to aid in real-time stratigraphic correlation. Whole-round core sections were run through the Whole-Round Multisensor Logger (WRMSL; measuring *P*-wave velocity, density, and magnetic susceptibility) and the Natural Gamma Radiation Logger (NGRL).

Typically, core sections were allowed to reach equilibrium with laboratory temperature (after ~4 h) prior to running through the whole-round core logging systems (see **"Physical properties"** for exceptions). However, when the sediment had higher concentrations of gas, sections were immediately run through the STMSL and the WRMSL prior to gas expansion of the cores. When liner sections were fractured from coring disturbance and patched on the catwalk, the resulting section diameter was too wide to fit through the magnetic susceptibility loop on the WRMSL and was measured on the STMSL instead (see the Laboratory Information Management System [LIMS] database for sections where this was required). Each section from a given core was split lengthwise from bottom to top into working and archive halves. Investigators should note that older material, especially lonestones, might have been transported upward on the split face of each section during splitting. The working half of each section was run on the Section Half Measurement Gantry, which includes the *P*-wave caliper (PWC) and vane

shear, prior to being sampled for shipboard analysis (biostratigraphy, physical properties, geochemistry, and bulk X-ray diffraction [XRD] mineralogy). The archive half of each section was scanned on the Section Half Imaging Logger (SHIL) and measured for color reflectance and magnetic susceptibility on the Section Half Multisensor Logger (SHMSL). At the same time, archive halves were described macroscopically and microscopically by means of smear slides. Finally, archive halves were run through the cryogenic magnetometer. Both halves of the core were then put into labeled plastic tubes that were sealed and transferred to cold storage space aboard the ship.

At the end of the expedition, all archive and working halves were transported from the ship to permanent cold storage at the Gulf Coast Repository at Texas A&M University (USA).

Sample depth calculations

The primary depth scale types are based on the measurement of the drill string length deployed beneath the rig floor (drillers depth below rig floor [DRF] and drillers depth below seafloor [DSF]), the length of each core recovered (core depth below seafloor [CSF] and core composite depth below seafloor [CCSF]), and the length of the logging wireline deployed (wireline log depth below rig floor [WRF], wireline log depth below seafloor [WSF], and wireline log matched depth below seafloor [WMSF]). All units are in meters. Depths of samples and measurements are calculated at the applicable depth scale either by fixed protocol (e.g., CSF) or by combinations of protocols with user-defined correlations (e.g., CCSF). The definition of these depth scale types and the distinction in nomenclature should keep the user aware that a nominal depth value at two different depth scale types usually does not refer to exactly the same stratigraphic interval in a hole.

Depths of cored intervals are measured from the drill floor based on the length of drill pipe deployed beneath the rig floor (DRF scale). The depth of the cored interval is referenced to the seafloor (DSF scale) by subtracting the seafloor depth at the time of the first hole from the DRF depth of the interval. In most cases, the seafloor depth is the length of pipe deployed minus the length of the mudline core recovered. However, some of the seafloor depths were determined by offset or by tagging the seafloor with the camera system in place.

Standard depths of cores on the CSF-A scale are determined based on the assumptions that (1) the top depth of a recovered core corresponds to the top depth of its cored interval (DSF scale) and (2) the recovered material is a contiguous section even if core segments are separated by voids when recovered. Voids in the core are closed by pushing core segments together, if possible, during core handling. This convention is also applied if a core has incomplete recovery, in which case the true position of the core within the cored interval is unknown and should be considered a sample depth uncertainty, up to the length of the core barrel used, when analyzing data associated with the core material. Standard depths of subsamples and associated measurements (CSF-A scale) are calculated by adding the offset of the subsample or measurement from the top of its section, as well as the lengths of all higher sections in the core, to the top depth of the cored interval.

A soft to semisoft sediment core from less than a few hundred meters below seafloor expands upon recovery (typically a few percent to as much as 15%), so the length of the recovered core exceeds that of the cored interval. Therefore, a stratigraphic interval may not have the same nominal depth at the DSF and CSF scales in the same hole. When core recovery (the ratio of recovered core to cored interval) is >100%, the CSF depth of a sample taken from the bottom of a core will be deeper than that of a sample from the top of the subsequent core (i.e., the data associated with the two core intervals overlap on the CSF-A scale).

Core composite depth scales (CCSF) are constructed for sites, whenever feasible, to mitigate the CSF-A core overlap problem as well as the coring gap problem and to create as continuous a stratigraphic record as possible. Using shipboard core logger–based physical properties data, verified with core photos, core depths in adjacent holes at a site are vertically shifted to correlate between cores recovered in adjacent holes. This process produces the CCSF-A depth scale. The correlation process results in affine tables, indicating the vertical shift of cores on the CCSF scale relative to the CSF-A scale. Once the CCSF scale is constructed, a splice can be defined that best represents the stratigraphy of a site by utilizing and splicing the best portions of individual sections and cores from each hole. This process produces the CCSF-D depth scale, which is strictly correct only along the splice. Because of core expansion, the CCSF-A/D depths of stratigraphic intervals are typically 10%–15% deeper than their CSF-A depths. CCSF-A depth scale construction also reveals that coring gaps on the order of 1–1.5 m typically occur between two subsequent cores, despite the apparent >100% recovery. Based on discussions between Expedition 341 participants, we suggest that these gaps may be produced by either rebound during piston coring or vertical rise of the floor of the borehole between coring runs in response to overburden reduction. Lastly, in order to compare intervals along the splice with drilling data, logging data, and seismic

data, a final depth scale, CCSF-B, is created by correcting the CCSF-D depth scale back to the true drilled interval. For detailed depth scale definitions, see **"Stratigraphic correlation."**

When coring multiple holes to establish composite depths and continuous spliced records, drilling depths were corrected for tides. At each site, tides were predicted at 30 min intervals throughout the time of coring, using the Oregon State University Tidal Prediction Software (copyright Oregon State University 2012, G. Egbert and L. Erofeeva, and used by permission). Tidal variations during Expedition 341 were up to 4 m over a diurnal–semidiurnal cycle, so proper tide corrections were needed to obtain complete composite sections and splices (see **"Stratigraphic correlation"**). The first APC core at each site established the reference depth of the mudline below sea level at the time of coring. For each core taken after the first mudline core, drilling advances were based on recovery plus a correction for the deviation of the sea level (as predicted from the tide model) relative to the reference sea level for the first core at the site. Tidal deviations at the time of each coring operation define the drilldown between cores. During each coring operation, the drill string is advanced either less than the previous core's recovery (for a falling tide) or greater the previous recovery (for a rising tide).

Lithostratigraphy

The primary lithostratigraphic procedures used during Expedition 341 included visual core description, sediment classification, digital color imaging, XRD, and smear slide preparation and description. Color spectrophotometry and point source magnetic susceptibility data acquired by the Lithostratigraphy group during core description are described in detail in **"Physical properties."** Percent carbonate, percent organic (CHNS), major element, and trace element geochemical measurements on sediment and sedimentary rocks collected by the Lithostratigraphy group are described in detail in **"Geochemistry."**

Core preparation

The technique applied for splitting cores into working and archive halves (either using a piano wire or a saw) affected the appearance of the split core surface. In soft sediment, the wire tended to drag mud across the split core surface, thereby obscuring the clasts, which may have resulted in an emphasis on muddier lithologies in the visual core descriptions (VCDs). Cutting by saw allowed for the identification of sedimentary structures, clast distribution, and clast composition at much greater detail. However, intervals of low density (e.g., diatom-rich mud and ooze) were often disturbed by water introduced during sawing. Splitting method choices were made by considering the physical properties data (density and magnetic susceptibility) determined on whole-round cores, and the saw was used when gamma ray attenuation (GRA) bulk density and magnetic susceptibility values both were high, indicating clast-rich, indurated lithologies.

Prior to core description and high-resolution digital color imaging, the quality of the split core surface of the archive half of each core was assessed, and when necessary (e.g., the surface was irregular or smeared), the split core surface was scraped lightly with a flexible plastic nonmagnetic card. Cleaned split core sections were then described in conjunction with measurements by the SHIL, discussed below, and SHMSL (see **"Physical properties"**).

Visual core descriptions

Macroscopic and smear slide descriptions of each section (nominally 0–150 cm long) were recorded on handwritten visual core description forms (Fig. **F1**). All handwritten forms were digitally preserved as PDF files (see LITH in **"Supplementary material"**). Standard sedimentological observations of lithology, sedimentary structures, color, bioturbation, and accessories were entered into the form, as well as specific comments, when necessary, on these features. Information in the Accessories column includes documentation of macroscopic biogenic remains, such as shells, worm tubes, and isolated gravel-sized clasts such as lonestones. When possible, clasts were described as sedimentary, igneous (plutonic or volcanic), or metamorphic (foliated or nonfoliated). Further, consideration of whole-round magnetic susceptibility and natural gamma ray data supported the identification and interpretation of distinct sedimentary features or intervals within the cores (e.g., reduced magnetic susceptibility and lower density often indicate the occurrence of diatom oozes).

Color

Sediment color was determined qualitatively for core intervals using Munsell Soil Color Charts (Munsell Color Company, Inc., 2009).

DESClogik data capture software

Visual core description forms were compiled and entered into the LIMS database using the DESClogik application. Direct entry of descriptive and interpretive information in the program was performed using Tabular Data Capture mode. Before core description began, a spreadsheet template was constructed

in Tabular Data Capture mode. Two templates containing category columns for texture and relative abundance of biogenic/mineralogic components were configured specifically for recording smear slide and thin section data, respectively. Another template containing category columns for texture and relative abundance of tephric components was configured specifically for recording volcanic grains. Data entered in DESClogik were then uploaded into the LIMS database.

Standard graphical report

A one-page graphical representation of each section was generated using the LIMS2Excel application and a commercial program (Strater, Golden Software). VCDs are generated with a CSF-A depth scale, split-core high-resolution color images, graphic lithology, volcanic grain content, drilling disturbance, bioturbation intensity, sedimentary structures, lithologic accessories (e.g., clast abundance or macrofossils), age, magnetic susceptibility, GRA bulk density, color reflectance (b*), and shipboard sample collection (Fig. F2). Graphic lithologies, sedimentary structures, and other visual observations shown on the VCDs by graphic patterns and symbols are explained in Figure F3.

Smear slides

To aid in lithologic classification, smear slide microscope analysis was used to determine mineralogy, microfossil, and volcanic constituents and abundance. Toothpick samples were taken from representative sections of lithology and at a frequency of at least one sample per core (~9.5 m). Each slide was prepared by completely mixing the sediment with several drops of distilled water on a glass microscope slide and dried on a hot plate at 50°C. The dried sample was then mounted in Norland optical adhesive 61 and fixed in an ultraviolet light box. Type and relative abundance of biogenic, volcanic, and mineralogic components were estimated (Fig. F4) for each smear slide using a transmitted-light petrographic microscope equipped with a camera. Data were entered into the LIMS database using a custom tabular template in DESClogik. Images of some smear slides were taken and uploaded into DESClogik as well.

Lithologic classification scheme

The lithologic description for granular sediments was based on the classification schemes used during Ocean Drilling Program (ODP) Leg 178 (Shipboard Scientific Party, 1999), IODP Expedition 317 (Expedition 317 Scientists, 2011), and IODP Expedition 318 (Expedition 318 Scientists, 2011).

The principal sediment/sedimentary rock name was based on the relative abundance of components present, including siliciclastic, carbonate, biogenic, and/or volcanic grains. If well indurated or cemented, the modifier of "stone" was used. These sediments were classified using Figure F5, based on Expedition 317. The principal name of sediments with >50% siliciclastic grains was based on an estimate of the grain sizes present. The Wentworth (1922) scale was used to define size classes:

- If no gravel was present, the principal sediment/rock name was determined based on the relative abundances of sand, silt, and clay (after Shepard, 1954) (Fig. F5).
- If the sediment/rock contains siliciclastic gravel, then the principal name was determined from the relative abundance of gravel (>2 mm) and sand/mud ratio of the clastic matrix following the classification of Moncrieff (1989) and used during Expedition 318 (Fig. F6).

The primary name for sediment/rock with >50% biogenic grains was "ooze," modified by the most abundant specific biogenic grain type that forms 50% or more of the sediment or rock (Fig. F7). For example, if diatoms exceed 50%, then the sediment is called "diatom ooze." However, if the sediment is composed of 40% diatoms and 15% sponge spicules, then the sediment was termed "biosiliceous ooze." This scheme was also used with carbonate biogenic grains.

Major and minor modifiers for biogenic sediment were also applied to the principal sediment/rock names following the scheme of Expedition 318 (Expedition 318 Scientists, 2011):

- Major modifiers are those components with abundances between 25% and 50% and are indicated by the suffix "rich" (e.g., "diatom-rich").
- Minor modifiers are those components with abundances of 10%–25% and are indicated by the suffix "-bearing" (e.g., "diatom-bearing").

The products of volcanic eruptions can be introduced into the sedimentary environment at the drill sites by both primary (air fall and sedimentation through the water column) and secondary (e.g., reworking by sediment-gravity flows, ice rafting, etc.) processes. The term "volcaniclastic-bearing" was used for sediment containing between 10% and 50% volcanic grains without consideration of the origin and environment (Brown, 2007; Fisher and Schmincke, 1984). "Volcaniclastic-rich" was used for sediment with 50%–90% volcanic grains. The principal name of a sediment/rock with >90% primary volcanic grains, such as glass shards and other pyroclastic components, was "ash" (Fisher and Schmincke,

1984) (Fig. F8). Using this definition, ash is defined as unconsolidated, fine (<2 mm) pyroclastic material, whereas the term "tuff" is used for the consolidated or lithified counterpart.

Bed/Lamination and thickness

Boundaries between different lithologies are classified as sharp or gradational. Bedding and lamination are defined following Mazzullo et al. (1988):

- Thinly laminated (1–3 mm thick),
- Laminated (3 mm to 1 cm),
- Very thin bedded (1–3 cm),
- Thin bedded (3–10 cm),
- Medium bedded (10–30 cm),
- Thick bedded (30–100 cm), and
- Very thick bedded (>100 cm).

For units in which two lithologies are closely interbedded (the individual beds are <15 cm thick and alternate between one lithology and another), three "interbedded" lithology names are used as primary units (Fig. F3) modified from Expedition 317 (Expedition 317 Scientists, 2011): interbedded sand and mud, interbedded silt and mud, and interbedded mud and diamict. When beds are distributed throughout a different lithology (e.g., beds of sand several centimeters to tens of centimeters thick within a mud bed), they are logged individually and the associated bed thickness and grain size ranges are described.

Bioturbation

Ichnofabric description included the extent of bioturbation and notation of distinctive biogenic structures. To assess the degree of bioturbation semiquantitatively, a modified version of the Droser and Bottjer (1986) ichnofabric index scheme was used (1 = no apparent bioturbation, 2 = slight bioturbation, 3 = moderate bioturbation, 4 = heavy bioturbation, and 5 = complete bioturbation) (Fig. F9). Massive mud may be deposited rapidly in a glacial environment and record no evidence of bioturbation; therefore, it was assigned a value of 1. However, mud may also completely lack sedimentary structures because of complete bioturbation (e.g., 5 on the scale), which may be accompanied by color mottling. This index is graphed using the numerical scale in the Bioturbation intensity column of the VCDs. Recognizable biogenic structures and trace fossils were noted and logged in the LIMS database through DESClogik.

Clast abundance

Clast abundance was determined by counting lonestones and diamict clasts that were visible on the archive-half sediment surface. The working half was examined when only holes or depressions caused by lonestones and diamict clasts were observed in the archive half. Size, lithology, and shape of lonestones and diamict clasts were determined whenever possible (i.e., without disrupting the sediment surface). Only lonestones and diamict clasts larger than 2 mm were counted. In the case of isolated lonestones contained in mud, the number of clasts per described subunit of a core section was entered into DESClogik. When the number of clasts per subunit of a core section became relatively common, the number of lonestones was not directly counted. The modifiers "with dispersed," "with common," or "with abundant" clasts and "clast-rich" and "clast-poor" then accounted for the clast abundance following the Moncrieff (1989) classification (Fig. F6). Details on size, lithology, shape, and the specific lithology of observed lonestones and diamict clasts are provided in the written core descriptions and/or the DESClogik General interval comments column.

Core disturbance

Core disturbance from the drilling process may alter the cores slightly (bent/bowed bedding contacts) or greatly (complete disruption of stratigraphic sequence). To document drilling disturbances, the following classification scheme is used. Drilling disturbance of relatively soft or firm sediment was classified into three categories:

1. Slightly disturbed: bedding contacts are slightly bent or bowed in a concave-downward appearance.
2. Extremely disturbed: bedding is completely deformed and may show diapiric or minor flow structures.
3. Soupy: sediment is water saturated and shows no traces of original bedding or structure.

Drilling disturbance of harder sediment (i.e., lithified by compaction or cementation) was classified into four categories:

1. Slightly fractured or biscuited: core pieces are in place and have very little drilling slurry or brecciation.
2. Moderately fractured or biscuited: core pieces are from the cored interval and are probably in the correct stratigraphic sequence (although the entire section may not be represented); intact core pieces are broken into rotated discs (or "biscuits") as a result of the drilling process, and drilling mud has possibly flowed in.
3. Highly fractured or brecciated: pieces are from the cored interval and are probably in the correct stratigraphic sequence (although the entire section may not be represented), but the origi-

nal orientation is totally lost and drilling mud has flowed in.

4. Highly fractured or drilling slurry: pieces are from the cored interval and are probably in the correct stratigraphic sequence (although the entire section may not be represented), but the original orientation is totally lost; loose pieces of core material are mixed with the drilling slurry.

In addition to these categories for soft and hard sediment, several other terms were used to characterize drilling disturbances. Although many other forms of drilling disturbance were observed (Fig. **F3**), the most common types are as follows:

- Suck-in: completely disturbed stratigraphic record due to soft (often sandy) sediment sucked into the core liner while pulling the drill string upward. Characteristic features are vertical stratification and flow-in structures in the middle of the section.
- Washed gravel: fine material was probably lost during drilling, with only washed coarse material remaining, commonly pebbles or cobbles. This may result from problems recovering coarse-grained diamict.
- Flow-in: soupy, displaced sediment was drawn into the core liner during APC coring.
- Fall-in: downhole contamination results from the falling of loose material from the drill hole walls into the top of the core. The uppermost 10–15 cm of each core was inspected during description for potential fall-in.

In additional to drilling-related artifacts, disturbance also occurred during core handling. The split core surface of relatively high porosity lithologies occasionally was disturbed because of excess pressure applied by the point magnetic susceptibility SHMSL lander. Pore water sampling by rhizons also disturbed the sedimentary fabric within several centimeters of the sampling hole.

Digital color imaging

The SHIL captures continuous high-resolution images of the archive-half surface for analysis and description. Images were collected shortly after core splitting and core description in an effort to avoid color changes resulting from sediment drying and oxidation of the surface. The shipboard system uses a commercial line-scan camera lens (AF Micro Nikon; 60 mm; 1:2.8 D), with illumination provided by a custom assembly of three pairs of light-emitting diode strip lights that provide constant illumination over a range of surface elevations. Each pair of lights has a color temperature of 6,500 K and emits 90,000 lux at 76 mm. The resolution of the line-scan camera was set at 10 pixels/mm. Available files include the original high-resolution TIFF image with grayscale and ruler, as well as reduced JPEG images cropped to show only the section-half surfaces.

X-ray diffraction analysis

Samples for XRD analyses were selected from the working half, generally at the same depth as sampling for solid-phase geochemistry and smear slides. Additional samples were taken when distinct lithologic changes occurred. In general, one 5 cm^3 sample was taken of a representative lithology per core, typically in Section 1 or 2. Additional samples were occasionally taken and analyzed based on visual core observations (e.g., color variability and visual changes in lithology and texture) and smear slides. Samples taken once per core for XRD analysis also were generally analyzed for sedimentary inorganic (i.e., carbonate analysis) and organic (i.e., CHNS analysis) carbon in the Geochemistry Laboratory (see **"Geochemistry"**). Samples analyzed for bulk mineralogy were freeze-dried in the case of unlithified samples and ground by hand or in an agate ball mill as necessary. Prepared samples were top-mounted onto a sample holder and analyzed using a Bruker D-4 Endeavor diffractometer mounted with a Vantec-1 detector, using nickel-filtered CuKα radiation. The standard locked coupled scan was as follows:

Voltage = 37 kV.
Current = 40 mA.
Goniometer scan = 4°–70°2θ.
Step size = 0.0174°2θ.
Scan speed = 1 s/step.
Divergence slit = 0.3 mm.

Shipboard results yielded only qualitative results of the presence and relative abundances of the most common mineralogical components.

Diffractograms of bulk samples were evaluated with the aid of the EVA software package, which allowed for mineral identification and basic peak characterization (e.g., baseline removal and maximum peak intensity). Files were created that contained *d*-spacing values, diffraction angles, and peak intensities with and without the background removed. These files were scanned by the EVA software to find *d*-spacing values characteristic of a limited range of minerals, using aluminum oxide as an internal standard (Expedition 317 Scientists, 2011). Peak intensities were reported for each mineral to provide semiquantitative measures of mineral abundances downhole and among sites. Muscovite/illite and kaolinite/chlorite have similar diffraction patterns and were not distinguished shipboard. Digital files with the diffraction patterns are available from the LIMS database

(iodp.tamu.edu/tasapps/). The presence of expandable clay minerals was analyzed by treating the samples with ethylene glycol following Moore and Reynolds (1997).

Paleontology and biostratigraphy

Preliminary age assignments for Expedition 341 sediments were based on biostratigraphic analyses of diatoms, planktonic foraminifers, and radiolarians (Figs. F10, F11). Benthic foraminifers were used primarily for paleoenvironmental interpretation. Diatom datum depths were determined by examining core catcher samples, and, where appropriate, additional samples (sampling spacing of 1.5–0.25 m) were taken from the split core sections. Planktonic and benthic foraminifers and radiolarians were examined in core catcher samples only. The preservation, abundance, and zonal assignment for selected samples and for each microfossil group were entered via DESClogik into the LIMS database.

Diatoms

The diatom zonal scheme used here mainly follows biostratigraphic studies by Barron and Gladenkov (1995) (ODP Leg 145) and Yanagisawa and Akiba (1998). Datums are modified following the updated geologic timescale (Hilgen et al., 2012) (Figs. F12, F13). Two- or three-digit code numbers (D120–D20) are given to the primary and secondary biohorizons according to the Neogene North Pacific Diatom (NPD) zone code of Akiba (1986) and Yanagisawa and Akiba (1998).

Several taxonomic studies of diatoms preserved in northeast Pacific sediments are available. For the identification of diatoms to the lowest possible taxonomic level, we mainly followed Akiba and Yanagisawa (1986), Yanagisawa and Akiba (1990), and Barron and Gladenkov (1995). Concerning Pliocene and Pleistocene diatoms found in Expedition 341 sediments, a major taxonomic issue is the modification proposed for the taxonomy of *Neodenticula seminae* and *Neodenticula koizumii*, two key diatom biostratigraphic markers in northeast Pacific sediments. As discussed by Yanagisawa and Akiba (1990, 1998), valves of extant *N. seminae* closely resemble those of the extinct *N. koizumii* and the morphologically intermediate, extinct taxon *Neodenticula* sp. A (Yanagisawa and Akiba, 1998). The distinguishing feature among these taxa is the copula structure. Whereas the copula of *N. seminae* is closed, smooth, and rounded, that of *N. koizumii* and *Neodenticula* sp. A is open and pointed, if well preserved. When ambiguity occurred in identifying the species, counts of open versus closed copula were made to determine the first occurrence of *N. seminae* and the last occurrence of *N. koizumii*.

Method of study for diatoms

Smear slides of core catcher samples and of silty mud from split core sections that were expected to be diatomaceous (based on visual observation) were prepared by placing a drop of reverse osmosis water and a small amount of raw sediment (tip of a toothpick) onto a glass slide and then evaporating the water by heating on a hot plate. One to two drops of Norland optical adhesive was applied to the dry slide, which was then covered with a 22 mm × 22 mm glass coverslip. The adhesive was solidified by placing the slide under ultraviolet light for ~10 min. Smear slides were partially examined at 400× and/or 1000× for stratigraphic markers and other common taxa using a ZEISS Axioplan microscope.

The total abundance of diatoms and the species composition of the preserved diatom assemblage were determined for all slides. Total diatom abundance of the sediment was assessed according to Scherer and Koç (1996):

D = dominant (>60% valves).
A = abundant (~20%–60% valves).
C = common (~5%–20% valves).
F = few (2%–5% valves).
R = rare (<2% valves).
B = barren (no diatoms present).

The relative abundance of each diatom taxon, as reported in range charts, was estimated using the following qualitative scale:

A = abundant (>10 valves/field of view [FOV]).
C = common (1–10 valves/FOV).
F = few (≥1 valves/10 FOVs and <1 valve/FOV).
R = rare (≥3 valves/traverse of coverslip and <1 valve/10 FOVs).
X = present (<3 valves/traverse of coverslip, including fragments).

Diatom preservation categories, as reported in range charts, were described qualitatively according to Barron and Gladenkov (1995):

VG = very good (no breakage or dissolution).
G = good (majority of specimens complete, with minor dissolution and/or breakage, and no significant enlargement of the areolae or a dissolution of frustule rims detected).
M = moderate (minor but common areolae enlargement and dissolution of frustule rims, with a considerable amount of breakage of specimens).

P = poor (strong dissolution or breakage, some specimens unidentifiable, and strong dissolution of frustule rims and areolae enlargement).

Radiolarians

The sites drilled during Expedition 341 in the northeast Pacific are located near ODP Site 887 (Leg 145), where several authors have addressed radiolarian biostratigraphy. Shilov (1995) proposed a new Pliocene to Miocene radiolarian zonation based on Sites 881–887 (Leg 145). Morley and Nigrini (1995) identified several radiolarian biostratigraphic events. Recently, Kamikuri et al. (2004, 2007) conducted detailed investigations of the Neogene radiolarian biostratigraphy at Site 887. During Expedition 341, we used the radiolarian zonation and datums established by Kamikuri et al. (2007). However, radiolarian events in Kamikuri et al. (2007) were tied to Cande and Kent (1995). Here, we recalculated each radiolarian datum and interpreted zones based on the updated geologic timescale (Hilgen et al., 2012).

The radiolarian zonal scheme used here follows Kamikuri et al. (2004, 2007) and uses 49 index fossils from early Miocene to present (Figs. **F14, F15**). The radiolarian zones from Kamikuri et al. (2007) are restricted to the middle Miocene to Pleistocene and thus cannot be used for older sediments. In addition to the biodatums, we also determined the relative abundances of environmentally sensitive species following Pisias et al. (1997).

Method of study for radiolarians

To prepare samples for light microscopy observation, ~5 cm^3 of wet core catcher sediment was sieved and rinsed using a 63 µm mesh sieve. The >63 µm fraction was then processed with 10% v/v H_2O_2 and 15% v/v HCl to remove calcium carbonate and clay infillings. The sample was then resieved using a 63 µm mesh sieve, and smear slides were prepared using the same technique as for the diatom analyses. Opportunistic counts of radiolarian taxa from mudline samples were also made.

Total radiolarian abundances were determined based on light microscopic observations at 40× magnification using a ZEISS AXIOSKOP microscope as follows:

A = abundant (>300 specimens/slide).
C = common (200–300 specimens/slide).
F = few (100–200 specimens/slide).
R = rare (50–100 specimens/slide).
P = present (<50 specimens/slide).
B = barren (0 specimens/slide).

Radiolarian species abundances were determined by counting at least 300 specimens (where possible) and tabulated as follows:

A = abundant (>20 specimens/300 counts).
C = common (10–20 specimens/300 counts).
F = few (5–10 specimens/300 counts).
R = rare (1–5 specimens/300 counts).
P = present (1 specimen/300 counts).

Preservation was recorded as follows:

G = good (most of specimens complete, including fine structures).
M = moderate (several species with minor dissolution and/or breakage).
P = poor (most of specimens with common dissolution and/or breakage).

Foraminifers

Biostratigraphic datums are infrequent for both planktonic and benthic foraminifers in the high-latitude Pacific Ocean. For planktonic foraminifers, we used the biostratigraphic framework established for the California margin, which focuses on the evolution of the genus *Neogloboquadrina* (Fig. **F16**). This framework provides six fossil zones (CM1–CM6) and eight biostratigraphic datum events from 3.6 Ma to present (Kennett et al., 2000; Kucera and Kennett, 2000). Latitudinal variation of several biotic events (e.g., last occurrence of *Neogloboquadrina asanoi* = 2.0–2.4 Ma; Kucera and Kennett, 2000) within the California margin suggests that some datum events are diachronous, and there may be an age uncertainty when applying these bioevents in the southern Gulf of Alaska margin. Benthic foraminifers are limited in their biostratigraphic use but provide information on water depth, productivity, and oxygenation (Bergen and O'Neil, 1979; Gooday, 2003; Murray, 2006; Jorissen et al., 2007).

Method of study for foraminifers

We analyzed ~40 cm^3 of sediment from each core catcher sample for benthic and planktonic foraminifers. Samples were disaggregated in tap water and wet-sieved through a 63 µm mesh sieve. If the sample was semilithified and did not readily disaggregate, the sample was soaked in water with a detergent (Borax) or with a small amount of H_2O_2. After disaggregation, all washed samples were rinsed with reverse osmosis water. The coarse fraction was placed on filter paper or in a porcelain dish and dried in an oven at ~40°C. The sieve was placed in an ultrasonic bath and thoroughly checked for sample residues to minimize cross-contamination.

Faunal identifications were made using a ZEISS Discovery V8 binocular light microscope. Taxonomic

composition, relative abundance, and preservation state were observed in the >63 µm size fraction for benthic foraminifers and in the >125 µm size fraction for planktonic foraminifers. The >63 µm size fraction was also checked for the presence of planktonic foraminifers, but none were identified. Taxonomic identifications of benthic foraminifers at the species level were made largely following Todd and Low (1967), Smith (1973), Bergen and O'Neil (1979), and the Ellis and Messina catalog (**www.micropress.org/em**); generic identifications largely followed Loeblich and Tappan (1988). Taxonomic identifications of planktonic foraminifers followed Kennett and Srinivasan (1983) and Saito et al. (1981); detailed descriptions of the morphological variation in the genus *Neogloboquadrina* were taken from Kennett et al. (2000) and Kucera and Kennett (2000).

Semiquantitative estimates of the relative abundances of benthic foraminifers in relation to the total >63 µm size fraction and of planktonic foraminifers in relation to the total >125 µm size fraction were ranked as follows:

D = dominant (>30%).
A = abundant (>10%–30%).
F = few (>5%–10%).
R = rare (1%–5%).
P = present (<1%).
B = barren (no foraminifers present).

Relative abundances of taxa within the benthic foraminifers with respect to the total benthic foraminiferal assemblage (>63 µm) and relative abundances of taxa within planktonic foraminifers with respect to the total planktonic foraminiferal assemblage (>125 µm) were ranked as follows:

D = dominant (>30%).
A = abundant (>10%–30%).
F = few (>5%–10%).
R = rare (1%–5%).
P = present (<1%).

In addition to the relative abundance of planktonic foraminifer species, the relative abundance (%) of the dextral coiling *Neogloboquadrina pachyderma* was determined by counting specimens of *N. pachyderma* with respect to their coiling directions.

Preservation of foraminiferal tests was ranked as follows:

VG = very good (no breakage or dissolution).
G = good (minor dissolution or pitting on calcareous taxa and no recrystallization; <10% of specimens are broken).
M = moderate (frequent etching of calcareous taxa; 10%–30% of specimens are broken).
P = poor (frequent dissolution and recrystallization; >30% of specimens are broken).

Stratigraphic correlation

Expedition 341 scientific objectives required recovery of complete stratigraphic sections to the extent possible. Continuous sedimentary sections cannot be recovered from a single borehole because gaps in recovery occur between successive cores, even when 100% or more nominal recovery is attained (Ruddiman et al., 1987; Hagelberg, et al., 1995). Construction of a complete stratigraphic section, referred to as a splice, requires combining intervals from two or more holes cored at the same site. To maximize the probability of bridging gaps between cores, we attempt to offset between holes the depths below the seafloor from which cores are recovered. This practice maximizes the probability that missing sedimentary sections from within a given hole are recovered in one or more adjacent holes. At least two complete holes, and in many cases three or more holes, are needed to recover a complete section in the APC portion of a site. Additional complete holes are cored to allow options for construction of alternate splices, where possible.

Our methods for developing composite depths and splices followed the basic strategy that is now common practice on all high-resolution paleoceanographic expeditions. We used initial analyses of magnetic susceptibility and gamma density run on the STMSL to develop preliminary composite depths for purposes of making real-time drilling decisions (Mix, Tiedemann, Blum, et al., 2003). The depth scale was refined as more detailed information became available during drilling.

Our goals for stratigraphic correlation, in priority order, were to

- Guide drilling to ensure recovery of a complete stratigraphic section,
- Establish a composite depth scale,
- Define a stratigraphically complete and representative sampling splice,
- Evaluate and refine shipboard stratigraphic age models and their uncertainties by synthesizing all available age information in a common depth framework, and
- Develop preliminary reconstructions of sediment accumulation rates and mass fluxes.

As a result of this stratigraphic correlation process, several different depth models are created. Table **T1** and Figure **F17** summarize these various IODP depth models and their ODP equivalents. Detailed discus-

sion of the definitions of these depth scales, and the processes by which they are created, appear below.

Composite depth scale

The initial CSF-A depth scale is based on the length that the drill string is advanced core by core. This is equivalent to the ODP scale meters below seafloor (mbsf). The CSF-A scale is inaccurate because of ship heave (which is not compensated for during APC coring), tidal variations in sea level, and other sources of error. Before a splice can be constructed, the cores from the various holes must be stratigraphically correlated with each other. Such correlation transfers CSF-A depths into a composite depth scale referred to as core composite depth below seafloor (CCSF-A). The splice that results is known as core composite depth below seafloor method D (CCSF-D). Differences between these depth scales occur because features may be slightly offset between holes on the CCSF-A scale and the splice on the CCSF-D scale. These IODP depth scales are approximately equivalent to the ODP depth scale meters composite depth (mcd) and are further described below.

The CCSF-A scale is built by assuming that the uppermost sediment (commonly referred to as the "mudline") in the first core from one hole is the sediment/water interface. At each site, this selected core becomes the "anchor" in the composite depth scale and is usually the only one in which depths are the same on both the CSF-A and CCSF-A scales. From this anchor, core logging data are correlated among holes downsection. For each core, a (constant) depth offset, or affine value, chosen to best align observed lithologic variations to the equivalent cores in adjacent holes, is added to the CSF-A depth in sequence down the holes. It is not usually possible to align all features perfectly between holes, so where possible the affine values are chosen to maximize correlations at the levels that splice tie points are defined between holes.

During Expedition 341, an initial composite depth scale was created using magnetic susceptibility measured with a loop sensor and GRA data from the STMSL. The final CCSF-A scale and the splice for each site used additional data from, for example, the WRMSL, which measures GRA density (a function of grain density and porosity) and *P*-wave velocity (on the *P*-wave logger [PWL]). GRA and magnetic susceptibility data from the WRMSL generally replaced the STMSL data for correlation purposes; however, the STMSL data are retained in the database as a useful check on the final data and because some damaged sections fit through the STMSL but could not be run on the WRMSL. In some cases, small depth offsets were found for features within core sections measured by the STMSL and WRMSL; a common cause of this offset is gas expansion in the cores between the STMSL and WRMSL analyses. In these cases, attempts were made to define composite depths using the last data measured prior to core splitting. This was not always possible, however; some depth mismatches (typically on the scale of centimeters, but perhaps tens of centimeters) may exist between composite depths defined by whole-round sensing and the depths at which particular features appear in split cores.

Correlations based primarily on whole-round GRA and magnetic susceptibility data were augmented where needed by natural gamma radiation (NGR) data from the core logger and digital color parameters (L*a*b*) and magnetic susceptibility data obtained with a point sensor (MS-POINT) measured on the SHMSL. High-resolution color digital images analyzed on the SHIL, which provides color digital images, were incorporated into the correlation process using the Corelyzer software. Specific methods for WRMSL and SHMSL measurements are described in **"Physical properties,"** and SHIL measurements are described in **"Lithostratigraphy."** Most core logging data were collected at 2.5, 5, or 10 cm intervals, depending on time availability and core flow; SHIL data were pixel based.

Composite depth scale construction

The core logging data were imported into the specialized shipboard software program Correlator (version 1.695; Mac) and linked to digital core images with the program Corelyzer (version 2.0.2; Mac). Correlator enables construction of a composite depth scale for each hole at a given site by depth-shifting individual cores to maximize the correlation of reproducible features in the core logging data. For hole-to-hole correlations and for plotting results, data were masked to avoid incorporating anomalous data influenced by edge effects at section boundaries, at core tops, or in voids where no sediment was present; however, all original data were retained in the LIMS database.

Depth intervals within cores are not squeezed or stretched by Correlator; thus, it is not possible to align all the correlative features within each core. Differences between features in different holes may reflect small-scale differences in sedimentation and/or distortion caused by the coring and archiving processes. For example, the tops of APC cores may be stretched and the bottoms compressed, although this depends on lithology and the extent of lithification. In addition, sediment of unknown age occa-

sionally falls from higher levels in the borehole onto the tops of cores as they are recovered, and as a result the tops of some cores are not reliable.

Correlations among cores from adjacent holes are evaluated visually and statistically (by windowed cross-correlation). The depth offsets for each core that are necessary to convert CSF-A depths to the CCSF-A scale are recorded in an affine table for each site. The CCSF-A depth for any point within a core equals the CSF-A depth plus the affine offset. Correlation at finer resolution is not possible with Correlator because depth adjustments are applied linearly to individual cores. At this stage, no adjustments are made in the length of each core, such as numerically squeezing and stretching within cores. Finer scale adjustments of individual cores relative to the splice (e.g., Hagelberg et al., 1995; Pälike et al., 2005) or relative to logging data (e.g., Harris et al., 1995) can be done following the development of the composite section.

Ideally, the base of the continuous CCSF-A scale is the bottom of the deepest core recovered from the deepest hole. In practice, however, the base often occurs where core recovery gaps align across all holes and below which constructing a splice is impossible. Deeper cores cannot be tied directly into the overlying continuous CCSF-A scale. These cores are appended, and CCSF-A depths are calculated by adding a constant offset, which is usually the largest affine value from each hole. An exception to this case occurs when some cores from two or more holes deeper than the base of the splice can be correlated with each other, allowing the generation of a "floating" CCSF-A scale and splice for some intervals deeper than the continuous CCSF-A scale.

Corrected composite depth scale

The length of the CCSF-A depth scale at a given site is typically ~10%–20% greater than the length of the cored interval in any one hole as indicated by the CSF-A depth scale. Although the exact reasons for this apparent expansion of the sediment column are not completely known, it is commonly attributed to rebound following release of overburden in the deeper sections, stretching during the coring process, gas expansion during the core recovery process, and other factors (Moran, 1997).

Core composite depth below seafloor (CCSF-B) is a depth scale that is intended to correct the CCSF-A scale or the splice (CCSF-D) for empirically observed expansion. CCSF-B depths are produced by correcting CCSF-A or CCSF-D depths for the average affine growth value of the CCSF-A scale relative to the CSF-A scale over a sufficiently long interval that random variations in drill pipe advance due to ship heave, tides, and other factors are negligible. This scaling produces a complete composite stratigraphic sequence that is the same length as the total cored or drilled interval. The CCSF-B scale is a close approximation of actual drilling depths and is essential for comparison of core logging and downhole logging data and for estimation of sediment accumulation rates and mass fluxes. Because the CCSF-B scale provides an estimate of the sediment thickness before the sediment was removed from the borehole, the intervals measured between actual samples taken within each core section are better represented in the CCSF-A or CCSF-D (uncompressed) depth scales.

Splice

The splice is a composite stratigraphic section representing the complete record at a site. It is composed of core sections from adjacent holes such that coring gaps or sampling gaps, like those generated by taking of IW samples, in one hole are filled with core from an adjacent hole. The splice does not generally contain coring gaps, and an effort has been made to minimize inclusion of disturbed sections by examining core photographs. The splice guides core sampling for high-resolution studies. Tables and figures in each site chapter summarize the intervals from each hole used to construct the splice. The portion of the CCSF-A depth scale that is applied to the splice is referred to as the CCSF-D depth scale. Within the splice sections, CCSF-D is identical to CCSF-A.

Note, however, that because of stretching and squeezing within cores, some features may not correlate precisely between the splice and samples taken off the splice, even though all samples have CCSF-A depths. Therefore, the final composite depth scale, CCSF-D, is only formally defined within the primary splice.

The choice of splice tie points is a somewhat subjective exercise. Our method in the construction of a splice followed four rules. First, where possible, we avoided using the first and last sections of cores, where disturbance due to drilling artifacts (even if not apparent in core logging data) was most likely. Second, we attempted to incorporate those realizations of the stratigraphic section that in our judgment were most representative of the holes recovered. Third, we tried to minimize tie points (i.e., to use the longest possible sections within individual cores) in order to simplify sampling. Fourth, we tried to minimize use of intervals sampled during the ex-

pedition to leave room for high-resolution postexpedition sampling in the splice.

Tidal effects on coring depth

Tidal influence on APC shot depth was previously documented by correlation of affine offset changes and tide height during ODP Leg 202 (Mix, Tiedemann, Blum, et al., 2003). During Expedition 341, we calculated tide corrections at 30 min intervals for all APC drill sites based on the Oregon State University Tidal Prediction Software (OTPS; copyright Oregon State University 2012, G. Egbert and L. Erofeeva, used by permission). Predicted tidal variations on Expedition 341 were up to 4 m over a diurnal and semidiurnal cycle, so proper tide corrections were needed to obtain complete composite sections and splices. The first APC core at each site established the reference depth for tidal corrections, and all following cores were adjusted for the offset of the predicted tide at the time of coring relative to the initial reference depth. During each coring operation, the drill string was advanced either less than the previous core's recovery (for a falling tide) or greater than the previous core's recovery (for a rising tide) to make this correction. The tide corrections used for Sites U1417–U1419 are illustrated in Figure **F18.**

Age models and sedimentation rates

The composite depth models (in CCSF-B depths where available) were applied to datums of known ages (see **"Paleontology and biostratigraphy"** and **"Paleomagnetism"**). Stratigraphic datums from multiple holes were merged to estimate the most representative depths and uncertainties in both depth and age of unique events at each site. We then developed minimum and maximum depth models, based on visual linear fits between equally spaced age increments that spanned the reasonable uncertainty range of the well-constrained datums, after rejecting obvious outliers. We considered these minimum and maximum models to represent the ±2σ uncertainties in the age:depth relationship.

Given these models, we estimated sediment accumulation rates between age increments based on 500 Monte Carlo simulations in which Gaussian white noise of appropriate range was applied to the depth at each age level. The resulting 500 realizations of sedimentation rate estimates were used to calculate the central tendency (fiftieth percentile) and uncertainties spanning 68.2% probability (i.e., ±1σ). Note that these sedimentation rates are effectively averages and uncertainties over the selected age increments; they are not intended to represent instantaneous sedimentation rates. Uncertainties in sedimentation rate generally rose as narrower time increments were selected. Through an iterative process, the size of age increments at each site was selected such that variations in sedimentation rate were greater than their uncertainties.

Geochemistry

Geochemical methods were used to quantify volatile gases and concentrations of chemical elements and ions in IW and in sediment samples (both IW squeeze cakes and discrete samples from the working halves). The applied methods followed recommendations published by Manheim and Sayles (1974), Gieskes et al. (1991), and Murray et al. (2000), as detailed below. Additional IW and sediment subsamples were taken for shore-based research. Headspace and IW sampling resolutions are detailed in the "Geochemistry" sections of the respective site chapters.

Hydrocarbon sampling and analyses

Sediment plugs were taken with a stainless steel sample coring tool from the cut section tops directly adjacent to the deepest IW whole-round samples immediately after the core was cut on the catwalk. When the sediment became too lithified to extract using the sample coring tool, fragments of the core were chiseled out. About 5 cm^3 of sediment was put into a 20 cm^3 serum glass vial that was immediately sealed with a septum and metal crimp on the catwalk. The sample was then heated at 70°C for 30 min, and a 5 cm^3 headspace gas aliquot was removed from the vial with a glass syringe and injected into the gas chromatograph.

Headspace gas samples were analyzed using a Hewlett Packard 6890 gas chromatograph (GC) equipped with a 2.4 m × 3.2 mm stainless steel column packed with 100/120 mesh HayeSep R and a flame ionization detector. This instrument measures the concentrations of methane (C_1), ethane (C_2), ethene ($C_{2=}$), propane (C_3), and propene ($C_{3=}$). The glass syringe was directly connected to the GC with a 1 cm^3 sample loop. The carrier gas was helium. The GC oven temperature was programmed to ramp at 30°C/min from 90° to 100°C and at 15°C/min from 100° to 110°C, to remain at 110°C for 4.5 min, and then to ramp at 50°C/min to 150°C with a final holding time of 1.8 min. Data were collected and evaluated with an Agilent Chemstation data-handling program. Chromatographic response was calibrated against preanalyzed standards. The coefficients of variation for gas standards run after every 10 samples were 1%–5% and 1%–4% for methane and ethane, respectively.

Interstitial water sampling and chemistry

IW was extracted from 5 to 15 cm whole-round sediment samples, depending on the degree of induration—and hence expected IW content—of the sediment. Usually, IW whole-round samples were taken in the following depth resolution: at the base of Sections 2, 4, and 6 in Cores 1–3 (given full stroke; modified depending on mudline depth in Core 1); at the base of Sections 3 and 5 in Cores 4–6; and at the base of Section 3 from Core 7 downhole. In case of half APC system application, IW samples were taken at the base of Section 2. Before IW extraction, the whole-round samples were removed from the core liner using a plastic stamp and the outer surfaces were scraped with a clean steel spatula to minimize potential contamination by the coring process. Whole rounds were placed into a titanium and steel squeezing device and squeezed at ambient temperature with a hydraulic press at pressures from 5,000 to 30,000 psi, using modified versions of the standard ODP stainless steel squeezer of Manheim and Sayles (1974). IW samples were collected in 50 mL plastic syringes and filtered through 0.45 µm Whatman polyethersulfone disposable filters. Aliquots of IW samples were stored in several vials for shipboard and shore-based analyses (Table T2).

In addition to conventional IW squeezing, IW was also extracted in higher depth resolution (~50–100 cm) using rhizon samplers from APC Cores 1–5 at Sites U1417–U1419. These polymer-coated sticks (0.1 µm pore size) were inserted into the sediment through holes drilled into the core liners along the splitting line after the cores had passed through the WRMSL. Applying 12 mL plastic syringes with stoppers created a vacuum that extracted IW from the sediment.

The International Association of Physical Sciences Organizations (IAPSO) seawater standard was used for standardization of alkalinity and chloride concentrations for all measurements made on the ion chromatograph (IC) and for all inductively coupled plasma–atomic emission spectroscopy (ICP-AES) measurements (IAPSO composition in Gieskes et al., 1991). Sodium sulfide, ammonium chloride, potassium phosphate monobasic, and calcium carbonate were used to prepare calibration solutions and internal standards for ammonium and phosphate concentration measurements.

IW analyses followed the procedures outlined by Gieskes et al. (1991), Murray et al. (2000), and the user manuals for new shipboard instrumentation (www.iodp-usio.org/Tools_Labs/). IW was routinely analyzed for salinity with an Index Instruments digital refractometer. Alkalinity/pH and chloride concentrations were measured immediately after IW extraction by titration with 0.1 N HCl and 0.1 N $AgNO_3$ solutions, respectively, using Metrohm autotitrators.

Dissolved ammonium and phosphate were determined spectrophotometrically (Agilent Cary 100 double-beam UV/Vis spectrophotometer). Sulfate, chloride, calcium, sodium, magnesium, and potassium ion concentrations were determined with a Metrohm 850 Professional IC on 1:100 diluted aliquots in 18 MΩ water.

Minor elements (B, Ba, Fe, Li, Mn, Si, and Sr) were analyzed with a Teledyne Prodigy high-dispersion ICP-AES. Standards (IAPSO) and samples were diluted 1:20 with a 2% v/v HNO_3 solution in deionized water, containing 10 ppm yttrium (Y) as an internal standard. Wavelengths were selected according to the recommendations for shipboard analysis of Murray et al. (2000). Drift correction was automatically applied by the instrument software.

The coefficient of variation of the IAPSO standard (run after every tenth sample) on the IC was 3%–5% for all anions and cations, and the average ion concentrations measured throughout the expedition were within 1.5% (2.5% for K) of the standard values given by Gieskes et al. (1991). The coefficients of variation for ammonium and phosphate based on internal standards run after every tenth sample were 5% and 2%, respectively.

For ICP-AES analysis, quantification limits for the different elements/wavelengths (five times the absolute standard deviation of the calibration blank), as well as their relative standard deviations (calculated from triplicate measurements for samples with respective element concentrations above quantification limit), are given in Table T3. Relative standard deviations for multiple analyses of the IAPSO standard throughout the expedition were <5% for Sr, <6% for B, and <10% for Li and Si. For the elements Ba, Fe, and Mn, concentrations of the IAPSO standard were below quantification limit.

In case of limited IW recovery from sandy and/or lithified samples, the following list of analytical and sampling priorities was followed: ICP-AES, IC, ammonium/phosphate (spectrophotometric), chloride titration, alkalinity/pH titration, shipboard scientist IW splits, and shore-based scientist IW splits. This priority list, as well as the respective amounts and pretreatments of IW splits, are listed in Table T2.

Bulk sediment geochemistry

Total inorganic carbon (TIC) contents (wt%) were determined using a UIC 5015 CO_2 coulometer. Around 10 mg of freeze-dried ground sediment taken from IW squeeze cakes and discrete samples (collected by

lected by shipboard sedimentologists) were reacted with 1 M HCl. The liberated CO_2 was backtitrated to a colorimetric end point. Calcium carbonate content was calculated from the TIC content with the assumption that all TIC is present as calcium carbonate ($CaCO_3$):

$$\text{wt\% } CaCO_3 = \text{wt\% TIC} \times 8.33.$$

The coefficient of variation was ~1%.

Total carbon (TC) and total nitrogen (TN) contents were determined on aliquots of the freeze-dried ground samples using a Thermo Electron Flash Elemental Analyzer 1112 equipped with a Thermo Electron packed column CHNS/NCS (polytetrafluoroethylene; length = 2 m; diameter = 6 × 5) and thermal conductivity detector. Aliquots of ~10 mg of freeze-dried ground sediment were weighed into tin cups and combusted at 900°C in an oxygen stream. Nitrogen oxides were reduced to N_2, and the mixture of N_2, CO_2, and H_2O gases was separated by GC, with detection performed by thermal conductivity detector. The GC oven temperature was set at 65°C. Notably, this column needed to be replaced after every 100 analyses to avoid a gradual increase of TN content due to saturation of the N_2 column. All measurements were calibrated by comparison to the standard, ThermoFisher Scientific Soil Reference Material NC (TN = 0.21 wt%; TC = 2.29 wt%), and average TN and TC contents throughout the expedition were within 0.4% of these standard values. Repeated measurements of this standard gave coefficients of variation of 7.6% and up to 19% for TC and TN, respectively. Contents of total organic carbon (TOC) (wt%) were calculated as the difference between TC and TIC:

$$\text{wt\% TOC} = \text{wt\% TC} - \text{wt\% TIC}.$$

Physical properties

Shipboard measurements of the physical properties of all the cores recovered were undertaken to rapidly characterize lithologic units, providing information on hole-to-hole and site-to-site stratigraphic relationships and guiding drilling efforts to recover complete stratigraphic sequences at each site. The primary objectives for physical properties measurements during Expedition 341 include the following:

1. Performing real-time assessment of sediment recovery at each site to guide drilling (see **"Stratigraphic correlation"**),
2. Correlating lithostratigraphy to downhole geophysical logging data,
3. Facilitating the construction of synthetic seismograms and integration with seismic data,
4. Providing porosity information to assist in understanding sediment consolidation and deformation behavior,
5. Identifying the physical parameters responsible for facies changes,
6. Developing and verifying a glacial sequence stratigraphic framework, and
7. Establishing the composite depth scale, the splice record, and initial age models at each site (see **"Stratigraphic correlation"**).

Physical properties were first measured on whole-round core sections. A typical core is cut into sections of no more than 1.5 m, yielding as many as six full-length core sections and a shorter seventh section in the case of maximum core recovery. Two data logging systems were run on each whole-round core section: (1) the STMSL, which measured sections immediately after they were brought onboard, and (2) the WRMSL, which was used to measure core sections that had warmed to ambient laboratory temperature (at least 4 h) for Sites U1417 and U1418. During operations at Site U1419, core expansion due to gassy sediments was determined to be a greater source of error than temperature, and thus the warming to ambient temperature procedure was abandoned. Following this, for Sites U1420 and U1421 we ran the cores at some point after warming to the point at which condensation ceased to form on the PVC liner. The linear track of the STMSL includes a GRA bulk densitometer and a magnetic susceptibility loop. The WRMSL also includes both those instruments, as well as a compressional *P*-wave velocity sensor.

After WRMSL scanning, the whole-round sections were measured for NGR. Core sections were then split along their length into archive and working halves. The archive half was run through a third data logging system, the SHMSL, for measurement of reflectance spectroscopy and colorimetry, magnetic susceptibility, and laser split-core surface analysis.

Discrete samples of 10 cm^3 were collected from the working halves (~1/section) to measure wet bulk density, dry bulk density, water content, porosity, and grain density according to IODP moisture and density (MAD) procedures. Point measurements of *P*-wave velocity were collected on the working halves using the PWC (~2–3/core). Shear strength tests using the automated vane system were also conducted on the working halves (~2–3/core). A full discussion of all methodologies and calculations used in the *JOIDES Resolution* physical properties laboratory can be found in Blum (1997).

Special Task Multisensor Logger

STMSL measurements were used to acquire GRA bulk density and magnetic susceptibility data at a lower spatial resolution than on the WRMSL to rapidly correlate the different holes at each site in order to guide the drilling operations and ensure complete sediment recovery. The GRA bulk densitometer and magnetic susceptibility loop on the STMSL are similar to those on the WRMSL (see **"Whole-Round Multisensor Logger"**), although the warming of the core over the course of measurement produces drift of up to ~5 instrument units (IU) in magnetic susceptibility measurements. The along-section spacing distance between STMSL measurements varied between 2.5 and 5.0 cm, depending on the time available to process each new core through the shipboard laboratories.

Whole-Round Multisensor Logger

After collection of STMSL data, most cores were allowed to sit in the laboratory for as long as 4 h to equilibrate with room temperature, with the exception of cores expanding because of high methane content. These cores were logged as quickly as possible to minimize vertical physical core disturbance prior to splitting. Whole-round sections were then measured at high resolution on the WRMSL. These data, including GRA bulk density, magnetic susceptibility, and *P*-wave velocity, advance the primary scientific objectives of the expedition by providing information on lithostratigraphic variability associated with changes in regional tectonics, glacial activity, and ocean productivity. However, this information is also critical in establishing shipboard core-to-core correlation between drill holes and for the construction of the composite depth and splice stratigraphic sequences. To optimize WRMSL performance, all sensors were set to a consistent sampling interval of 2.5 cm. Measurement times were 5 s for the GRA bulk densitometer, 3 s for the magnetic susceptibility loop (the average of 3 measurements of 1 s), and 5 s for *P*-wave velocity. With handling, data initializing, and track movement, a 1.5 m section took ~10 min to scan. A 9.5 m core thus took ~1 h to pass through the WRMSL. *P*-wave velocity measurements were not collected for XCB or RCB acquired cores because of errors generated by an incompletely filled core liner.

Gamma ray attenuation bulk density

Bulk density is a reflection of water-saturated porosity, grain size, grain density (mineralogy), grain packing, and coring disturbance. To measure bulk density, the GRA densitometer uses a 10 mCi ^{137}Cs capsule as a gamma ray source (with the principal energy peak at 0.662 MeV) and a scintillation detector. The narrow collimated peak is attenuated as it passes through the center of the core. Incident photons are scattered by the electrons of the sediment by Compton scattering.

The attenuation of the incident intensity (I_0) is directly related to the electron density in the sediment core of diameter (D) that can be related to bulk density given the average attenuation coefficient (in micrometers) of the sediment (Evans, 1965; Harms and Choquette, 1965). Because the attenuation coefficient is similar for most common minerals and aluminum, bulk density is obtained through direct calibration of the densitometer using aluminum rods of different diameters mounted in a core liner filled with distilled water. Between holes, calibrations are performed from an aluminum plug with four different thickness steps of 2, 3, 4, and 5 cm mounted in a core liner filled with distilled water. In addition to this standard allowing for detection of instrument drift between holes and sites, the measurements provide a calibration curve to empirically relate the counts to density. As the instrument is volumetrically calibrated assuming the full interior diameter of the core liner is filled with sediment, any reduction in core diameter (such as can occur from XCB/RCB coring and/or clast-rich lithologies) will bias the results toward lower values (see VOLNORM in **"Supplementary material"**). In such cases of incomplete recovery, GRA bulk densities must be regarded as a minimum estimate.

Magnetic susceptibility

Magnetic susceptibility is a measure of the degree to which a material can be magnetized by an external magnetic field. It provides information on the magnetic composition of the sediments, which can often be related to mineralogical composition (e.g., terrigenous versus biogenic materials) and diagenetic overprinting. Magnetite and a few other iron oxides with ferrimagnetic characteristics have a specific magnetic susceptibility several orders of magnitude higher than clay, which has paramagnetic properties. Diamagnetic minerals (carbonate and silica) and plastics (core liner) have small negative values of magnetic susceptibility (e.g., Thompson and Oldfield, 1986). Sediments rich in biogenic carbonate and/or opal therefore have generally low to negative magnetic susceptibility values (e.g., Tauxe, 2010).

Magnetic susceptibility was measured using the noncontact pass-through "loop" sensor on the STMSL and WRMSL, with loop diameters of 90 and 80 mm, respectively. Because of its larger loop diameter, the initial data from the STMSL is of lower amplitude than the corresponding data from the WRMSL, although the half-height width of both response

curves is ~4.5 cm (Fig. F19). To compensate for the reduction in response function amplitude, all raw STMSL magnetic susceptibility measurements are multiplied by an instrument unit correction factor of 1.46, derived from the measured ratio of a series of six homogenized "standards" made shipboard from varying concentrations of sepiolite drilling mud and powdered iron (Fig. F20A). These standards ranged from ~10 to ~2500 IU on the WRMSL magnetic susceptibility loop, fully encompassing the range of values observed during the expedition.

The output of the magnetic susceptibility loop sensors can be set to centimeter-gram-second (cgs) units or SI units, which are the standard units used by IODP. However, to actually obtain dimensionless SI units (i.e., volume-specific low-field magnetic susceptibility), the instrument units stored in the IODP database must be multiplied by a correction factor to compensate for instrument scaling and the geometric ratio. Identifying this correction factor requires standards of known magnetic susceptibility, which were not available on the ship. Consequently, all magnetic susceptibility values from the loops reported here are in instrument units and have not been corrected to dimensionless SI units.

On the SHMSL, magnetic susceptibility was measured via "point" sensor at 2.5 cm intervals for the majority of core sections. In some intervals where a specific lithology of interest was identified, the sampling interval was decreased to as low as 1 cm. The point sensor requires flush contact with the split core, and results are negatively biased by rough surfaces associated with clast-rich lithologies and gassy sediments. A laser surface analyzer aids in the recognition of irregularities in the split core surface (e.g., cracks and voids), and data from this tool were recorded to provide an independent check on the fidelity of SHMSL measurements. STMSL MS-POINT data are reported in SI units. When downloading the depth data from LIMS, note that for some intervals there is an 0.5 cm offset between uploaded data and measured sample point data.

We evaluated the sensitivity of the SHMSL point sensor to the STMSL and WRMSL loop magnetic susceptibility measurements via the same six homogenized standards used to evaluate the relationship between the WRMSL and STMSL loop magnetic susceptibility (Fig. F20B). The relationship between the WRMSL and the STMSL magnetic susceptibility data is potentially nonlinear and should be interpreted with caution.

P-wave logger

Compressional wave (*P*-wave) velocity is dependent upon the incompressibility (bulk modulus) and rigidity (shear modulus) of a material. These two moduli vary with a material's lithology, porosity, cementation, bulk density, state of stress, temperature, and fabric or degree of fracturing. In marine sediments, velocity is additionally controlled by the occurrence and abundance of free gas and gas hydrate. Microscopic and macroscopic fracturing, as well as the presence of gas in the sediments, may attenuate the signal to the point where it is not possible to obtain data. Together with bulk density, velocity data are used to calculate acoustic impedance and reflection coefficients that can be used to construct synthetic seismograms and estimate the depths of seismic horizons.

P-wave velocities were measured on whole-round sections with the PWL on the WRMSL for cores that were acquired using the APC system. The PWL transmits a 500 kHz *P*-wave pulse through the core section at a specified repetition rate of 2/s. This signal is coupled to the sample by the plastic pole pieces of the transducers and by the pressure applied by the linear actuator. For the PWL, in contrast to the PWC, no water is used to improve coupling between the transducers and the liner because the pressure applied by the actuator is known to be sufficient for reliable *P*-wave measurements. The transmitting and receiving ultrasonic transducers are aligned so that wave propagation is perpendicular to the section's long axis.

A linear voltage differential transformer is used to measure the separation of the transducer to derive a travel path length for the signal (i.e., the slightly compressed core diameter). The ultrasonic *P*-wave velocity is then calculated after corrections have been made for system propagation delay, liner thickness, and liner material velocity. Calibrations were performed before each hole on the PWL using an acrylic cylinder milled to four calibration sections of 69.7, 64.8, 59.75, and 54.75 mm in diameter.

Natural Gamma Radiation Logger

NGR measurements provide insights into sediment composition and thus can be used to identify lithology. The NGRL measures gamma rays emitted from whole-round core sections arising primarily from the decay of long-period isotopes uranium (^{238}U), thorium (^{232}Th), and potassium (^{40}K). Typically, high counts identify fine-grained deposits containing K-rich clay minerals and their adsorbed U and Th atoms. NGR data can also help to correlate the core material recovered with the downhole logs for core-log integration.

The design and basic operation of the NGR detector unit is described in Vasiliev et al. (2011). The instrument contains eight sodium iodide detectors spaced

~20 cm apart. A measurement run consists of counting two positions on each core section for a total of 16 measurements per 150 cm section, yielding a depth resolution of 10 cm. Total detector counts are routinely summed for the range of 100–3000 keV. An energy calibration for each detector was routinely performed using ^{137}Cs and ^{60}Co sources to identify peaks at 662 and 1330 keV, respectively. Background measurements were done on an empty core liner for ~20,000 s (>5 h) on approach to each site or group of sites to minimize local cosmic-ray flux contributions to the statistical error.

The quality of the energy spectrum measured in a core depends on the concentration of radionuclides in the sample but also on the counting time, with longer measurement times yielding increasingly resolved spectra. We set the instrument to count for at least 5 min in both run positions, which should equate to a measurement error of <2.5% (Vasiliev et al., 2011). Readings at the ends of core sections are automatically corrected by the NGRL software using empirically derived correction factors (Vasiliev et al., 2011).

During Expedition 341 we used two of the available edge correction files for the NGRL software, both of which consist of a lookup table at 1 cm resolution. Correction coefficients decrease along a half-Gaussian curve as the section length within the measurement window increases; in the case of less than half the detector window seeing sediment, the measurement is discarded and the edge correction is applied to the next sensor in. The appropriate correction coefficient is determined by the distance between the section end and the center of the most proximal detector; for file "ngr_edge_correction_table_0.txt," in the case of a 0 cm offset between the outermost detectors and the edge of the core, the end detector counts are simply multiplied by 2 (see Vasiliev et al., 2011). For file "ngr_edge_correction_table_1.txt," the lookup table of the 0 offset file is shifted 1 cm, such that the former correction for a 1 cm offset becomes the correction factor for a 0 cm offset (Fig. **F21**). During Expedition 341, we applied edge correction file "ngr_edge_correction_table_1.txt" through the end of Site U1418. To use this edge correction, sections were loaded ~1 cm back from the leading edge of the boat to avoid overcorrection of the uppermost measurement. However, the loading position was inconsistent between operators, so we switched to loading sections flush with the leading edge of the boat coupled with edge-correction file "ngr_edge_correction_table_0.txt" prior to occupation of Site U1419.

To determine the position of the core for the lower edge correction, the NGR detector software requires that core lengths are manually entered. The measuring tape along the sample loading boat used to determine this length was moved relative to the leading edge of the core at several times prior to occupation of Site U1419; after this was discovered, the tape was zeroed relative to the leading edge of the boat, where it remained for the rest of the expedition. Lower edge corrections with the 0 cm offset file were variably high; to minimize this effect we systematically removed 1 cm from the actual section length for the application of the edge correction, rounding to the nearest centimeter. Although this in practice reduced notable errors in the edge correction, its necessity suggests that the sodium iodide detectors are not all positioned where the software believes they should be. Preliminary evaluation with a ^{137}Cs point source suggests variable along-section offsets in both the positive and negative direction. Although these position errors are likely quite small, an offset of 1 cm equates to an error of >10% near the center of the detector, and this may be a contributing factor to the inconsistency of the edge corrections.

Moisture and density

After whole-round cores were split into working and archive halves, the working halves were placed on the sampling table for collection of discrete samples to determine wet and dry bulk density, grain density, water content, and porosity. In soft sediment, ~10 cm^3 samples were collected with a plastic syringe. Samples were taken no more than once per core section and no less than three per core. Samples were placed in numbered, preweighed 16 mL Wheaton glass vials with a diameter matching that of the syringe for wet and dry sediment weighing, drying, and wet and dry volume measurements. The weights of wet and dry sample masses were determined to a precision of 0.005 g using two Mettler Toledo electronic balances and a computer averaging system to compensate for the ship's motion.

Dry sample volume was determined using a hexapycnometer system of a six-celled, custom-configured Micromeritics AccuPyc 1330TC helium-displacement pycnometer. The precision of each cell is 1% of the full-scale volume. Volume measurement was preceded by three purges of the sample chamber with helium warmed to ~28°C. Three measurement cycles were run for each sample. Periodically, a solid metallic reference volume was placed sequentially in one of the chambers to check for instrument drift and systematic error. The volumes of the numbered Wheaton vials were calculated before the expedition by multiplying each vial's weight against the average density of the vial glass. Dry mass and volume were measured after samples were heated in an oven at

105° ± 5°C for 24 h and allowed to cool in a desiccator for 15–20 min. The procedures for the determination of these physical properties comply with the American Society for Testing and Materials designation 2216 (ASTM International, 1990). The fundamental relation and assumptions for the calculations of all physical property parameters are discussed by Blum (1997) and summarized below in **"Mass and volume calculation"** and **"Calculation of bulk properties."**

Mass and volume calculation

Wet mass (M_{wet}), dry mass (M_{dry}), and dry volume (V_{dry}) were measured in the laboratory. The ratio of mass (rm) is a computational constant of 0.965 (i.e., 0.965 g of freshwater per 1 g of seawater). Salt precipitated in sediment pores during the drying process is included in the M_{dry} and V_{dry} values. The mass of the evaporated water (M_{water}) and salt (M_{salt}) in the sample are given by

$$M_{water} = M_{wet} - M_{dry}$$

and

$$M_{salt} = M_{water}\,[s/(1 - s)],$$

respectively, where s is the assumed saltwater salinity (0.035%) corresponding to a pore water density (ρ_{pw}) of 1.024 g/cm^3 and a salt density (ρ_{salt}) of 2.22 g/cm^3. The corrected mass of pore water (M_{pw}), volume of pore water (V_{pw}), mass of solids excluding salt (M_{solid}), volume of salt (V_{salt}), volume of solids excluding salt (V_{solid}), and wet volume (V_{wet}) are, respectively,

$$M_{pw} = (M_{wet} - M_{dry})/\mathrm{rm},$$

$$V_{pw} = M_{pw}/\rho_{pw},$$

$$M_{solid} = M_{wet} - M_{pw},$$

$$M_{salt} = M_{pw} - (M_{wet} - M_{dry}),$$

$$V_{salt} = M_{salt}/\rho_{salt},$$

$$V_{wet} = V_{dry} - V_{salt} + V_{pw},$$

and

$$V_{solid} = V_{wet} - V_{pw}.$$

Calculation of bulk properties

For all sediment samples, water content (w) is expressed as the ratio of mass of pore water to wet sediment (total) mass: $w = M_{pw}/M_{wet}$. Wet bulk density (ρ_{wet}), dry bulk density (ρ_{dry}), sediment grain density (ρ_{solid}), porosity (ϕ), and void ratio (VR) are calculated as follows:

$$\rho_{wet} = M_{wet}/V_{wet},$$

$$\rho_{dry} = M_{solid}/V_{wet},$$

$$\rho_{solid} = M_{solid}/V_{solid},$$

$$\phi = V_{pw}/V_{wet},$$

and

$$VR = V_{pw}/V_{solid}.$$

MAD properties reported and plotted in the "Physical properties" sections of all site chapters were calculated with shipboard-prepared Excel spreadsheets.

Section Half Measurement Gantry

Caliper *P*-wave velocity

For a description of the controls of *P*-wave velocity in marine sediments see ***"P*-wave logger."**

We used the PWC to vertically measure *P*-wave velocity across the working half of split cores (*x*-axis), regardless of drilling method. These measurements were taken no more than once per section and no less than three times per full core. Additional PWC measurements were taken in heterogeneous sections (e.g., significant lonestone content). As with the PWL, the PWC transmits a 500 kHz *P*-wave pulse through the core section at a specified repetition rate of 2/s, coupled to the sample by the plastic pole pieces of the transducers and by the pressure applied by the linear actuator. Water is used to improve coupling between the transducers and the liner/sediment surface. The transmitting and receiving ultrasonic transducers are aligned so that wave propagation is perpendicular to the section's long axis.

Traveltime is determined by signal processing software that automatically detects the first arrival of the *P*-wave signal to a precision of 50 ms. It is challenging for an automated routine to pick the first arrival of a potentially weak signal with significant background noise. The search method skips the first positive amplitude and finds the second positive amplitude using a detection threshold limit, typically set to 30% of the maximum amplitude of the signal. It then finds the preceding zero crossing and subtracts one period to determine the first arrival. To avoid extremely weak signals, minimum signal strength can be set (0.02 V) and weaker signals will be ignored. To avoid cross-talk signals from the receiver at the be-

ginning of the record, a delay (typically 0.01 ms) can be set to force the amplitude search to begin in the quiet interval preceding the first arrival. In addition, a trigger (4 V) to initiate the arrival search process and the number of waveforms to be stacked can also be set. We used stacks of five measurements for Sites U1417–U1419. For Sites U1420 and U1421, we increased the number of stacks to 15 in order to increase the signal-to-noise ratio when measuring velocities in the mostly diamict intervals. Even with the stacking parameters, the auto-picking feature failed when the signal-to-noise ratio was high or when the picking threshold was exceeded. In some of these cases, we were able to manually pick the first arrivals.

As with the PWL, a linear voltage differential transformer is used to measure the separation of the transducer to derive a travel path length for the signal (i.e., the slightly compressed core diameter). The ultrasonic *P*-wave velocity is then calculated after corrections have been made for system propagation delay, liner thickness, and liner material velocity. We calibrated the system every 3–4 h, depending on when we detected significant drift. Calibrations were performed on acrylic cylinders of varying lengths: 45, 39.9, 30.03, 20.02, and 15.07 mm.

Vane shear tests

Shear strength of a material describes the point at which a significant structural failure occurs in response to an applied shear stress. During Expedition 341, sediment shear strength was measured by vane shear in the laboratory, as it is suited for measuring the shear strength of very soft to stiff marine sediments. Vane tests are useful for determining the undrained shear strength of undisturbed clay- or silt-rich samples. These shear strength tests are not suitable for coarser grained sediments or sediment containing silt or sand laminations. The typical sampling rate was one measurement per core section until the sediment became too firm for vane insertion. Samples were generally taken in undisturbed fine-grained sediment.

The automated vane system test was conducted using the Giesa automated vane shear system. This system consists of a controller and a gantry for shear vane insertion. A four-bladed miniature vane (diameter = height = 12.7 mm) was pushed carefully into the sediment of the working halves until the top of the vane was level with the sediment surface. The vane was then rotated at a constant rate of 90°/min to determine the torque required to cause a cylindrical surface to be sheared by the vane. The measurement was continued until the plot curve showed a decrease. This destructive measurement was done with the rotation axis parallel to the bedding plane. The torque required to shear the sediment along the vertical and horizontal edges of the vane is a relatively direct measurement of shear strength. Undrained shear strength, s_u, is given as a function of pressure in SI units of pascals (kPa = N/m^2).

Diffuse spectral reflectance

Measurements of diffuse spectral reflectance were carried out using an Ocean Optics USB4000 spectrophotometer. This instrument measures the diffuse reflectance spectra of the split core from the ultraviolet to near-infrared range (380–900 nm) at 2 nm increments. Spectral data are also converted to the International Commission on Illumination L*a*b* color space, where L* ranges from black to white, a* from green to red, and b* from blue to yellow (e.g., St-Onge et al., 2007).

Accurate diffuse spectral reflectance measurements using the SHMSL requires flush contact between the instrument sensors and the split core. A built-in laser surface analyzer aids the recognition of irregularities in the split core surface (i.e., cracks and voids), and data from this tool were recorded in order to provide an independent check on the fidelity of SHMSL measurements and to filter the data in order to remove data irregularities caused by gaps or drilling disturbance.

Heat flow

The APCT-3 consists of electronic components, including battery packs, a data logger, and a platinum resistance-temperature device calibrated over a temperature range of 0°–30°C. Descriptions of the tool and data analysis principles can be found in Pribnow et al. (2000) and Graber et al. (2002) and references therein. The thermal time constant of the cutting shoe assembly where the APCT-3 is inserted is ~2–3 min. The only modification to normal APC procedures required to obtain temperature measurements is to hold the corer in place 5–10 min near the seafloor to record bottom water temperatures and to hold it for ~10 min in the hole after cutting the core. During this time, the APCT-3 logs temperature data on a microprocessor contained within the instrument as it approaches equilibrium with the in situ temperature of the sediments. The tool can be preprogrammed to record temperatures at a range of sampling rates. A sampling rate of 10 s was used during Expedition 341.

A typical temperature history recorded by the APCT-3 is shown in Figure **F22.** It consists of (a) a mudline temperature record lasting 5 min, followed by (b) a pulse of frictional heating when the piston is fired,

(c) a period of thermal decay that is monitored for ~10 min, (d) a frictional pulse upon removal of the corer, and (e) a second mudline temperature measurement for 5 min. The in situ temperature is determined by extrapolating from the thermal decay that follows the frictional pulse when the piston is fired. Details of this process and the associated uncertainties are discussed in the individual site chapters.

Paleomagnetism

Paleomagnetism studies aboard the *JOIDES Resolution* during Expedition 341 comprised routine measurements of the natural remanent magnetization (NRM) of archive-half sections before and after alternating field (AF) demagnetization. Remanence measurements and AF demagnetizations were performed using a long-core superconducting rock magnetometer (SRM) (2-G Enterprises model 760-R). This instrument is equipped with a direct-current superconducting quantum interference device (DC-SQUID) and has an inline AF demagnetizer capable of reaching peak fields of 80 mT. The spatial resolution measured by the width at half-height of the pickup coils response is <10 cm for all three axes, although they can in some circumstances sense a magnetization over a core length of 30 cm. The noise level of the cryogenic magnetometer is ~2×10^{-10} Am^2 or 2×10^{-5} A/m for a ~100 cm^3 split core sample. The practical noise level is, however, affected by the magnetization of the core liner (~2×10^{-5} A/m) and by the background magnetization of a clean measurement tray (<5×10^{-6} A/m). Using the software package SRM Section developed during IODP Expedition 321T, the tray was cleaned and measured as needed and the background magnetization subtracted from subsequent core measurements.

The remanent magnetization of archive halves of all core sections was measured unless precluded or made unreliable by drilling-related deformation. Measurements were made at intervals of 1, 2.5, or 5 cm with leader and trailer lengths of 15 cm. The measurement interval, number of demagnetization steps, and peak field used reflected the quality, the demagnetization characteristics of the recovered sediments, the severity of the drill string magnetic overprint, the desire to keep peak AFs low (usually 20 mT), and the need to maintain core flow through the laboratory. Higher AFs of up to 40 mT were occasionally used for sections recovered using the XCB and RCB systems. Using a track speed setting of 10 cm/s, one step of a three-axis AF demagnetization and subsequent section measurement at 2.5 cm intervals took ~5.5 min. For measurement at intervals of 2.5 cm without AF demagnetization, ~3 min was needed. If time allowed, a four-step demagnetization and measurement scheme with peak fields of 20 mT was deployed following NRM measurement. To speed up core flow, the 5 and 15 mT steps were often dropped. Low peak demagnetization fields ensure that archive halves remain useful for shore-based higher resolution U-channel or cube studies of magnetic remanence.

Measurements were undertaken using the standard IODP magnetic coordinate system (+x = vertical upward from the split surface of archive halves, +y = left-hand split surface when looking upcore, and +z = downcore). Data were stored using the standard IODP file format and manually checked for quality. Void depths and otherwise disturbed intervals were manually noted on the "cryomag log sheets" and later taken into account. Lonestones and other visible debris that might hinder paleomagnetic measurements were removed prior to SRM measurement (and replaced after) or accounted for when processing data.

During APC coring, full-length nonmagnetic, full-length steel, and half-length steel core barrels were used (see **"Coring and drilling operations"**). Orientation was attempted at one hole for each APC-cored site using the FlexIT orientation tool on selected APC cores beginning at Core 3H. This instrument uses three orthogonally mounted fluxgate magnetometers to record orientation with respect to magnetic north of the double lines scribed on the core liner. The tool also has three orthogonally mounted accelerometers that monitor the movement of the drill assembly and help determine when the most stable, and thus most useful, core orientation data are gathered. Declination, inclination, and temperature are recorded internally at regular intervals until the tool's memory capacity is filled. Tools were switched every 8–12 h or when necessary. The azimuthal reference line is the double orientation line on the core liner and remains on the working half after the core is split.

Where shipboard AF demagnetization appears to have isolated the characteristic remanent magnetization (ChRM), paleomagnetic inclinations, and/or declinations of the highest demagnetization step, typically 20 mT was used to make an initial designation of magnetic polarity zones. The Astronomically Tuned Neogene Timescale (ATNTS2012) (Hilgen et al., 2012) within the Geological Timescale 2012 (Gradstein et al., 2012) was used as a reference for the ages of correlative Cenozoic polarity chrons.

The magnetic susceptibility of whole-core sections was measured on two separate core logging systems. Whole-core sections were measured on the STMSL to rapidly acquire magnetic susceptibility data for stra-

tigraphic correlation (see **"Stratigraphic correlation"**). After whole cores were or were not warmed to room temperature, except for those in gassy sediments, measurements were made as part of the WRMSL (see **"Physical properties"**). Additionally, point-source magnetic susceptibility measurements were made on the archive halves of cores using the SHMSL. When time allowed, the partially demagnetized NRM intensities of selected core intervals were normalized by the WRMSL to assess the potential for deriving shore-based estimates of relative paleointensity of geomagnetic field.

Downhole logging

Downhole logs are measurements of physical, chemical, and structural properties of the formation surrounding a borehole that are made after completion of drilling. The data are rapidly collected, continuous with depth (at vertical sampling intervals ranging from 2.5 to 150 mm), and measured in situ. These equate to vertical resolutions that are intermediate between laboratory measurements on core samples and geophysical surveys. Downhole logs are thus useful in calibrating the interpretation of geophysical survey data and provide a necessary link for the integrated understanding of physical properties at a range of spatial scales.

Downhole logs can be interpreted in terms of the stratigraphy, lithology, mineralogy, and geochemical composition of the penetrated formation. They also provide information on the condition, shape, and size of the borehole and on possible deformation induced by drilling and/or formation stress. Where core recovery is incomplete or cored material is disturbed, log data may help to characterize the borehole section and fill in between sampled intervals. Where core recovery is good, log and core data complement one another and may be interpreted jointly.

Logging operations

During wireline logging operations, logs are recorded with a variety of logging tools combined into several tool strings, which are run down the hole after completion of drilling operations. Three primary tool strings were initially planned for Expedition 341 (Fig. **F23;** Table **T4**): the triple combo string (spectral and natural gamma ray, porosity, density, resistivity, and magnetic susceptibility), the Formation MicroScanner (FMS)-sonic string (spectral and natural gamma ray, sonic velocity, and resistivity images), and the Versatile Seismic Imager (VSI) string (vertical seismic profile [VSP] and gamma ray). A fourth tool string, the Magnetic Susceptibility Sonde (MSS) string (magnetic susceptibility and spectral and natural gamma ray) was also deployed at one site (U1417). These tool strings may be modified in response to expected borehole conditions or tool performance. In addition, because of concerns about borehole condition and time limitations near the end of the expedition, a modified tool string was designed for Sites U1420 and U1421 to record the highest priority measurements needed to meet primary science objectives. This Sonic-induction string (natural gamma ray, sonic velocity, and resistivity) is shown in Figure **F24,** and individual tools are listed in Table **T4.**

In preparation for logging, boreholes are flushed of debris by circulating viscous drilling fluid and filled with seawater or a seawater-based logging gel (sepiolite mud mixed with seawater; approximate density = 8.8 lb/gal, or 1.055 g/cm^3) to help stabilize the borehole walls. Heavier logging fluid (sepiolite mud mixed with seawater, weighted with barite) may be used where borehole conditions call for additional stabilization. The BHA is pulled up to a depth of 80–100 m DSF, depending on the stability of the hole. Each tool string is then lowered downhole by a seven-conductor wireline cable during sequential deployments. Each tool string deployment is a logging "run," starting with the assembly of the tool string and the necessary calibrations. A tool string is then sent down to the bottom of the hole while recording a partial set of data and then, except for the VSI string, is pulled up at a constant speed, typically 250–500 m/h, to record the primary data. The VSI string is held stationary at regularly spaced depths while shooting the seismic source. During each run, tool strings can be lowered down and pulled up the hole several times to evaluate reproducibility or to try to improve the quality of the data. Each lowering or hauling-up of the tool string while collecting data constitutes a "pass." During each pass, incoming data are recorded and monitored in real time on the surface minimum configuration multitasking acquisition and imaging system (MAXIS). A logging run is complete once the tool string has been returned to the rig floor and disassembled. A wireline heave compensator (WHC) was employed to minimize the effect of ship's heave on the tool string's position in the borehole.

Logged properties and tool measurement principles

The main logging measurements recorded during Expedition 341 are listed in Table **T5.** More detailed descriptions of individual tools and their geological applications may be found in Ellis and Singer (2007), Goldberg (1997), Rider (1996), Lovell et al. (1998), Schlumberger (1989, 1994), and Serra (1984, 1986,

1989). A complete list of acronyms for the Schlumberger tools and measurement curves is available at www.apps.slb.com/cmd/.

Natural radioactivity

The Hostile Environment Natural Gamma Ray Sonde (HNGS) was used to measure natural gamma radioactivity in the formation. It uses two bismuth germanate scintillation detectors and five-window spectroscopy to determine concentrations of potassium (in weight percent), thorium (in parts per million), and uranium (in parts per million). The radioactive isotopes of these three elements dominate NGR emissions in most rocks and sediments. The HNGS filters out gamma ray energies below 500 keV, eliminating sensitivity to bentonite or KCl in the drilling mud and improving measurement accuracy. The HNGS also provides a measure of the total gamma ray emission (HSGR) and uranium-free or computed gamma ray emission (HCGR) that are measured in American Petroleum Institute units (gAPI). The HNGS response is influenced by the borehole diameter; therefore, HNGS data are corrected for borehole diameter variations during acquisition.

The Enhanced Digital Telemetry Cartridge (EDTC) was used primarily to communicate data from the tool strings in the borehole to the surface. The EDTC also includes a sodium iodide scintillation detector that measures the total natural gamma ray emissions. It is not a spectral tool, but it provides high-resolution total gamma radiation for each pass, which allows precise depth match processing between logging runs and passes. The inclusion of a gamma ray tool (either HNGS or EDTC) in every tool string allows for use of gamma ray data for depth correlation between logging strings and passes.

Porosity

Formation porosity was measured with the Accelerator Porosity Sonde. This sonde includes a minitron neutron generator that produces fast (14.4 MeV) neutrons and five neutron detectors (four epithermal and one thermal) positioned at different spacing from the minitron. The tool's detectors count neutrons that arrive at the detectors after being scattered and slowed by collisions with atomic nuclei in the formation.

The highest energy loss occurs when neutrons collide with hydrogen nuclei, which have practically the same mass as the neutron (the neutrons simply bounce off of heavier elements without losing much energy). If the hydrogen (i.e., water) concentration is low, as in low-porosity formations, neutrons can travel farther before being captured and the count rates increase at the detector. The opposite effect occurs in high-porosity formations where the water content is high. The raw porosity value is often an overestimate because hydrogen atoms bound in minerals such as clays or contained in hydrocarbons also contribute to the measurement.

Upon reaching thermal energies (0.025 eV), the neutrons are captured by the nuclei of Cl, Si, B, and other elements, resulting in a gamma ray emission. This neutron capture cross section (Σ_f) is also measured by the tool.

Density

Formation density was measured with the Hostile Environment Litho-Density Sonde (HLDS). The HLDS normally consists of a radioactive cesium (^{137}Cs) gamma ray source (661 keV) and far- and near-gamma ray detectors mounted on a shielded skid, which is pressed against the borehole wall by a hydraulically activated eccentralizing arm. Gamma rays emitted by the source undergo Compton scattering by electrons in the formation. The number of scattered gamma rays that reach the detectors is proportional to the density of electrons in the formation, which is in turn related to bulk density. Porosity may also be derived from this bulk density if the matrix density is known.

The HLDS also measures the photoelectric effect (PEF) caused by absorption of low-energy gamma rays. Photoelectric absorption occurs when gamma rays reach <150 keV after being repeatedly scattered by electrons in the formation. The PEF is determined by comparing counts from the far detector in the high-energy region, where only Compton scattering occurs, with those in the low energy region, where count rates depend on both reactions. The far detector is used because it has a greater depth of investigation (tens of centimeters). The response of the short-spaced detector, mostly influenced by mudcake (minimally present in riserless drilling because seawater-based mud is used) and borehole rugosity, is used to correct the density measurement for these effects. Because PEF depends on the atomic number of the elements in the formation, it also varies according to the chemical composition of the minerals present and can be used for the identification of some minerals. For example, the PEF of calcite = 5.08 b/e$^-$, illite = 3.03 b/e$^-$, quartz = 1.81 b/e$^-$, and kaolinite = 1.49 b/e$^-$.

Good contact between the tool and borehole wall is essential for high-quality HLDS logs. Poor contact results in underestimation of density values. Both the density correction and caliper measurements of borehole diameter are used to check the contact quality.

Electrical resistivity

The High-Resolution Laterolog Array (HRLA) provides six electrical resistivity measurements with different depths of investigation (including the borehole, or mud resistivity, and five measurements of formation resistivity with increasing penetration into the formation). This sonde sends a focused current into the formation and measures the intensity necessary to maintain a constant drop in voltage across a fixed interval, providing a direct resistivity measurement. The array has one central (source) electrode and six electrodes above and below it, which serve alternatively as focusing and returning current electrodes. By rapidly changing the role of these electrodes, a simultaneous resistivity measurement at six penetration depths is achieved. The tool is designed to ensure that all signals are measured at exactly the same time and tool position and to reduce the sensitivity to "shoulder bed" effects when crossing sharp beds thinner than the electrode spacing. The design of the HRLA, which eliminates the need for a surface reference electrode, improves formation resistivity evaluation compared to the traditional dual induction method. The HRLA is run centralized in the borehole for optimal results, so knuckle joints are used to centralize the HRLA while allowing the eccentralized density and porosity tools to maintain good contact with the borehole wall (Fig. **F23**).

The Phasor Dual Induction–Spherically Focused Resistivity Tool (DIT) was used rather than the HRLA to measure electrical resistivity in boreholes where unstable hole conditions presented greater risk to logging tools. The DIT provides three measures of resistivity at different depths of investigation into the formation. The two induction devices (deep and medium depths of penetration) transmit high-frequency alternating current through coil transmitters, creating a magnetic field that induces a secondary current in the formation. These currents produce a new inductive signal, proportional to the conductivity of the formation, which is measured by the receiving coils. Measured conductivities are then converted to resistivity (in ohm-meters). Spherically focused resistivity is measured by an electrode device that sends a current into the formation while maintaining a constant voltage drop. The amount of current necessary to keep a constant voltage gives a direct measure of resistivity. This device uses electrodes to focus the current flow into the formation so that equipotential surfaces are spherical and has a shallower depth of investigation and a higher vertical resolution than induction measurements.

Typically, igneous minerals found in crustal rocks, calcite, silica, and hydrocarbons are electrical insulators, whereas ionic solutions like pore water are conductors. Electrical resistivity, therefore, can be used to evaluate porosity (via Archie's law) for a given salinity and resistivity of pore water.

Magnetic susceptibility

The MSS, a wireline tool designed by Lamont-Doherty Earth Observatory (LDEO), measures the ease with which particular formations are magnetized when subjected to a magnetic field. The ease of magnetization, or susceptibility, is ultimately related to the concentration and composition (size, shape, and mineralogy) of magnetizable material within the formation. These measurements provide one of the best methods for investigating stratigraphic changes in mineralogy and lithology because the measurement is quick, repeatable, and nondestructive and because different lithologies often have strongly contrasting susceptibilities. High-resolution susceptibility measurements can aid significantly in paleoclimatic and paleoceanographic studies, where construction of an accurate and complete stratigraphic framework is critical to reconstructing past climatic changes.

A single-coil sensor provides high-resolution measurements (~10 cm vertical resolution) with a shallow depth of investigation (~3 cm penetration into the borehole wall). A dual-coil sensor provides lower resolution measurements (~40 cm vertical resolution), with greater depth of investigation (~20 cm penetration into the borehole wall), and because of its more robust nature acts as a quality control for the high-resolution measurements. The MSS can be run as a component in a Schlumberger tool string, using a specially developed data translation cartridge. For quality control and environmental correction, the MSS also measures internal tool temperature and *z*-axis acceleration.

Acoustic velocity

The Dipole Shear Sonic Imager (DSI) measures the transit times between sonic transmitters and an array of eight receivers. The recorded waveforms are then used to calculate the sonic velocity of the formation. The omnidirectional monopole transmitter emits high-frequency (5–15 kHz) pulses to extract the compressional wave velocity of the formation, as well as the shear wave velocity when it is faster than the *S*-wave velocity of the borehole fluid. It combines replicate measurements, thus providing a measurement of compressional wave velocity through sediment that is relatively free from the effects of formation damage and an enlarged borehole (Schlumberger, 1989). The same transmitter can be fired in sequence at a lower frequency (0.5–1 kHz) to generate Stoneley waves that are sensitive to fractures and variations in

permeability. Along with the monopole transmitters found on most sonic tools, the DSI also has two cross-dipole transmitters, which allow an additional measurement of shear wave velocity. Dipole measurements are necessary to measure shear velocities in "slow" formations, where shear wave velocity is slower than the *S*-wave velocity in the borehole fluid. Such slow formations are typically encountered in deep-ocean drilling. The two shear wave velocities measured from the two orthogonal dipole transmitters can be used to identify sonic anisotropy associated with the local stress regime.

Resistivity images

The FMS produces high-resolution images of borehole wall microresistivity that can be used for detailed lithostratigraphic and structural interpretation. The tool has four orthogonally oriented pads, each with 16 button electrodes that are pressed against the borehole walls. The electrodes are arranged in two diagonally offset rows of eight electrodes each. A focused current is emitted from the button electrodes into the formation, with a return electrode near the top of the tool. Resistivity of the formation at the button electrodes is derived from the intensity of current passing through the button electrodes. Processing transforms these measurements into oriented high-resolution images that reveal the geologic structures of the borehole wall based on their conductivity. Features such as bedding, stratification, fracturing, slump folding, and bioturbation can be resolved. The images are oriented to magnetic north so that fabric analysis can be carried out and the dip and direction (azimuth) of planar features in the formation can be measured. In addition, when the corresponding planar features can be identified in the recovered core samples, individual core pieces can be reoriented with respect to true north.

The maximum extension of the FMS caliper arms is 15 inches (~38 cm). In boreholes with a diameter larger than this maximum, the pad contact at the end of the caliper will be inconsistent, and the FMS images may appear out of focus and overestimate conductivity. Irregular borehole walls will also adversely affect the images if contact with the wall is poor. Approximately 30% of a borehole with a diameter of 25 cm is imaged during a single pass. Coverage may be increased by a second run. The vertical resolution of FMS images is ~5 mm.

Acceleration and inclinometry

The General Purpose Inclinometry Tool (GPIT) was included in the FMS-sonic tool string to calculate tool acceleration and orientation during logging. Tool orientation is defined by three parameters: tool deviation, tool azimuth, and relative bearing. The GPIT utilizes a three-axis inclinometer and a three-axis fluxgate magnetometer to record the orientation of the FMS as the magnetometer records the magnetic field components (F*x*, F*y*, and F*z*). Thus, the FMS images can be corrected for irregular tool motion, and the dip and direction (azimuth) of features in the FMS image can be determined. Corrections for cable stretching and/or ship heave using GPIT acceleration data (A*x*, A*y*, and A*z*) allow precise determinations of log depths.

Vertical seismic profile

In a VSP experiment, a borehole seismic tool is anchored against the borehole wall at regularly spaced intervals and records acoustic waves generated by a seismic source positioned just below the sea surface. The main purpose of this experiment is to provide a direct measurement of the time necessary for seismic waves to travel from the surface to a given depth and to tie the observations in the well, recorded as a function of depth, to the reflections in the seismic survey data, recorded as a function of time.

The VSI used for the VSP is a three-axis geophone accelerometer that is anchored to the borehole wall by a caliper arm prior to recording. The orientation of the horizontal components, x and y, varies with sensor rotation during logging, but tool orientation is recorded. During Expedition 341, the VSI was anchored against the borehole wall at ~50 m intervals, and 5–10 recordings were typically taken at each station. The recorded waveforms were stacked, and a one-way traveltime was determined from the first breaks for each station. The seismic source used was a Sercel G-gun parallel cluster composed of two 250 inch^3 air guns separated by 1 m. It was positioned by one of the ship cranes off the port side of the ship at a total horizontal offset from the top of the wellhead of ~30 m and maintained at a fixed water depth (typically between 2 and 7 m).

In accordance with the requirements of the National Environmental Policy Act and the Endangered Species Act, all seismic activities were conducted during daytime and Protected Species Observers kept watch for protected species (marine mammals, sea turtles, and endangered marine species) for the duration of the zero-offset VSP. Any sighting of protected species within the exclusion zone of 940 m for deepwater depths (>1000 m) and 1410 m for intermediate water depths (100–1000 m) would interrupt the survey for 60 min after the last sighting or until the protected species were seen leaving the exclusion zone. Protected Species Observers began observations 1 h prior to the use of the seismic source, which started

with a 30 min ramp-up procedure, gradually increasing the operational pressure and firing rate to provide time for undetected protected species to vacate the area. The same ramp-up procedure would be used when resuming activity after any interruption because of the sighting of protected species or whenever the gun was not fired for more than 30 min.

Auxiliary logging equipment

Cable head

The Schlumberger logging equipment head (or cable head) measures tension at the very top of the wireline tool string, which diagnoses difficulties in running the tool string up or down the borehole or when exiting or entering the drill string or casing. The logging equipment head-mud temperature (LEH-MT) used during Expedition 341 also includes a thermal probe to measure the borehole fluid temperature.

Telemetry cartridges

Telemetry cartridges are used in each tool string to allow the transmission of the data from the tools to the surface. The EDTC also includes a sodium iodide scintillation detector to measure the total natural gamma ray emission of the formation. This gamma ray log was used to match depths between different passes and runs. In addition, it includes an accelerometer that can be used in real time to evaluate the efficiency of the WHC.

Joints and adapters

Because the tool strings combine tools of different generations and with various designs, they include several adapters and joints between individual tools to allow communication, provide isolation, avoid interferences (mechanical and acoustic), terminate wiring, or position the tool properly in the borehole. Knuckle joints in particular were used to allow some of the tools such as the HRLA to remain centralized in the borehole, while the overlying HLDS was pressed against the borehole wall.

All these additions are included and contribute to the total length of the tool strings in Figures **F23** and **F24.**

Wireline heave compensator

The WHC system, which was first used during Expedition 320T (February 2009), is designed to compensate for the vertical motion of the ship and maintain a steady motion of the logging tools. It uses vertical acceleration measurements made by a motion reference unit (MRU), located under the rig floor near the center of gravity of the ship, to calculate the vertical motion of the ship. It then adjusts the length of the wireline by varying the distance between two sets of pulleys through which the cable passes. Real-time measurements of uphole (surface) and downhole acceleration are made simultaneously by the MRU and EDTC, respectively. An LDEO-developed software package allows these data to be analyzed and compared in real time, displaying the actual motion of the logging tool string and enabling monitoring of the efficiency of the compensator.

Logging data flow and depth scales

Data for each wireline logging run were monitored in real time and recorded using the Schlumberger MAXIS 500 system. These data were then copied to the shipboard processing stations for preliminary processing. Typically, the main pass of the triple combo is used as a reference to which other passes are interactively depth matched. The initial logging data are referenced to the rig floor (WRF). After depth matching, all the logging depths were shifted to a seafloor reference (WSF) based on the step in the gamma radiation at the sediment/water interface and preliminarily depth matched to remove offsets between different logging passes. Potential sources of error in depth matching include sea state, uncompensated heave, wireline stretch, and errors in the reference log used, and the magnitude of uncertainty is typically on the order or centimeters to meters (IODP Depth Scales Terminology, v. 2.0, 2010). These data were made available to the science party within a few days of their acquisition.

The downhole log data were also transferred onshore to LDEO for standardized data processing. The main part of the processing is rigorous depth matching to remove depth offsets between different logging passes, which results in a new depth scale: wireline log matched depth below seafloor (WMSF). Also, corrections are made to certain tools and logs (e.g., FMS images are corrected for tool acceleration), documentation for the logs (with an assessment of log quality) is prepared, and data are converted to ASCII for the conventional logs and to SEG-Y for the VSP data. Schlumberger GeoQuest's GeoFrame software package is used for most of the processing. The standardized processed data are made available (in ASCII and DLIS formats) shortly after the expedition through the IODP logging database (**iodp.ldeo.columbia.edu/DATA/index.html**).

For a summary of borehole and downhole logging depth scales used on Expedition 341, see Table **T6.**

Log data quality

The principal influence on log data quality is the condition of the borehole wall. If the borehole diam-

eter varies over short intervals because of washouts during drilling or ledges made of layers of harder material, the logs from tools that require good contact with the borehole wall (i.e., the FMS and density tools) may be degraded. Deep investigation measurements such as gamma ray, resistivity, and sonic velocity, which do not require contact with the borehole wall, are generally less sensitive to borehole conditions. Very narrow ("bridged") sections will also cause irregular log results. The quality of the borehole is improved by minimizing the circulation of drilling fluid while drilling, conditioning by flushing the borehole to remove debris, and logging as soon as possible after drilling and conditioning are completed.

The quality of the logging depth determination depends on several factors. The depth of the logging measurements is determined from the length of the cable payed out from the winch on the ship. The seafloor (mudline) is identified on the natural gamma log by the abrupt reduction in gamma ray count at the water/sediment boundary. Discrepancies between DSF, CSF-A, and WMSF depths occur because of core expansion, incomplete core recovery, tides, or incomplete heave compensation for the drilling depth. In the case of log depth, discrepancies between successive runs occur because of incomplete heave compensation, incomplete correction for cable stretch, and cable slip. In the case of very fine sediments in suspension, the mudline can be an elusive datum. Tidal changes in sea level also will have an effect. The hydraulic WHC was used to adjust the wireline length for rig motion during wireline logging operations, to minimize the wireline tool motion caused by ship heave.

References

Akiba, F., 1986. Middle Miocene to Quaternary diatom biostratigraphy in the Nankai Trough and Japan Trench, and modified lower Miocene through Quaternary diatom zones for middle-to-high latitudes of the north Pacific. *In* Kagami, H., Karig, D.E., Coulbourn, W.T., et al., *Init. Repts. DSDP,* 87: Washington, DC (U.S. Govt. Printing Office), 393–481. **doi:10.2973/dsdp.proc.87.106.1986**

Akiba, F., and Yanagisawa, Y., 1986. Taxonomy, morphology and phylogeny of the Neogene diatom zonal marker species in the middle-to-high latitudes of the North Pacific. *In* Kagami, H., Karig, D.E., Coulbourn, W.T., et al., *Init. Repts. DSDP,* 87: Washington, DC (U.S. Govt. Printing Office), 483–554. **doi:10.2973/dsdp.proc.87.107.1986**

ASTM International, 1980. Standard method for laboratory determination of water (moisture) content of soil, rock and soil-aggregate mixtures. In *Annual Book of ASTM Standards:* Philadelphia (Am. Soc. Testing Mater.).

Barron, J.A., and Gladenkov, A.Y., 1995. Early Miocene to Pleistocene diatom stratigraphy of Leg 145. *In* Rea, D.K., Basov, I.A., Scholl, D.W., and Allan, J.F. (Eds.), *Proc. ODP, Sci. Results,* 145: College Station, TX (Ocean Drilling Program), 3–19. **doi:10.2973/odp.proc.sr.145.101.1995**

Bergen, F.W., and O'Neil, P., 1979. Distribution of Holocene foraminifera in the Gulf of Alaska. *J. Paleontol.,* 53(6):1267–1292. **http://www.jstor.org/stable/1304134**

Blum, P., 1997. Physical properties handbook: a guide to the shipboard measurement of physical properties of deep-sea cores. *ODP Tech. Note,* 26. **doi:10.2973/odp.tn.26.1997**

Brown, D.J., 2007. A guide to the use of volcaniclastic nomenclature in engineering investigations. *Q. J. Eng. Geol. Hydrogeol.,* 40(1):105–112. **doi:10.1144/1470-9236/06-007**

Cande, S.C., and Kent, D.V., 1995. Revised calibration of the geomagnetic polarity timescale for the Late Cretaceous and Cenozoic. *J. Geophys. Res.: Solid Earth,* 100(B4):6093–6095. **doi:10.1029/94JB03098**

Droser, M.L., and Bottjer, D.J., 1986. A semiquantitative field classification of ichnofabric. *J. Sediment. Res.,* 56(4):558–559. **doi:10.1306/212F89C2-2B24-11D7-8648000102C1865D**

Ellis, D.V., and Singer, J.M., 2007. *Well Logging for Earth Scientists* (2nd ed.): New York (Elsevier).

Evans, H.B., 1965. GRAPE—a device for continuous determination of material density and porosity. *Trans. SPWLA Annu. Logging Symp.,* 6(2):B1–B25. **https://www.spwla.org/SymposiumTransactions/grape-device-continuous-determination-material-density-and-porosity**

Expedition 317 Scientists, 2011. Methods. *In* Fulthorpe, C.S., Hoyanagi, K., Blum, P., and the Expedition 317 Scientists, *Proc. IODP,* 317: Tokyo (Integrated Ocean Drilling Program Management International, Inc.). **doi:10.2204/iodp.proc.317.102.2011**

Expedition 318 Scientists, 2011. Methods. *In* Escutia, C., Brinkhuis, H., Klaus, A., and the Expedition 318 Scientists, *Proc. IODP,* 318: Tokyo (Integrated Ocean Drilling Program Management International, Inc.). **doi:10.2204/iodp.proc.318.102.2011**

Fisher, R.V., and Schmincke, H.-U., 1984. *Pyroclastic Rocks.*:Berlin (Springer-Verlag).

Gieskes, J.M., Gamo, T., and Brumsack, H., 1991. Chemical methods for interstitial water analysis aboard *JOIDES Resolution. ODP Tech. Note,* 15. **doi:10.2973/odp.tn.15.1991**

Goldberg, D., 1997. The role of downhole measurements in marine geology and geophysics. *Rev. Geophys.,* 35(3):315–342. **doi:10.1029/97RG00221**

Gooday, A.J., 2003. Benthic foraminifera (Protista) as tools in deep-water paleoceanography: environmental influences on faunal characteristics. *Adv. Mar. Biol.,* 46:1–90. **doi:10.1016/S0065-2881(03)46002-1**

Graber, K.K., Pollard, E., Jonasson, B., and Schulte, E. (Eds.), 2002. Overview of Ocean Drilling Program engineering tools and hardware. *ODP Tech. Note,* 31. **doi:10.2973/odp.tn.31.2002**

Gradstein, F.M., Ogg, J.G., Schmitz, M.D., and Ogg, G.M. (Eds.)., 2012. *The Geological Time Scale 2012:* Amsterdam (Elsevier).

Hagelberg, T.K., Pisias, N.G., Shackleton, N.J., Mix, A.C., and Harris, S., 1995. Refinement of a high-resolution, continuous sedimentary section for studying equatorial Pacific Ocean paleoceanography, Leg 138. *In* Pisias, N.G., Mayer, L.A., Janecek, T.R., Palmer-Julson, A., and van Andel, T.H. (Eds.), *Proc. ODP, Sci Results,* 138: College Station, TX (Ocean Drilling Program), 31–46. **doi:10.2973/odp.proc.sr.138.103.1995**

Harms, J.C., and Choquette, P.W., 1965. Geologic evaluation of a gamma-ray porosity device. *Trans. SPWLA Annu. Logging Symp.,* 6(2):C1–C37.

Harris, S., Hagelberg, T., Mix, A., Pisias, N.G., and Shackleton, N.J., 1995. Sediment depths determined by comparisons of GRAPE and logging density data during Leg 138. *In* Pisias, N.G., Mayer, L.A., Janecek, T.R., Palmer-Julson, A., and van Andel, T.H. (Eds.), *Proc. ODP, Sci. Results,* 138: College Station, TX (Ocean Drilling Program), 47–57. **doi:10.2973/odp.proc.sr.138.104.1995**

Hilgen, F.J., Lourens, L.J., and Van Dam, J.A., 2012. The Neogene period. *In* Gradstein, F.M., Ogg, J.G., Schmitz, M.D., and Ogg, G.M. (Eds.), *The Geologic Time Scale:* Oxford (Elsevier), 923–978. **doi:10.1016/B978-0-444-59425-9.00029-9**

Jorissen, F.J., Fontanier, C., and Thomas, E., 2007. Paleoceanographical proxies based on deep-sea benthic foraminiferal assemblage characteristics. *In* Hillaire-Marcel, C., and De Vernal, A. (Eds.), *Proxies in Late Cenozoic Paleoceanography.* Dev. Mar. Geol., 263–325. **doi:10.1016/S1572-5480(07)01012-3**

Kamikuri, S., Nishi, H., and Motoyama, I., 2007. Effects of late Neogene climatic cooling on North Pacific radiolarian assemblages and oceanographic conditions. *Palaeogeogr., Palaeoclimatol., Palaeoecol.,* 249(3–4):370–392. **doi:10.1016/j.palaeo.2007.02.008**

Kamikuri, S., Nishi, H., Motoyama, I., and Saito, S., 2004. Middle Miocene to Pleistocene radiolarian biostratigraphy in the northwest Pacific Ocean, ODP Leg 186. *Isl. Arc,* 13(1):191–226. **doi:10.1111/j.1440-1738.2003.00421.x**

Kennett, J.P., Rozo-Vera, G.A., and Machain Castillo, M.L., 2000. Latest Neogene planktonic foraminiferal biostratigraphy of the California margin. *In* Lyle, M., Koizumi, I., Richter, C., and Moore, T.C. (Eds.), *Proc. ODP, Sci. Results,* 167: College Station, TX (Ocean Drilling Program), 41–62. **doi:10.2973/odp.proc.sr.167.212.2000**

Kennett, J.P., and Srinivasan, M.S., 1983. *Neogene Planktonic Foraminifera: A Phylogenetic Atlas:* Stroudsburg, PA (Hutchinson Ross).

Kucera, M., and Kennett, J.P., 2000. Biochronology and evolutionary implications of late Neogene California margin planktonic foraminiferal events. *Mar. Micropaleontol.,* 40(1–2):67–81. **doi:10.1016/S0377-8398(00)00029-3**

Loeblich, A.R., and Tappan, H., 1988. *Foraminiferal Genera and Their Classification* (Vol. 2): New York (Van Nostrand Reinhold Co.).

Lovell, M.A., Harvey, P.K., Brewer, T.S., Williams, C., Jackson, P.D., and Williamson, G., 1998. Application of FMS images in the Ocean Drilling Program: an overview. *In* Cramp, A., MacLeod, C.J., Lee, S.V., and Jones, E.J.W. (Eds.), *Geological Evolution of Ocean Basins: Results from the Ocean Drilling Program.* Geol. Soc. Spec. Publ., 131(1):287–303. **doi:10.1144/GSL.SP.1998.131.01.18**

Manheim, F.T., and Sayles, F.L., 1974. Composition and origin of interstitial waters of marine sediments, based on deep sea drill cores. *In* Goldberg, E.D. (Ed.), *The Sea* (Vol. 5): *Marine Chemistry: The Sedimentary Cycle:* New York (Wiley), 527–568.

Mazzullo, J.M., Meyer, A., and Kidd, R.B., 1988. New sediment classification scheme for the Ocean Drilling Program. *In* Mazzullo, J., and Graham, A.G. (Eds.), *Handbook for shipboard sedimentologists*. ODP Tech. Note, 8:44–67. **doi:10.2973/odp.tn.8.1988**

Mix, A.C., Tiedemann, R., Blum, P., et al., 2003. *Proc. ODP, Init. Repts.,* 202: College Station, TX (Ocean Drilling Program). **doi:10.2973/odp.proc.ir.202.2003**

Moncrieff, A.C.M., 1989. Classification of poorly-sorted sedimentary rocks. *Sediment. Geol.,* 65(1–2):191–194. **doi:10.1016/0037-0738(89)90015-8**

Moore, D.M., and Reynolds, R.C., Jr., 1997. *X-ray Diffraction and the Identification and Analysis of Clay Minerals* (2nd ed.): New York (Oxford Univ. Press).

Moran, K., 1997. Elastic property corrections applied to Leg 154 sediment, Ceara Rise. *In* Shackleton, N.J., Curry, W.B., Richter, C., and Bralower, T.J. (Eds.), *Proc. ODP, Sci. Results,* 154: College Station, TX (Ocean Drilling Program), 151–155. **doi:10.2973/odp.proc.sr.154.132.1997**.

Morley, J.J., and Nigrini, C., 1995. Miocene to Pleistocene radiolarian biostratigraphy of North Pacific Sites 881, 884, 885, 886, and 887. *In* Rea, D.K., Basov, I.A., Scholl, D.W., and Allan, J.F. (Eds.), *Proc. ODP, Sci. Results,* 145: College Station, TX (Ocean Drilling Program), 55–91. **doi:10.2973/odp.proc.sr.145.107.1995**

Munsell Color Company, Inc., 2009. *Munsell Soil Color Chart*: Grand Rapids, MI (Munsell Color Co., Inc.).

Murray, J.W., 2006. *Ecology and Applications of Benthic Foraminifera*: Cambridge (Cambridge Univ. Press).

Murray, R.W., Miller, D.J., and Kryc, K.A., 2000. Analysis of major and trace elements in rocks, sediments, and interstitial waters by inductively coupled plasma–atomic emission spectrometry (ICP-AES). *ODP Tech. Note,* 29. **doi:10.2973/odp.tn.29.2000**

Pälike, H., Moore, T., Backman, J., Raffi, I., Lanci, L., Parés, J.M., and Janecek, T., 2005. Integrated stratigraphic correlation and improved composite depth scales for ODP Sites 1218 and 1219. *In* Wilson, P.A., Lyle, M., and Firth, J.V. (Eds.), *Proc. ODP, Sci. Results,* 199: College Station, TX (Ocean Drilling Program), 1–41. **doi:10.2973/odp.proc.sr.199.213.2005**

Pisias, N.G., Roelofs, A., and Weber, M., 1997. Radiolarian-based transfer functions for estimating mean surface ocean temperatures and seasonal range. *Paleoceanography,* 12(3):365–379. **doi:10.1029/97PA00582**

Pribnow, D., Kinoshita, M., and Stein, C., 2000. *Thermal Data Collection and Heat Flow Recalculations for Ocean Drilling Program Legs 101–180:* Hanover, Germany (Inst. Joint Geosci. Res., Inst. Geowiss. Gemeinschaftsauf. [GGA]). **http://www-odp.tamu.edu/publications/heatflow/ODPReprt.pdf**

Rider, M.H., 1996. *The Geological Interpretation of Well Logs* (2nd ed.): Caithness (Whittles Publ.).

Ruddiman, W.F., Cameron, D., and Clement, B.M., 1987. Sediment disturbance and correlation of offset holes drilled with the hydraulic piston corer: Leg 94. *In* Ruddiman, W.F., Kidd, R.B., Thomas, E., et al., *Init. Repts. DSDP,* 94: Washington, DC (U.S. Govt. Printing Office), 615–634. **doi:10.2973/dsdp.proc.94.111.1987**

Saito, T., Thompson, P.R., and Breger, D., 1981. *Systematic Index of Recent and Pleistocene Planktonic Foraminifera:* Tokyo (Univ. of Tokyo).

Savrda, C.E., Krawinkel, H., McCarthy, F.M.G., McHugh, C.M.G., Olson, H.C., and Mountain, G., 2001. Ichnofabrics of a Pleistocene slope succession, New Jersey margin: relations to climate and sea-level dynamics. *Palaeogeogr., Palaeoclimatol., Palaeoecol.,*171(1–2):41–61. **doi:10.1016/S0031-0182(01)00266-8**

Scherer, R.P., and Koç, N., 1996. Late Paleogene diatom biostratigraphy and paleoenvironments of the northern Norwegian-Greenland Sea. *In* Thiede, J., Myhre, A.M., Firth, J.V., Johnson, G.L., and Ruddiman, W.F. (Eds.), *Proc. ODP, Sci. Results,* 151: College Station, TX (Ocean Drilling Program), 75–99. **doi:10.2973/odp.proc.sr.151.155.1996**

Schlumberger, 1989. *Log Interpretation Principles/Applications:* Houston (Schlumberger Educ. Serv.), SMP–7017.

Schlumberger, 1994. *IPL Integrated Porosity Lithology:* Houston (Schlumberger Wireline Testing), SMP-9270.

Serra, O., 1984. *Fundamentals of Well-Log Interpretation* (Vol. 1): *The Acquisition of Logging Data:* Amsterdam (Elsevier).

Serra, O., 1986. *Fundamentals of Well-Log Interpretation* (Vol. 2): *The Interpretation of Logging Data.* Amsterdam (Elsevier).

Serra, O., 1989. *Formation MicroScanner Image Interpretation:* Houston (Schlumberger Educ. Serv.), SMP-7028.

Shepard, F.P., 1954. Nomenclature based on sand-silt-clay ratios. *J. Sediment. Petrol.,* 24(3):151–158. **http://jsedres.sepmonline.org/cgi/reprint/24/3/151.pdf**

Shilov, V.V., 1995. Miocene–Pliocene radiolarians from Leg 145, North Pacific. *In* Rea, D.K., Basov, I.A., Scholl, D.W., and Allan, J.F. (Eds.), *Proc. ODP, Sci. Results,* 145: College Station, TX (Ocean Drilling Program), 93–116. **doi:10.2973/odp.proc.sr.145.111.1995**

Shipboard Scientific Party, 1999. Explanatory notes. *In* Barker, P.F., Camerlenghi, A., Acton, G.D., et al., *Proc. ODP, Init. Repts.,* 178: College Station, TX (Ocean Drilling Program), 1–66. **doi:10.2973/odp.proc.ir.178.104.1999**

Smith, P.B., 1973. Foraminifera of the North Pacific Ocean. *U.S. Geol. Surv. Prof. Pap.,* 766. **http://pubs.usgs.gov/pp/ 0766/report.pdf**

St-Onge, G., Mulder, T., Francus, P., and Long, B., 2007. Continuous physical properties of cored marine sediments. *In* Hillaire-Marcel, C., and de Vernal, A. (Eds.), *Proxies in Late Cenozoic Paleoceanography.* Dev. Mar. Geol., 1:63–98. **doi:10.1016/S1572-5480(07)01007-X**

Tauxe, L., 2010. *Essentials of Paleomagnetism:* Berkeley, California (Univ. California Press).

Thompson, R., and Oldfield, F., 1986. *Environmental Magnetism:* London (Allen and Unwin).

Todd, R., and Low, D., 1967. Recent foraminifera from the Gulf of Alaska and southeastern Alaska. *U.S. Geol. Surv. Prof. Pap.,* 573-A. **http://pubs.usgs.gov/pp/0573a/report.pdf**

Vasiliev, M.A., Blum, P., Chubarian, G., Olsen, R., Bennight, C., Cobine, T., Fackler, D., Hastedt, M., Houpt, D., Mateo, Z., and Vasilieva, Y.B., 2011. A new natural gamma radiation measurement system for marine sediment and rock analysis. *J. Appl. Geophys.,* 75:455–463. **doi:10.1016/j.jappgeo.2011.08.008**

Wentworth, C.K., 1922. A scale of grade and class terms for clastic sediments. *J. Geol.,* 30(5):377–392. **doi:10.1086/622910**

Yanagisawa, Y., and Akiba, F., 1990. Taxonomy and phylogeny of the three marine diatom genera, *Crucidenticula, Denticulopsis* and *Neodenticula. Bull. Geol. Surv. Jpn.,* 41:197–301.

Yanagisawa, Y., and Akiba, F., 1998. Refined Neogene diatom biostratigraphy for the northwest Pacific around Japan, with an introduction of code numbers for selected diatom biohorizons. *Chishitsugaku Zasshi,* 104(6):395–414. **doi:10.5575/geosoc.104.395**

Publication: 22 November 2014
MS 341-102

Figure F1. Core description form, Expedition 341.

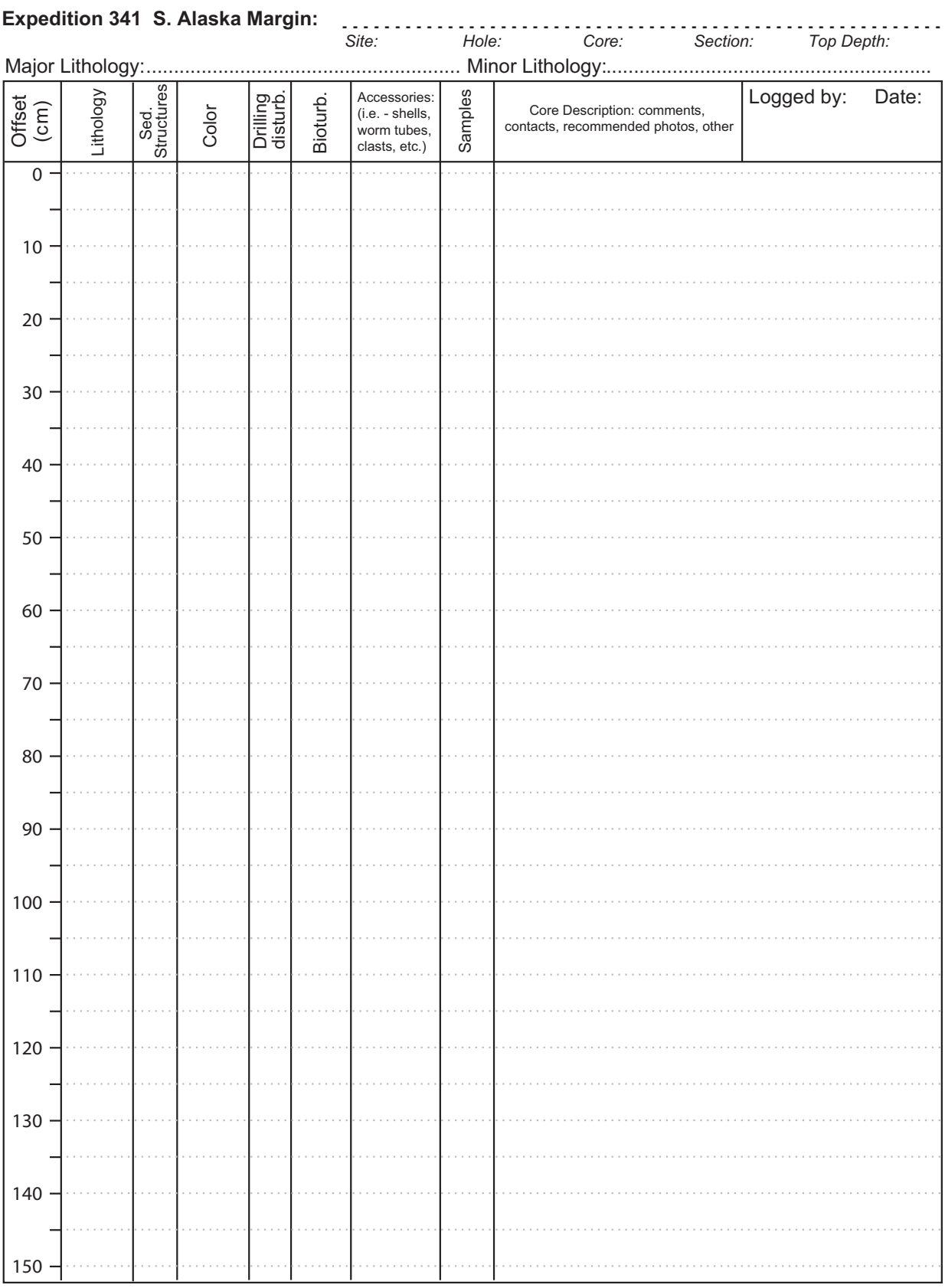

Figure F2. Example of a graphical visual core description (VCD) form, Expedition 341.

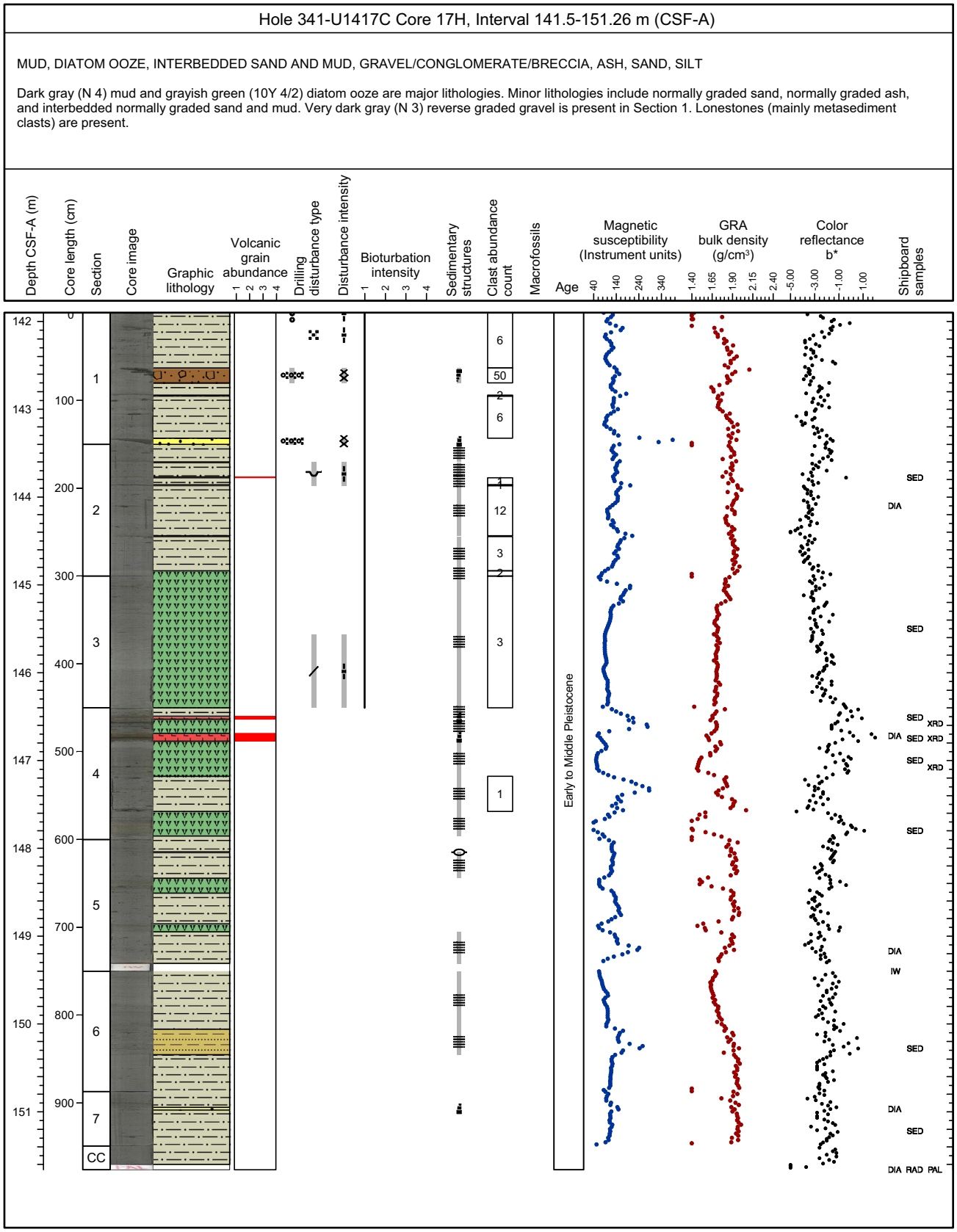

Figure F3. Legend for standard graphic report, Expedition 341.

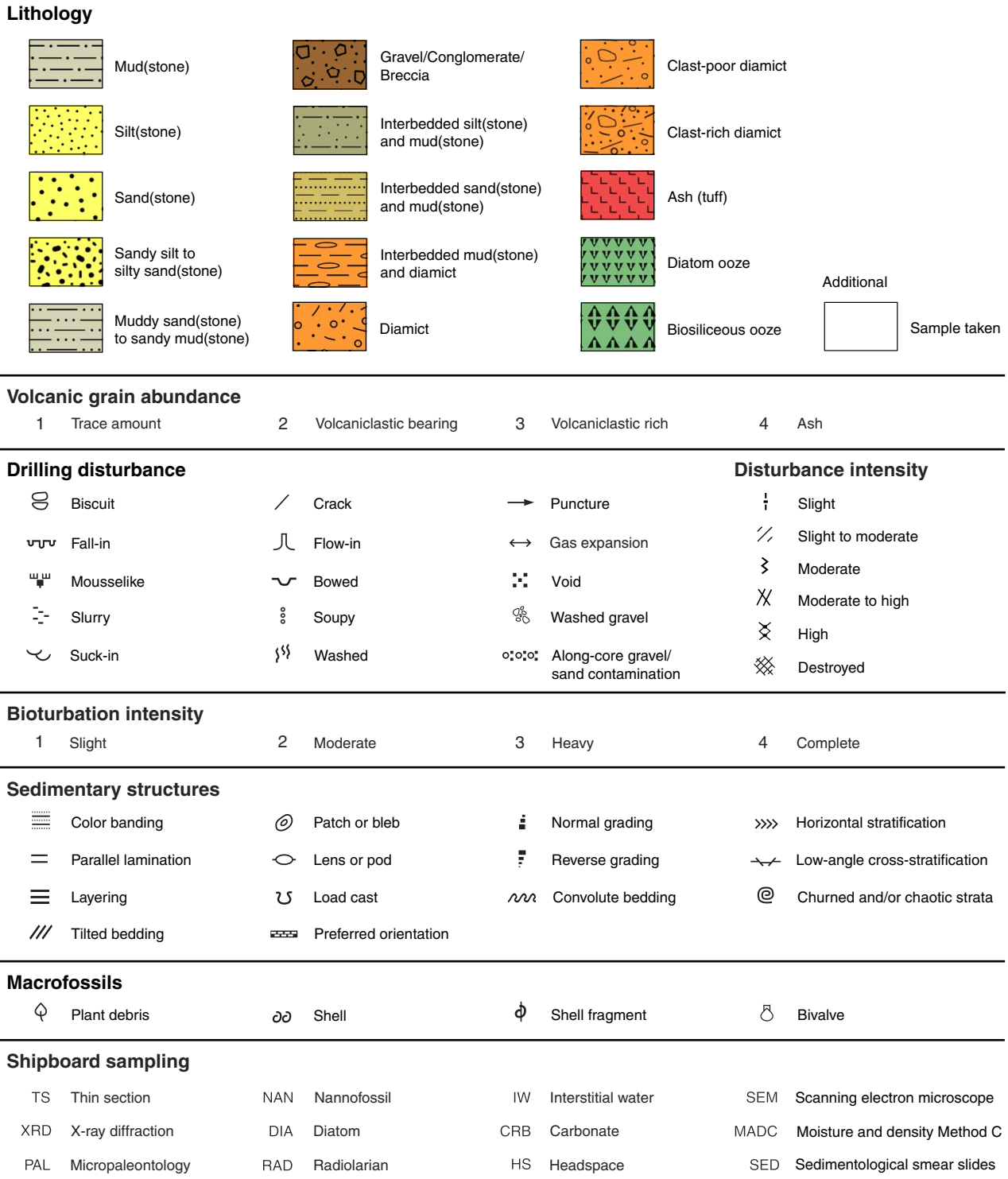

Figure F4. Smear slide description form, Expedition 341.

IODP Expedition 341 SMEAR SLIDE DESCRIPTION WORKSHEET

Leg	Site	Hole	Core	Section	Interval (cm) Top	Bottom

Observer	

Siliciclastic texture (%)		
Sand	Silt	Clay

Percent	Component
SILICICLASTIC GRAINS/MINERALS	
	Framework minerals
	Quartz
	Feldspar
	K-feldspar (Orthoclase, Microcline...)
	Plagioclase
	Rock fragments
	Sedimentary
	Igneous
	Metamorphic
	Accessory/trace minerals
	Micas
	Biotite
	Muscovite
	Chlorite
	Clay minerals
	Glauconite
	Chert
	Zircon
	Ferromagnesium minerals
	Authigenic minerals
	Barite
	Phosphorite/Apatite
	Zeolite
	Opaque minerals
	Pyrite
	Magnetite
	Fe-oxide
	Carbonates
	Calcite
	Dolomite

Percent	Component
VOLCANICLASTIC GRAINS	
	Crystal grain
	Vitric grain (glass, pumice)
	Lithic grain
	Palagonite
BIOGENIC GRAINS	
	Calcareous
	Foraminifers
	Nannofossils
	Pteropods
	Siliceous
	Radiolarians
	Diatoms
	Silicoflagellates
	Sponge spicules
	Dinoflagellates
	Others
	Pollen
	Organic debris
	Plant debris

Comments:

Fossil preservation	Abundance code
G = good	<1% = TR (trace)
M = moderate	1-5% = R (rare)
P = poor	5-25% = C (common)
	25-75% = A (abundant)
	>75% = D (dominant)

Figure F5. Ternary plots of lithology naming scheme, Expedition 341. Modified from Expedition 317 Scientists (2011). Lower ternary plot follows Shepard (1954).

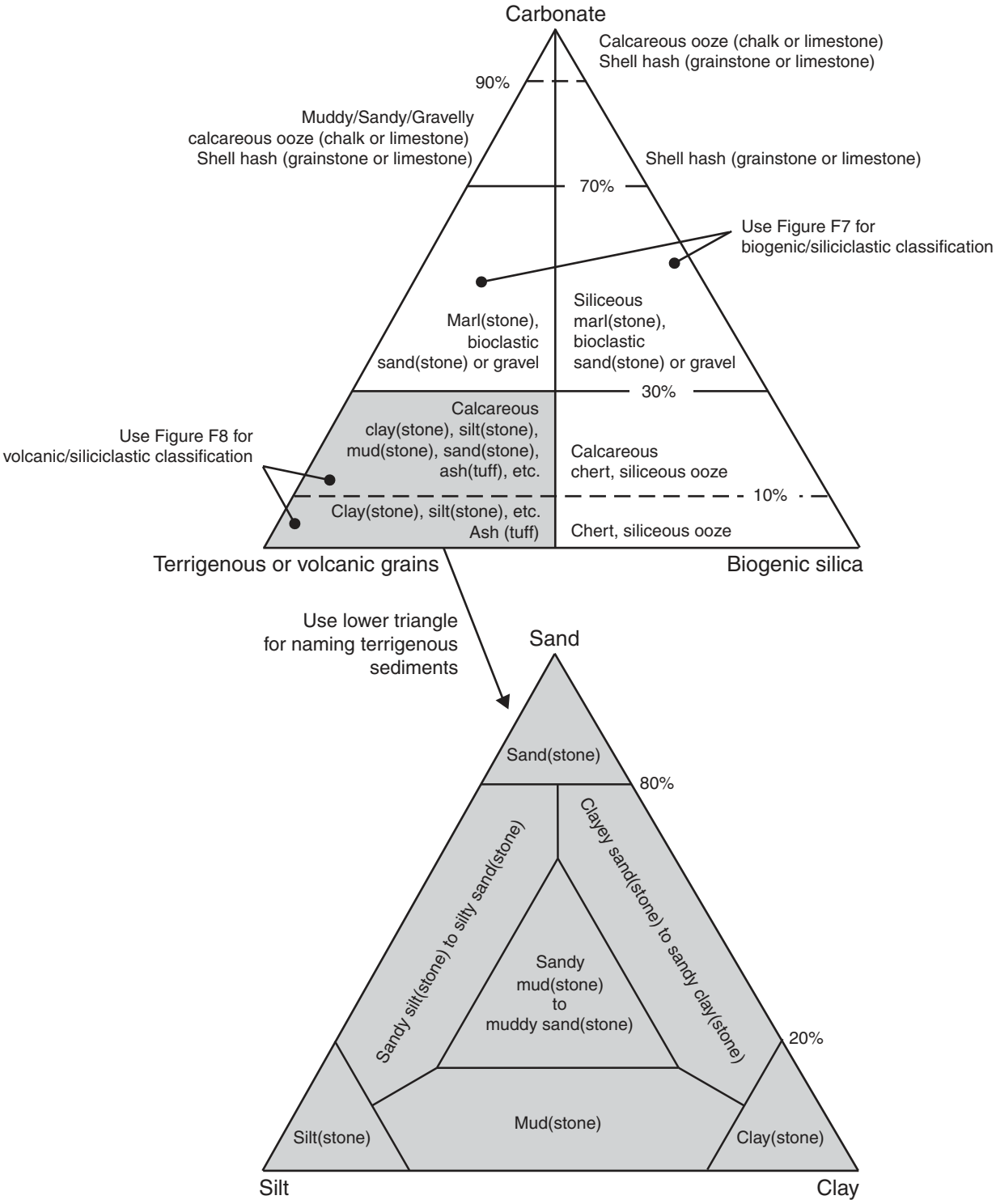

Figure F6. Classification scheme for siliciclastic clastic sediment/rock containing a gravel component, Expedition 341. After Moncrieff (1989).

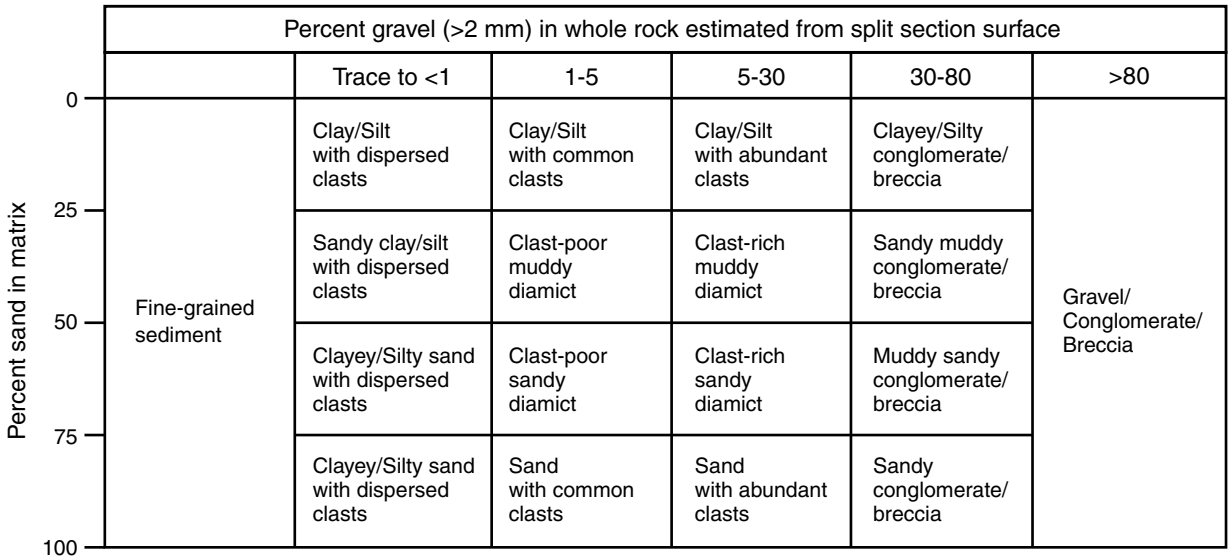

Figure F7. Classification scheme for sediments that are mixtures of biogenic (e.g., diatoms) and siliciclastic components, Expedition 341.

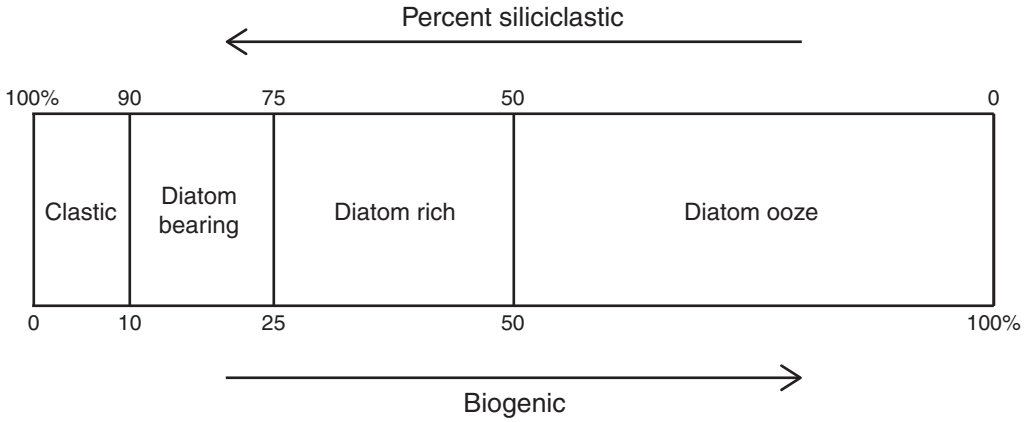

Figure F8. Classification scheme for sediments that are mixtures of volcanic grains and siliciclastic components, Expedition 341.

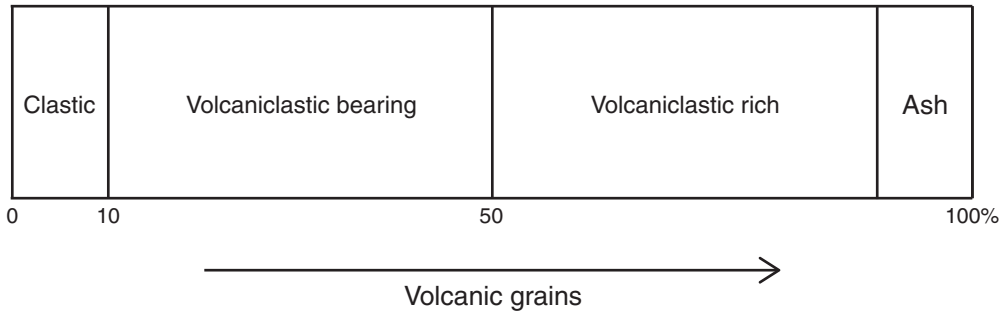

Figure F9. Ichnofabric index legend, Expedition 341. Modified from Droser and Bottjer (1986) and Savrda et al. (2001).

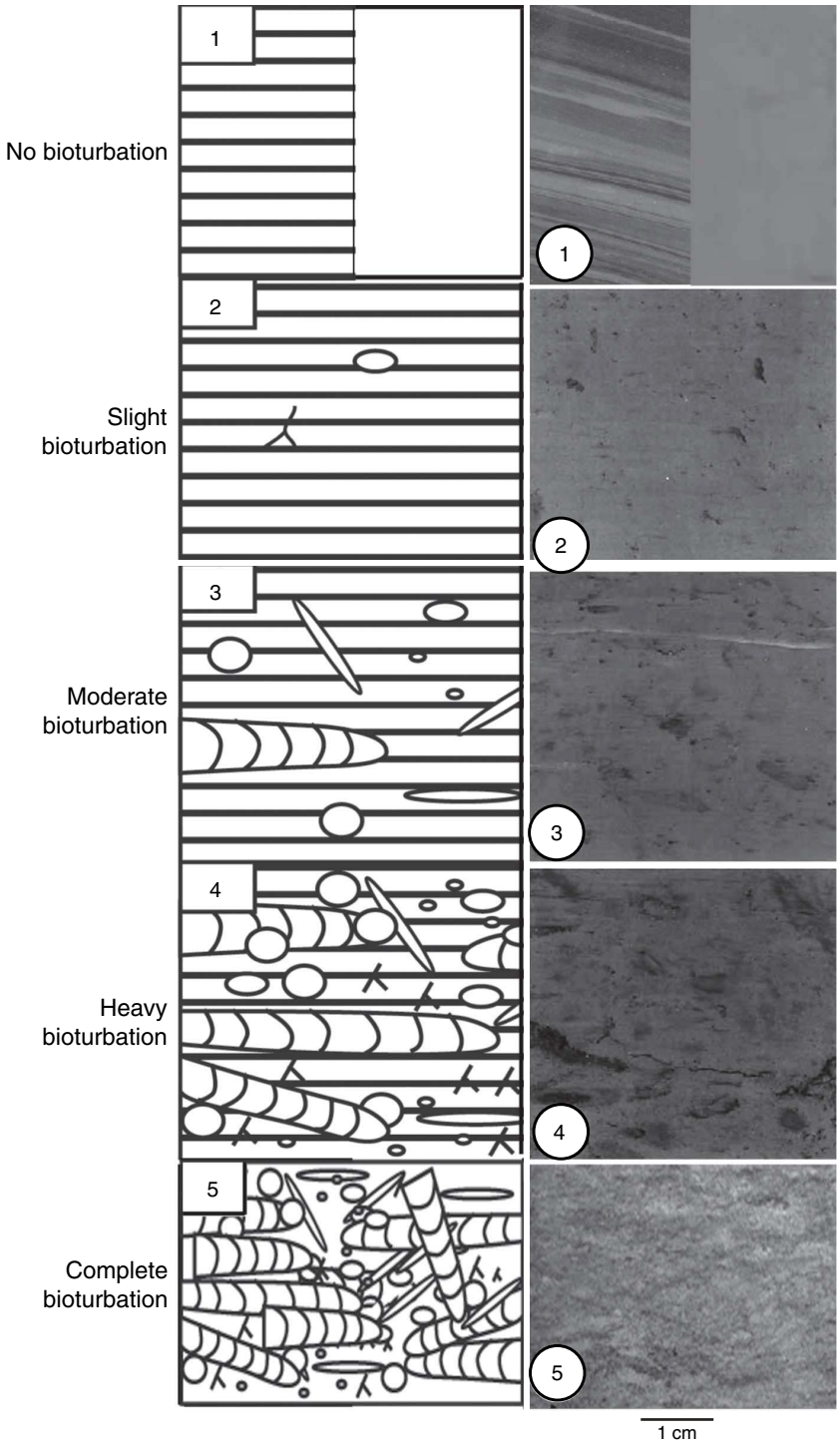

Figure F10. Integrated chronostratigraphy based on diatom, radiolarian, and planktonic foraminiferal biozones from present to late Miocene (0–11.5 Ma) used during Expedition 341. Magnetostratigraphy, stages, and epochs after the updated geologic timescale (Hilgen et al., 2012). NPD = Neogene North Pacific Diatom zone of Yanagisawa and Akiba (1998), CM = California margin.

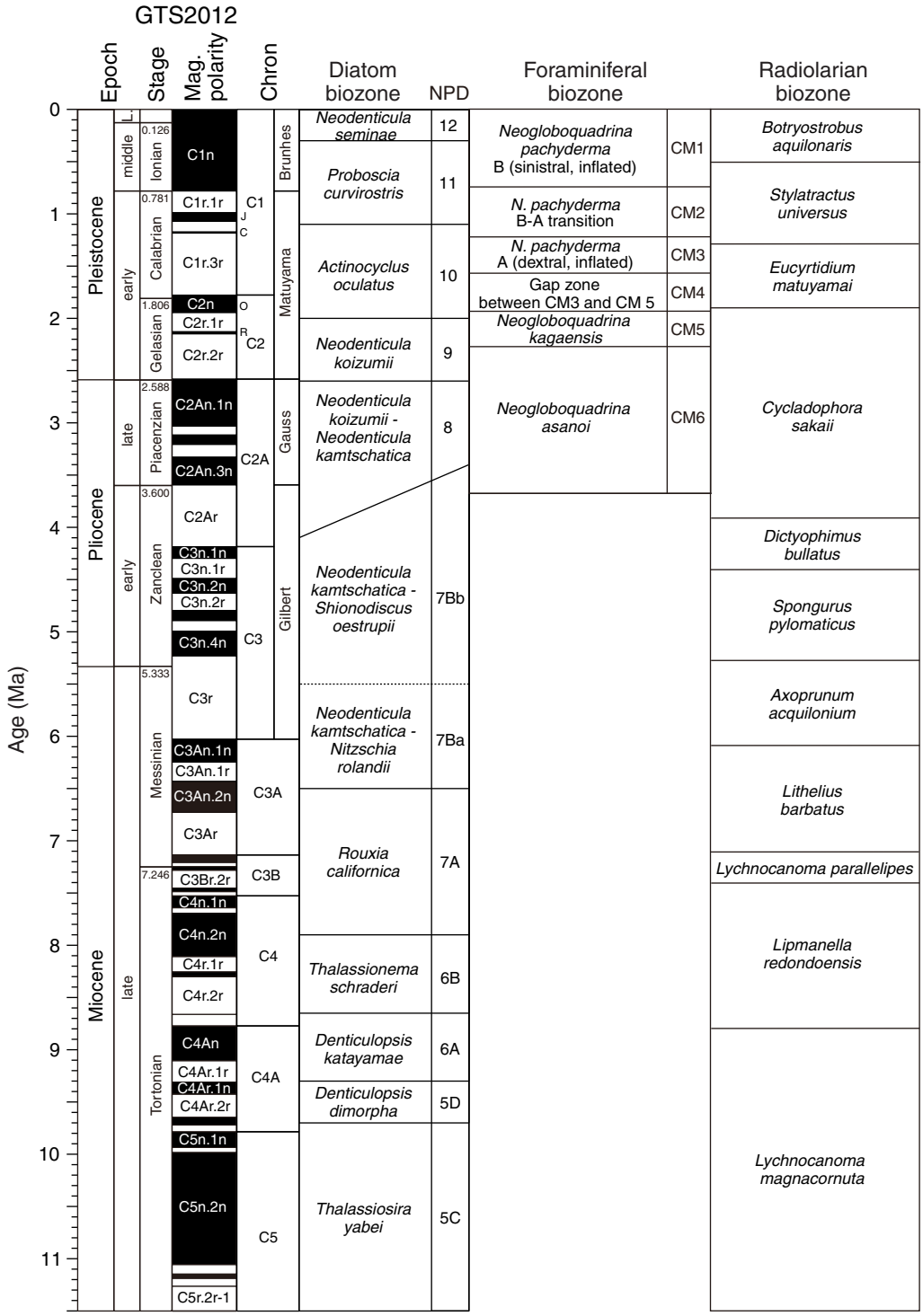

Figure F11. Integrated chronostratigraphy based on diatom and radiolarian biozones from late to early Miocene (11–23 Ma) used during Expedition 341. Magnetostratigraphy, stages, and epochs after the updated geologic timescale (Hilgen et al., 2012). NPD = Neogene North Pacific Diatom zone of Yanagisawa and Akiba (1998).

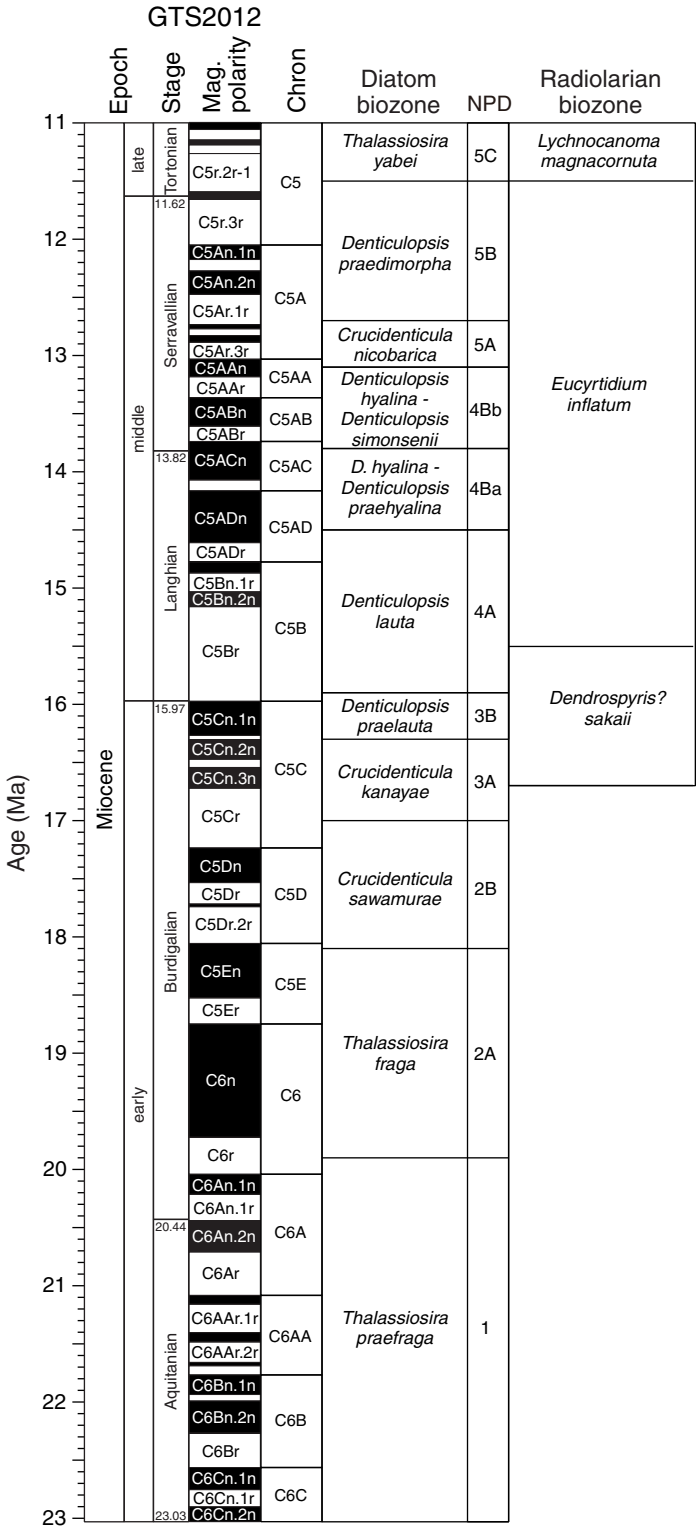

Figure F12. Diatom biozones and biohorizons from present to early Miocene (0–11.5 Ma) used during Expedition 341. Magnetostratigraphy, stages, and epochs after the updated geologic timescale (Hilgen et al., 2012). NPD = Neogene North Pacific Diatom zone of Yanagisawa and Akiba (1998). Biozone boundaries are in bold.

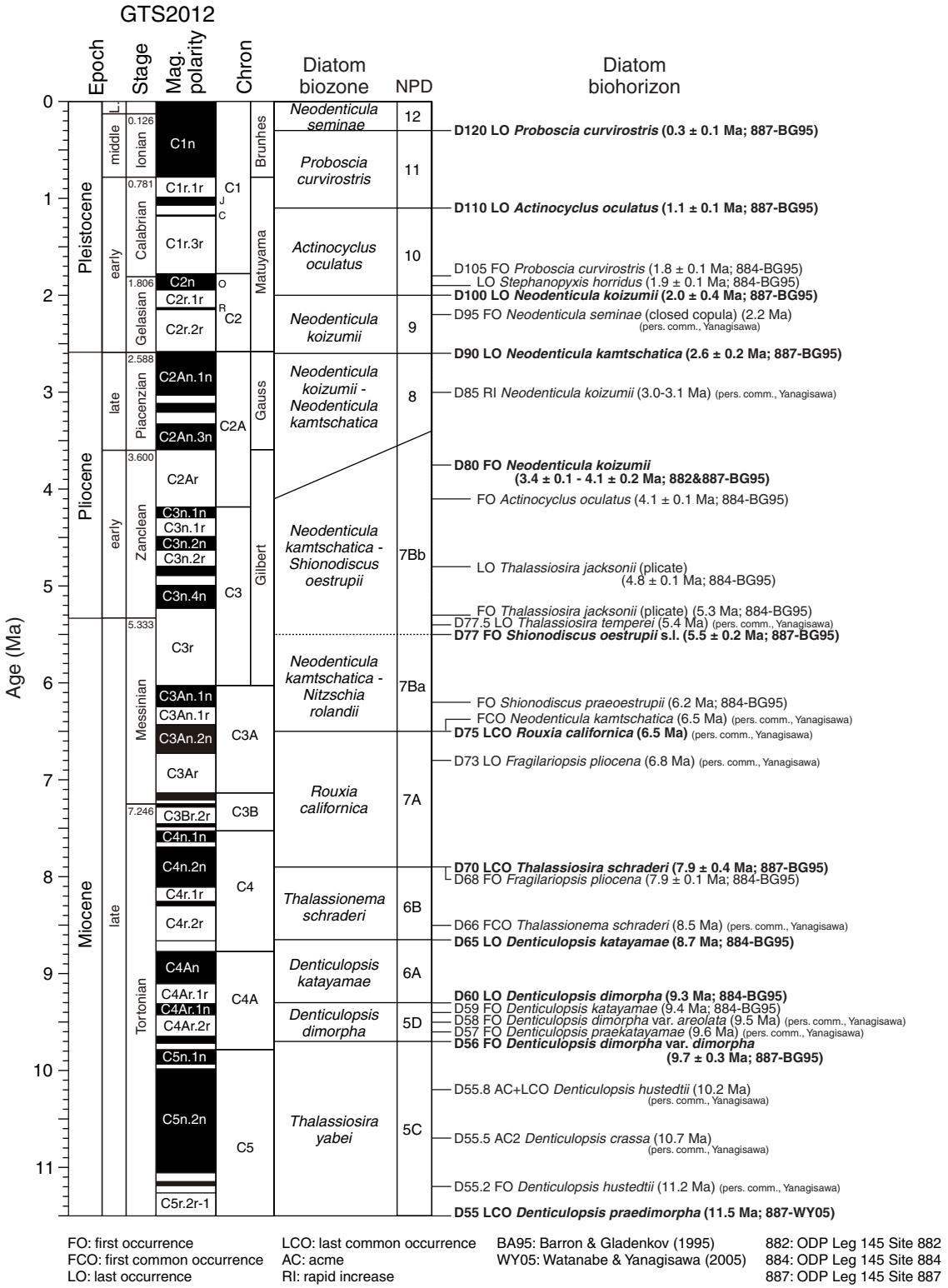

Figure F13. Diatom biozones and biohorizons from late to early Miocene (11–23 Ma) used during Expedition 341. Magnetostratigraphy, stages, and epochs after the updated geologic timescale (Hilgen et al., 2012). NPD = Neogene North Pacific Diatom zone of Yanagisawa and Akiba (1998). Biozone boundaries are in bold.

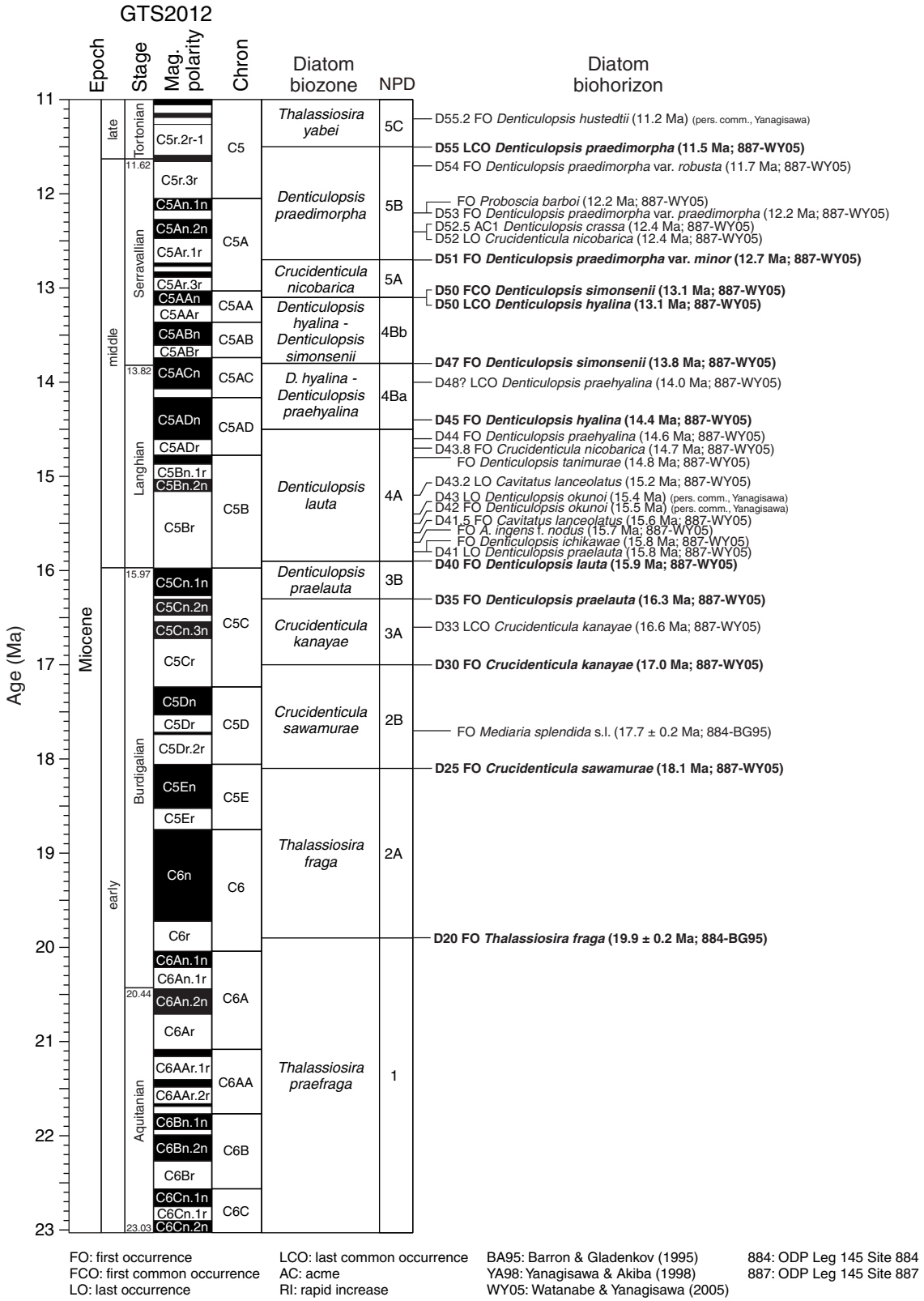

Figure F14. Radiolarian biozones and biohorizons from present to early Miocene (0–11.5 Ma) used during Expedition 341. Magnetostratigraphy, stages, and epochs after the updated geologic timescale (Hilgen et al., 2012). Biozone boundaries are in bold.

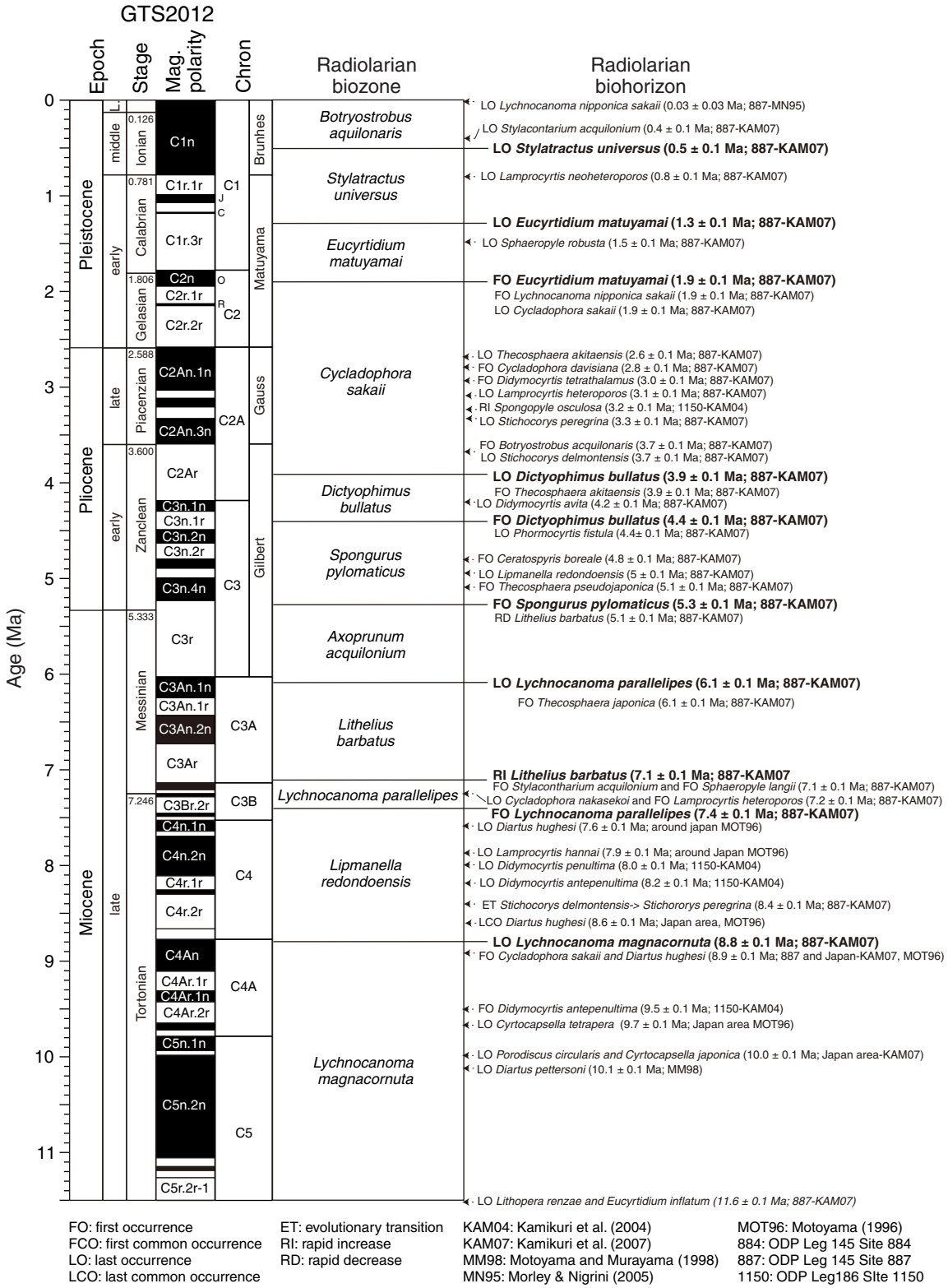

Figure F15. Radiolarian biozones and biohorizons from early to late Miocene (11–23 Ma) used during Expedition 341. Magnetostratigraphy, stages, and epochs after the updated geologic timescale (Hilgen et al., 2012). Biozone boundaries are in bold.

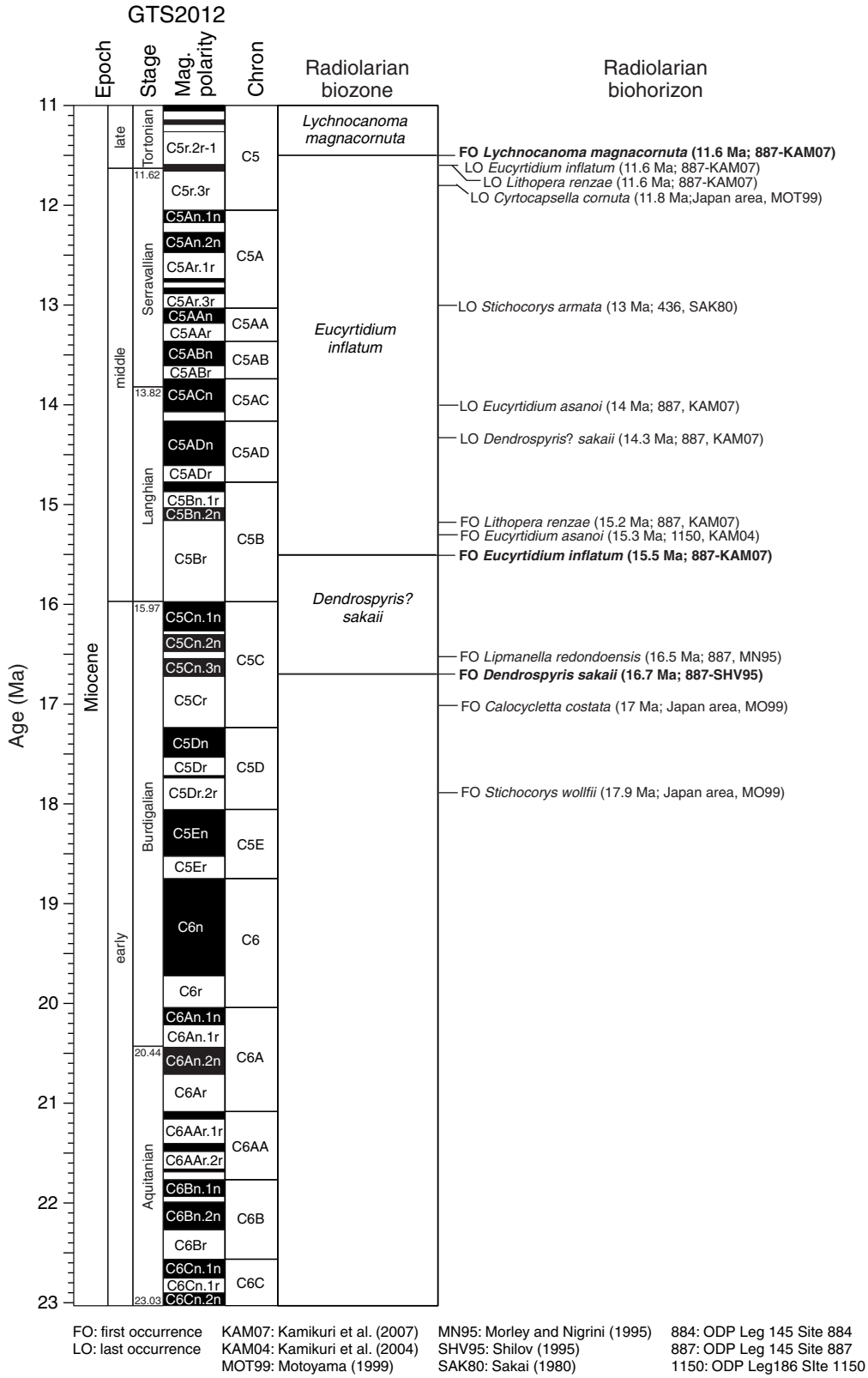

Figure F16. Planktonic foraminiferal biozones and biohorizons from present to Pliocene (0–3.6 Ma) used during Expedition 341. Magnetostratigraphy, stages, and epochs after the geologic timescale (Hilgen et al., 2012). CM = California margin. Biozone boundaries are in bold.

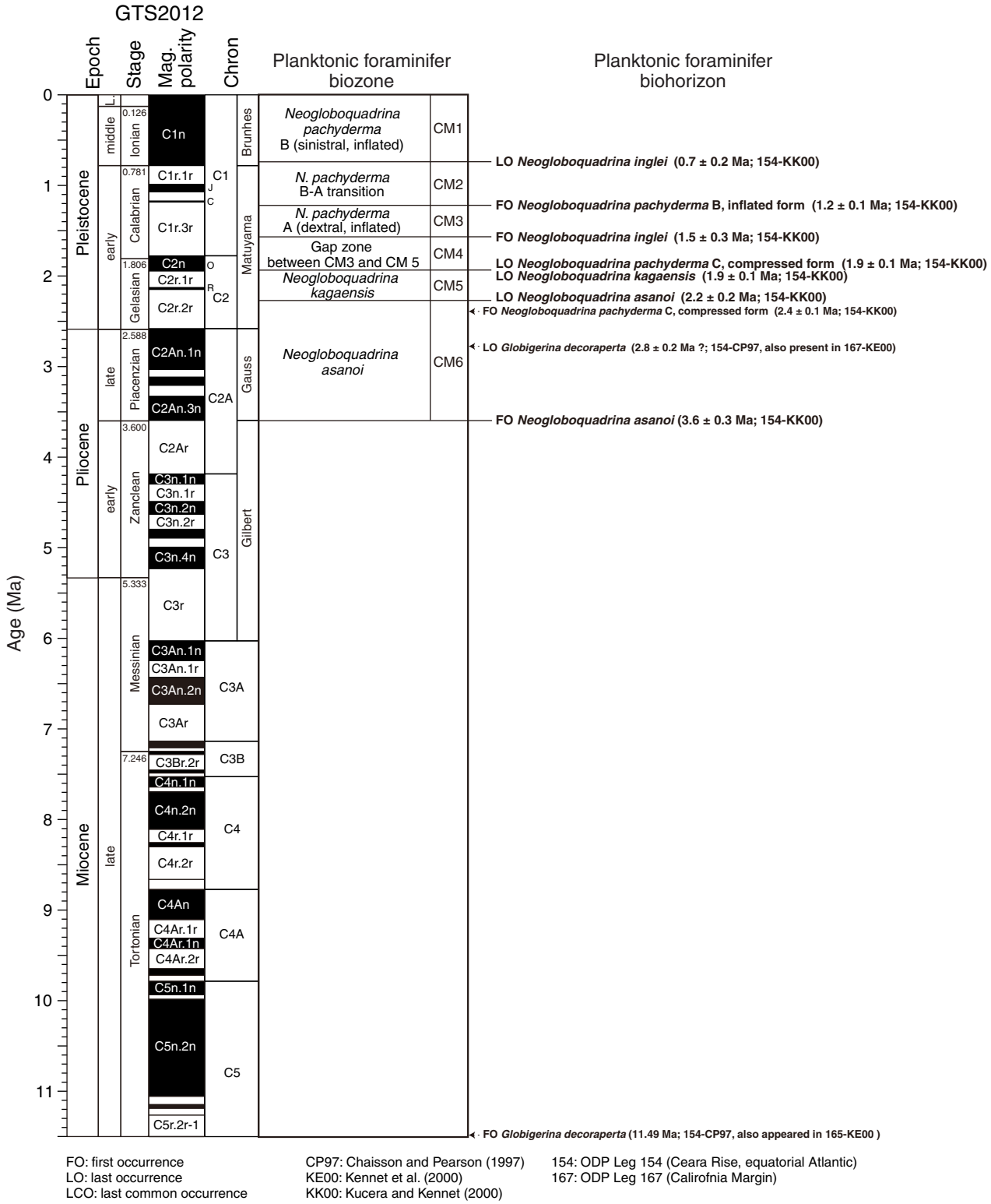

Figure F17. Schematic illustration of depth scales used during Expedition 341. The black section in individual cores reflects the interval used to construct a continuous splice (black continuous sequence). Note the expansion in depth (affine growth) in the CCSF-A and CCSF-D depth scales. The CCSF-B scale corrects for this apparent expansion. See text for details.

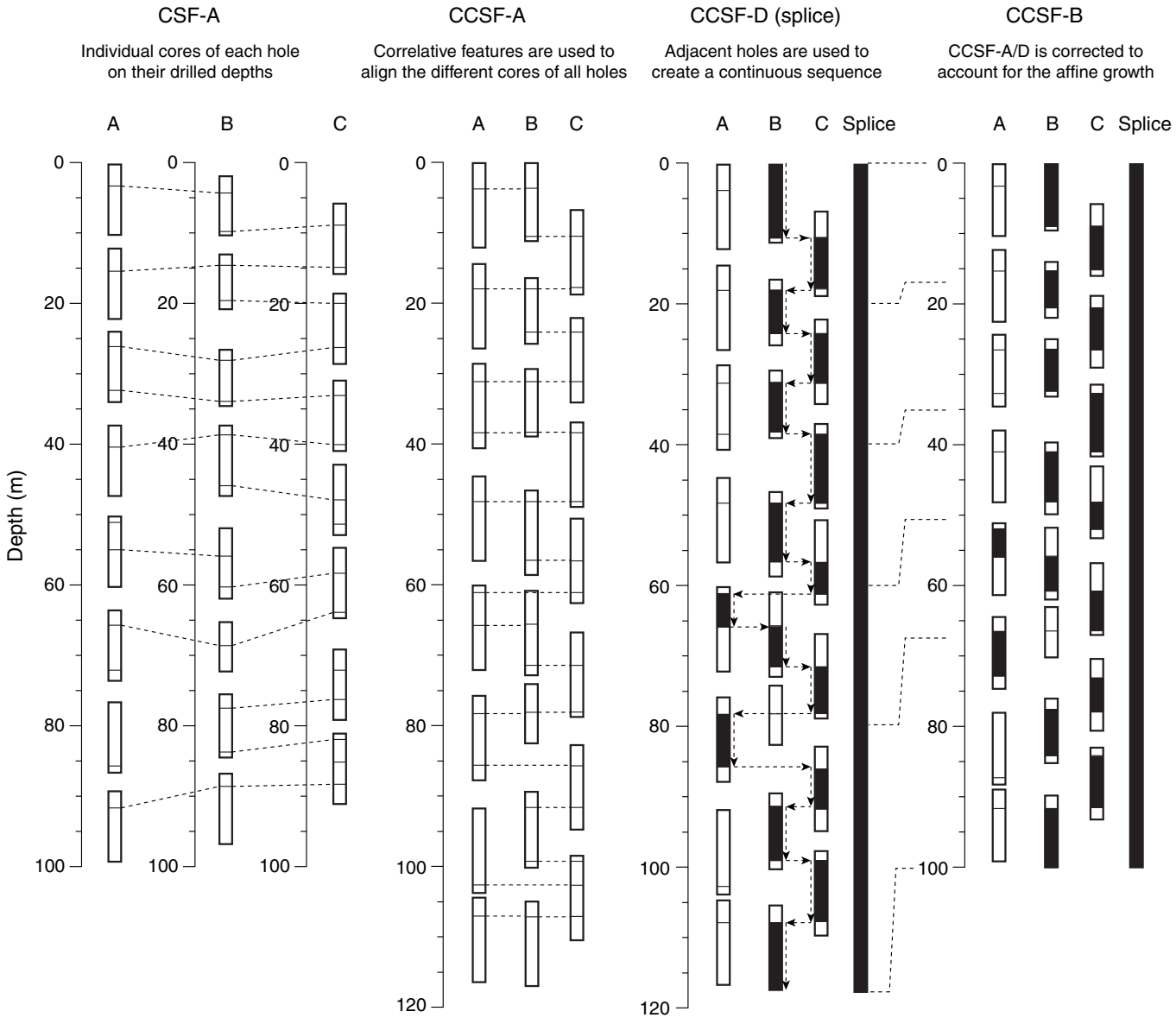

Figure F18. Tide corrections used during drilling at Sites (**A**) U1417, (**B**) U1418, and (**C**) U1419. MSL = mean sea level.

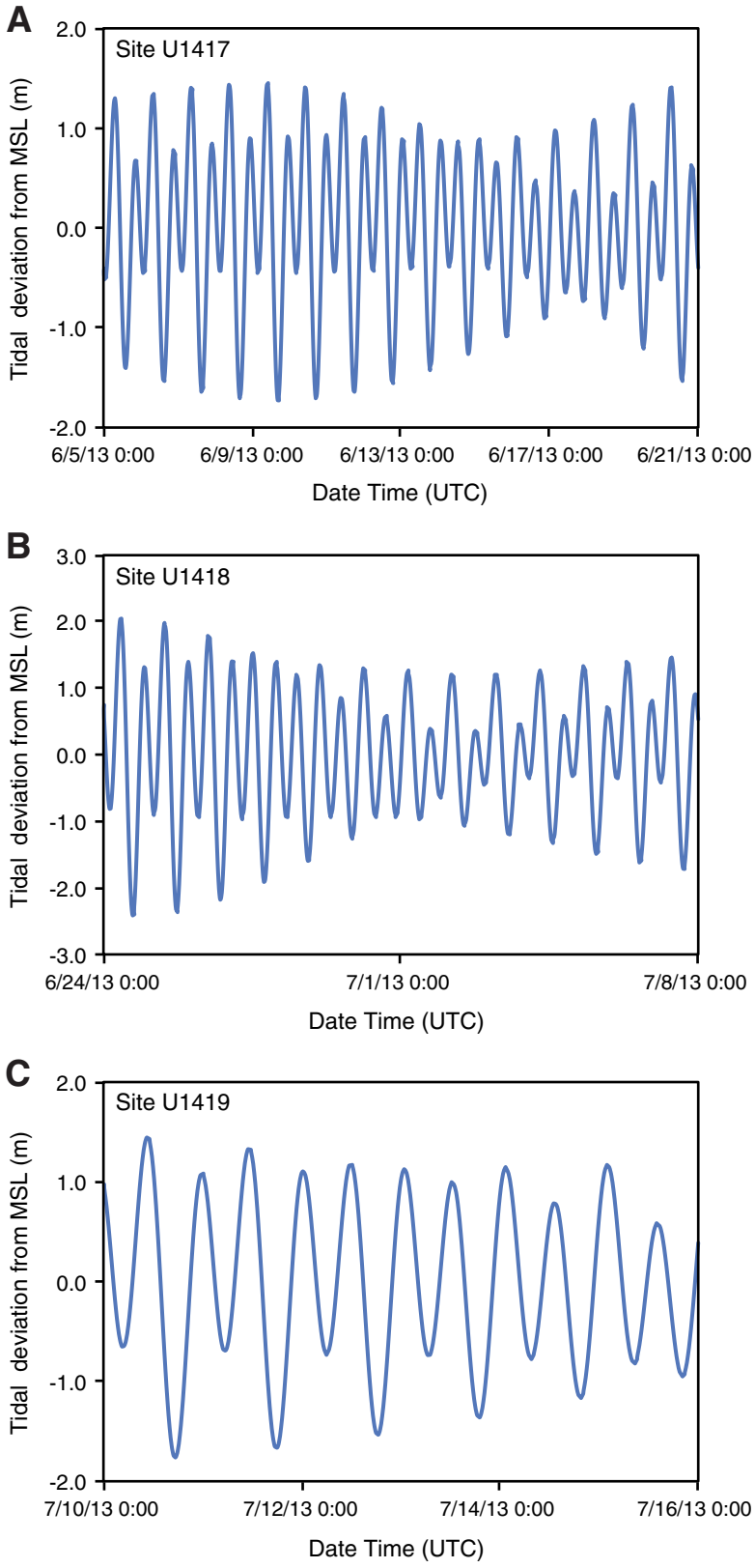

Figure F19. Response functions of the 80 mm Whole-Round Multisensor Logger (WRMSL) and 90 mm Special Task Multisensor Logger (STMSL) loop magnetic susceptibility (MS) sensors. Dashed bars denote half-height width.

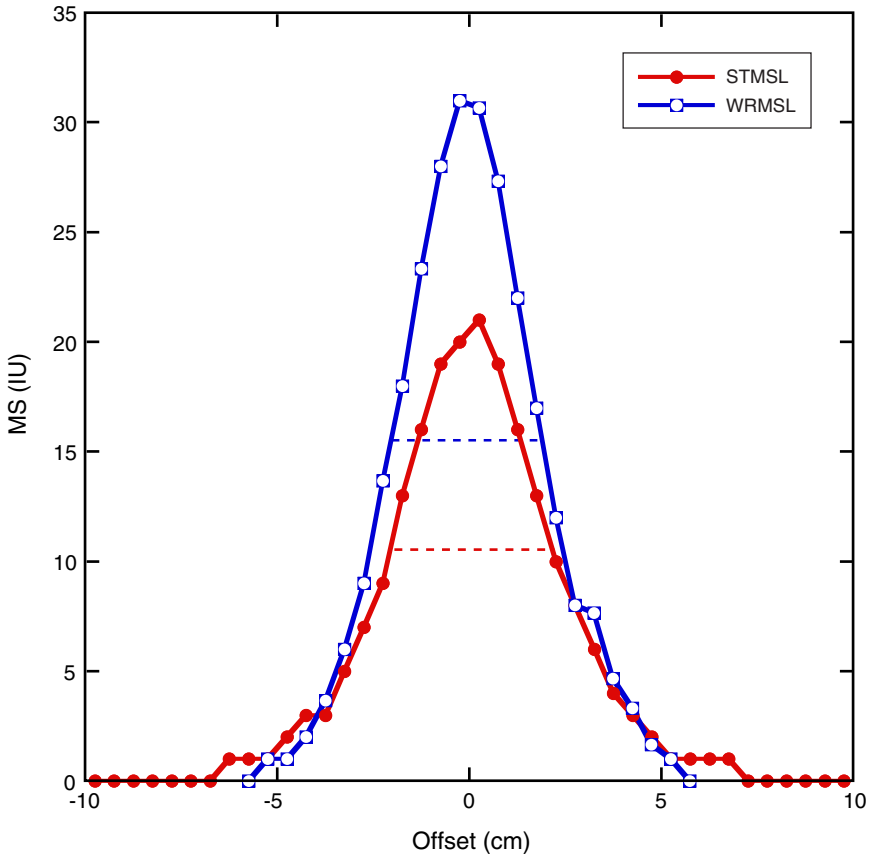

Figure F20. Relationship between Whole-Round Multisensor Logger (WRSML), Special Task Multisensor Logger (STMSL), and Section Half Multisensor Logger (SHMSL) magnetic susceptibility (MS) calculated from 6 standards. Each 30 cm standard was run through all three instruments at 0.5 cm resolution three times, and the central 20 cm were averaged to generate a single value for each run. The averages of the three runs for each standard are plotted with 1σ standard deviations for (**A**) STMSL vs. WRMSL and (**B**) SHMSL vs. WRMSL. The standard deviations of these three runs are plotted on both axes but fall within the symbol in the case of the loop MS data. In the case of the WRMSL vs. SHMSL data, both a linear regression (black) and a second-order polynomial regression (red) are shown.

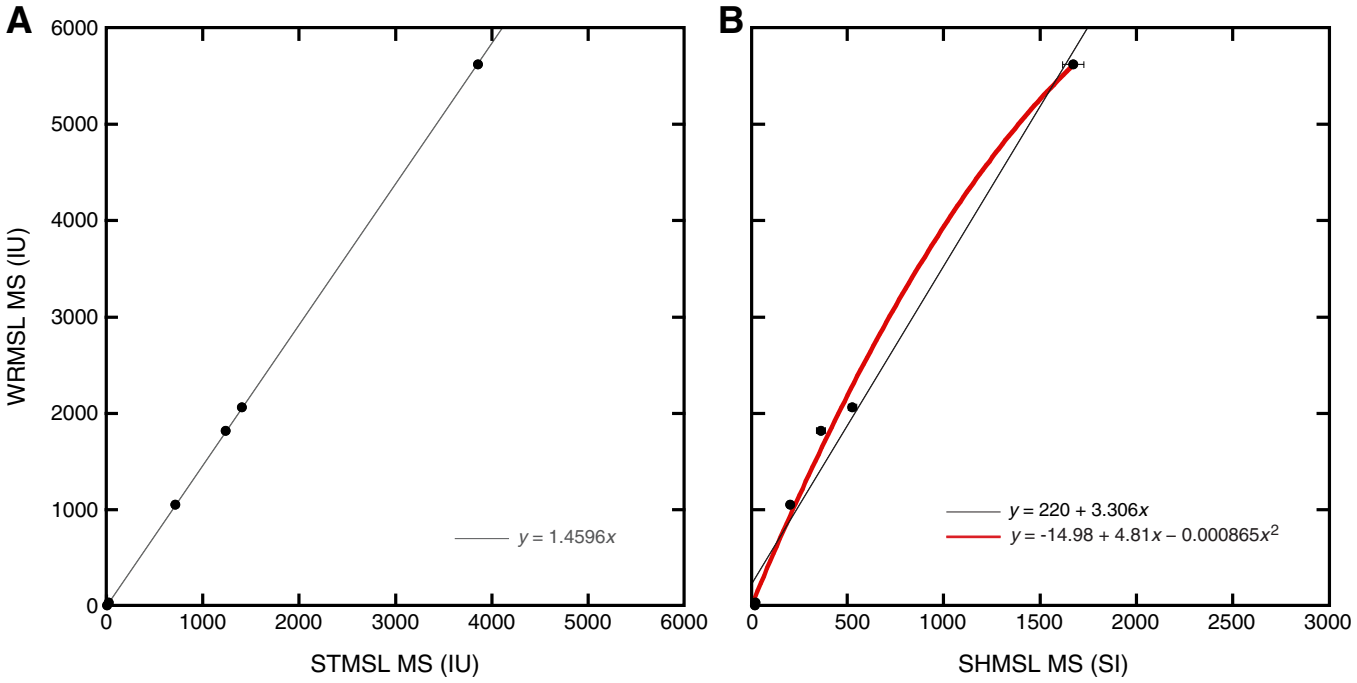

Figure F21. Edge correction coefficients proscribed by "ngr_edge_correction_table_0.txt" (0) and "ngr_edge_correction_table_1.txt" (1). Offsets reflect the presumed distance between the detector center and the edge of the core.

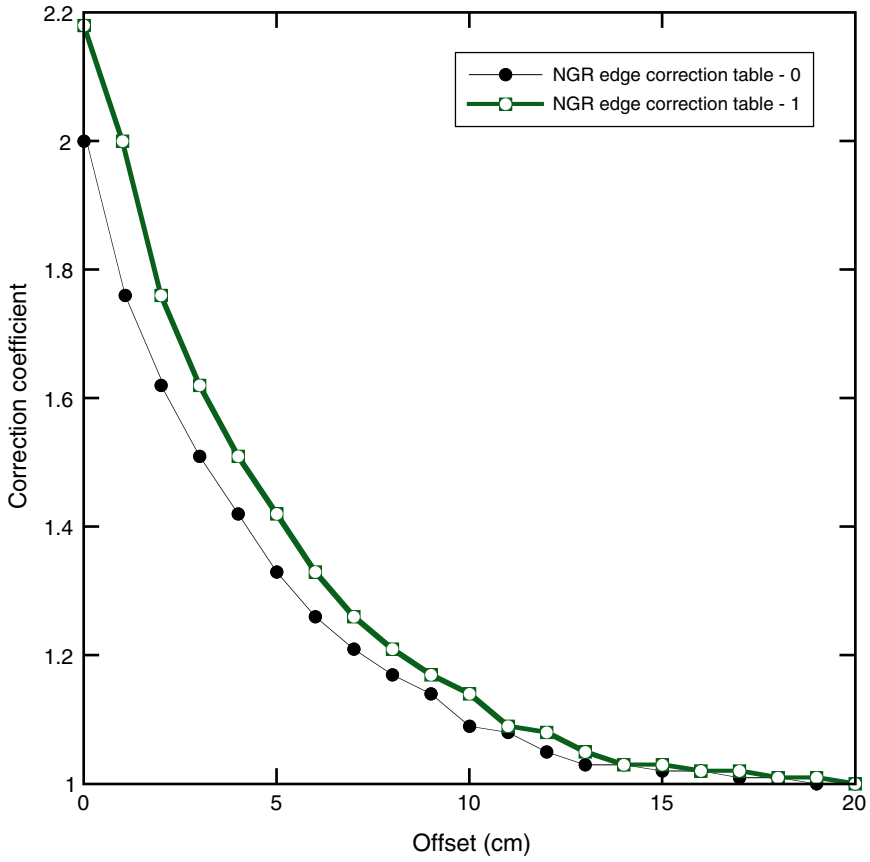

Figure F22. An example of an advanced piston corer temperature tool (APCT-3) temperature history showing (a) the first 5 min mudline measurement, (b) frictional heating associated with the piston firing, (c) the 10+ min measurement of thermal decay in the borehole, (d) frictional heating associated with core removal, and (e) the second 5 min mudline measurement.

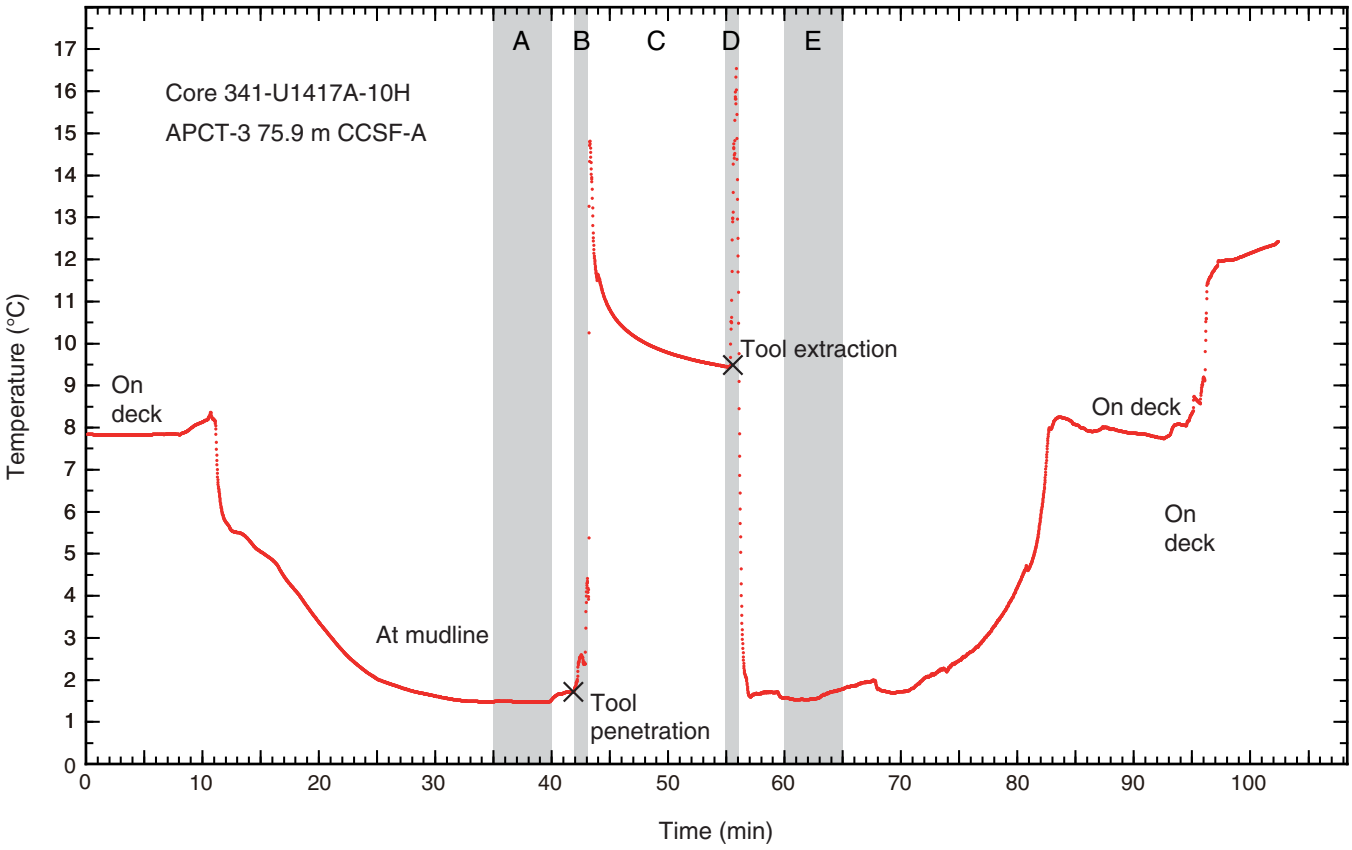

Figure F23. Wireline tool strings deployed during Expedition 341: triple combo, FMS-sonic, VSI, and MSS (see **"Downhole logging"** for more information). LEH-MT = logging equipment head-mud temperature, EDTC = Enhanced Digital Telemetry Cartridge, HNGS = Hostile Environment Natural Gamma Ray Sonde, APS = Accelerator Porosity Sonde, HLDS = Hostile Environment Litho-Density Sonde, HRLA = High-Resolution Laterolog Array, MSS = Magnetic Susceptibility Sonde, FMS = Formation MicroScanner, DSI = Dipole Shear Sonic Imager, GPIT = General Purpose Inclinometry Tool, VSI = Versatile Seismic Imager.

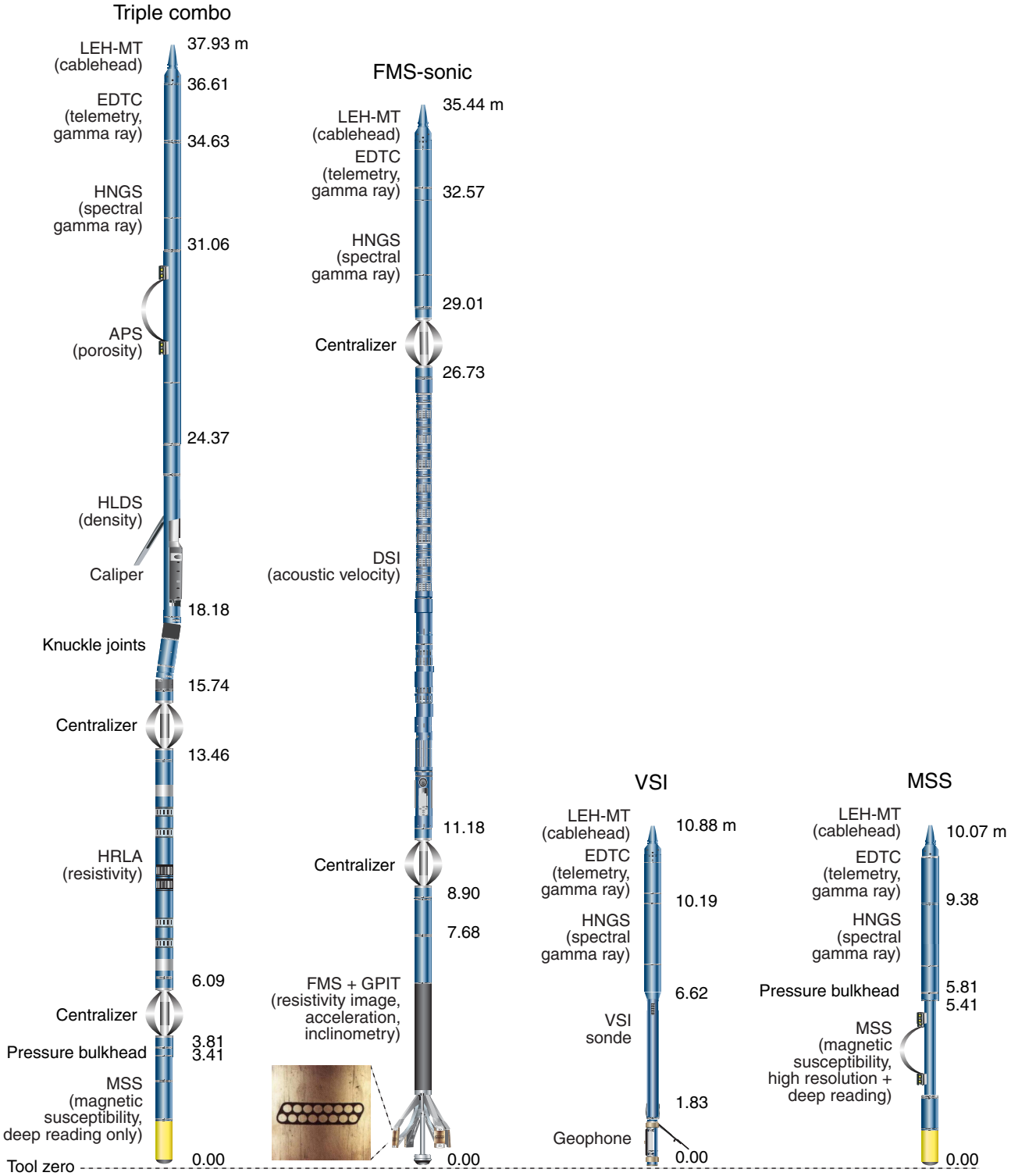

Figure F24. Sonic-induction tool string deployed in boreholes with uncertain hole conditions during Expedition 341. LEH-MT = logging equipment head-mud temperature, EDTC = Enhanced Digital Telemetry Cartridge, HLDS = Hostile Environment Litho-Density Sonde, DSI = Dipole Shear Sonic Imager, DIT = Phasor Dual Induction–Spherically Focused Resistivity Tool.

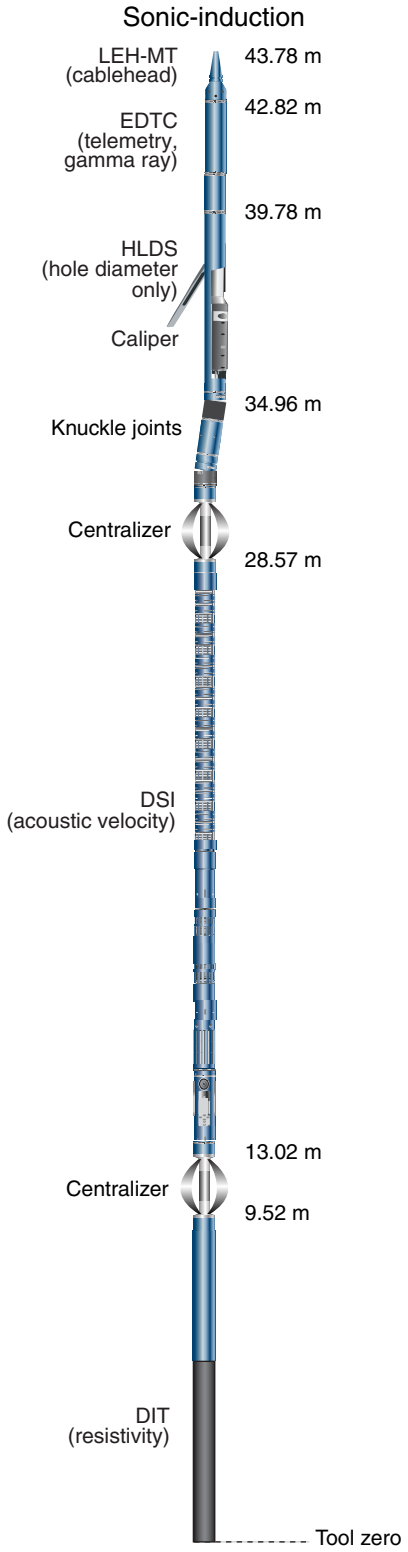

Table T1. Core depth scales used as part of IODP Expedition 341.

IODP depth scale	Complete name	ODP equivalent name	Definition
CSF-A	Core depth below seafloor	Meters below seafloor (mbsf)	Initial drilling depth.
CCSF-A	Core composite depth below seafloor, appended	Meters composite depth (mcd)	Composite depth scale in which cores from all holes are aligned by adding an affine value specific to each core.
CCSF-D	Splice	Splice	Composite sequence representing the complete stratigraphy at a site. It is composed of core sections from adjacent holes such that coring gaps or sampling gaps in one hole are filled with sediment from an adjacent hole.
CCSF-B	Corrected composite depth scale		Corrects for the affine growth and is the same length as the total depth cored. It is constructed by applying the specific equations determined for various depth intervals at each site.

For downhole logging depth scales, see Table **T6.**

Table T2. Sampling plan for interstitial water analyses to cover shipboard analytical priorities and shore-based sample requests.

Priority (if IW is limited)	Amount required (mL)	Splitting and preparation
ICP-AES major elements	0.1	2.5 mL IW into 5 mL cryovial, add 10 mL HNO_3 concentrated (include IW split for onshore trace metals analysis)
ICP-AES minor elements	0.5	
IC	0.1	5 mL IW into 5 mL cryovial, store in fridge until respective analysis
Phosphate (photometric)	0.3	
Ammonium (photometric)	0.1	
Chlorinity (titration)	0.5	
Alkalinity/pH (titration)	3	3 mL into 5 mL cryovial, titrate fast after squeezing
IW splits (onshore: $\delta^{18}O$, chlorinity, silica)	2–12	2–12 mL in 2–6 mL cryovials, freeze/cool (depending on onshore analysis)
IW splits (onshore: DIC, Ca/Sr/S isotopes)	2–12	2–12 mL into 2–6 mL (cryo)vials, cool, DIC sample toxified with $HgCl_2$

IW = interstitial water, ICP-AES = inductively coupled plasma–atomic emission spectroscopy, IC = ion chromatograph, DIC = dissolved inorganic carbon.

Table T3. Quantification limits for inductively coupled plasma–atomic emission spectroscopy (ICP-AES) analyses of all wavelengths measured at Sites U1417–U1421 and relative standard deviations (RSDs) for all wavelengths based on samples with element concentrations above the respective quantification limits.

	B (μM) 249.677	B (μM) 249.772	**Ba (μM) 455.403**	Ba (μM) 493.409	**Fe (μM) 239.563**	Fe (μM) 259.940	**Li (μM) 670.784**	**Mn (μM) 257.610**	Mn (μM) 259.372	Si (μM) 250.690	**Si (μM) 251.611**	Sr (μM) 407.771	Sr (μM) 421.552	**Sr (μM) 460.733**
Site U1417 ICP-AES minor elements														
Quantification limits (5 × StdDev of blank)	**17.64**	4.38	**0.33**	0.56	**2.02**	0.65	**3.01**	**0.33**	0.63	19.56	**24.13**	0.21	0.24	**2.53**
RSD% for IW values above quantification limits	**<9**	<9	**<8**	—	**<10**	—	**<10**	**<6**	<7	<7	**<8**	<7	<6	**<7**
Site U1418 ICP-AES Minor elements														
Quantification limits (5 × StdDev of blank)	**42.25**	13.08	**0.56**	0.34	**1.94**	1.08	**6.04**	**0.74**	0.56	23.76	**9.99**	Rejected	Rejected	**4.04**
RSD% for IW values above quantification limits	**<8**	<9	**<5**	<5	**<12**	<13	**<14**	**<6**	<7	<6	**<7**	Rejected	Rejected	**<6**
Site U1419 ICP-AES Minor elements														
Quantification limits (5 × StdDev of blank)	**50.75**	8.23	**0.46**	0.85	**0.81**	0.28	**7.16**	**0.23**	0.34	10.14	**4.36**	Rejected	Rejected	**3.58**
RSD% for IW values above quantification limits	**<6**	<5	**<7**	<6	**<11**	<13	**<8**	**<6**	<9	<5	**<6**	Rejected	Rejected	**<4**

StdDev = standard deviation, IW = interstitial water. Bold = selected wavelengths for respective elements. — = not calculated; rejected = values not reportable.

Table T4. Downhole measurements made by wireline tool strings, Expedition 341.

Tool string	Tool	Measurement	Sampling interval (cm)	Vertical resolution (cm)
Triple combo with MSS	EDTC	Total gamma ray	5 and 15	30
	HNGS	Spectral gamma ray	15	20–30
	HLDS	Bulk density, borehole diameter	2.5 and 15	38
	APS	Neutron porosity	5 and 15	36
	HRLA	Resistivity	15	30
	MSS	Magnetic susceptibility (deep reading sensor only)	4	40
FMS-sonic	EDTC	Total gamma ray	5 and 15	30
	DSI	Acoustic velocity	15	107
	GPIT	Tool orientation and acceleration	4	15
	FMS	Microresistivity, borehole diameter	0.25	0.50
Versatile Seismic Imager	VSI	One-way acoustic traveltime	Stations at 10–50 m	NA
	EDTC	Total gamma ray	5 and 15	30
MSS with HNGS	HNGS	Spectral gamma ray	15	20–30
	MSS	Magnetic susceptibility, deep reading sensor (DR)	4	40
		Magnetic susceptibility, high resolution sensor (HR)	4	10
Sonic-induction	EDTC	Total gamma ray	5 and 15	30
	HLDS	Borehole diameter	15	30
	DSI	Acoustic velocity	15	107
	DIT	Resistivity	15.24	150–240

All tool names except MSS are trademarks of Schlumberger. Sampling interval based on optimal logging speed. Acoustic imaging approximate vertical resolution is at 500 kHz. NA = not applicable. For definitions of tool acronyms, see Table T5.

Table T5. Acronyms and units used for downhole wireline tools and measurements, Expedition 341.

Tool	Output	Description	Unit
EDTC		Enhanced Digital Telemetry Cartridge	
	GR	Total gamma ray	gAPI
	ECGR	Environmentally corrected gamma ray	gAPI
	EHGR	High-resolution environmentally corrected gamma ray	gAPI
HNGS		Hostile Environment Natural Gamma Ray Sonde	
	HSGR	Standard (total) gamma ray	gAPI
	HCGR	Computed gamma ray (HSGR minus uranium contribution)	gAPI
	HFK	Potassium	wt%
	HTHO	Thorium	ppm
	HURA	Uranium	ppm
APS		Accelerator Porosity Sonde	
	APLC	Near/array limestone corrected porosity	Dec. fraction
	STOF	Computed standoff	inch
	SIGF	Formation capture cross section	Capture units
HLDS		Hostile Environment Litho-Density Sonde	
	RHOM	Bulk density	g/cm^3
	PEFL	Photoelectric effect	$barn/e^-$
	LCAL	Caliper (measure of borehole diameter)	inch
	DRH	Bulk density correction	g/cm^3
HRLA		High-Resolution Laterolog Array	
	RLAXXX	Apparent resistivity from Computed Focusing Mode XXX	Ωm
	RT	True resistivity	Ωm
	MRES	Borehole fluid resistivity	Ωm
MSS		Magnetic Susceptibility Sonde	
	LSUS	Magnetic susceptibility, deep reading (DR)	Uncalibrated units
	HSUS	Magnetic susceptibility, high resolution (HR)	Uncalibrated units
FMS		Formation MicroScanner	
	C1, C2	Orthogonal hole diameters	inch
	P1AZ	Pad 1 azimuth	°
		Spatially oriented resistivity images of borehole wall	
GPIT		General Purpose Inclinometry Tool	
	DEVI	Hole deviation	°
	HAZI	Hole azimuth	°
	Fx, *Fy*, *Fz*	Earth's magnetic field (three orthogonal components)	°
	Ax, *Ay*, *Az*	Acceleration (three orthogonal components)	m/s^2
DSI		Dipole Shear Sonic Imager	
	DTCO	Compressional wave slowness	µs/ft
	DTSM	Shear wave slowness	µs/ft
	DT1	Shear wave slowness, lower dipole	µs/ft
	DT2	Shear wave slowness, upper dipole	µs/ft
VSI		Versatile Seismic Imager	
	1WTT	Acoustic traveltime	s
DIT		Phasor Dual Induction–Spherically Focused Resistivity Tool	
	IDPH	Deep induction resistivity	Ωm
	IMPH	Medium induction resistivity	Ωm
	SFLU	Shallow spherically focused resistivity	Ωm

For the complete list of acronyms used in IODP and for additional information about tools, consult IODP-USIO Science Services, LDEO, at **iodp.ldeo.columbia.edu/TOOLS_LABS/tools.html.**

Table T6. Borehole and downhole logging depth scales, Expedition 341.

Depth scale	Complete name	Definition
DSF	Drillers depth below seafloor	The length of all drill string components between seafloor and target.
WRF	Wireline log depth below rig floor	Length of wireline and sensor offset between the rig floor and the target.
WSF	Wireline log depth below seafloor	WRF with seafloor depth below rig floor subtracted.
WSSF	Wireline log speed-corrected depth below seafloor	WSF corrected with accelerometer data.
WMSF	Wireline log matched depth below seafloor	Depth derived by correlation between reference run and all additional runs to make a set of WSF runs internally consistent.